

Phased Array Theory and Technology

ROBERT J. MAILLOUX, FELLOW, IEEE

Invited Paper

Abstract—This review of array antennas highlights those elements of theory and hardware that are a part of the present rapid technological growth. The growth and change in array antennas include increased emphasis on "special-purpose" array techniques such as conformal and printed circuit arrays, wide angle scanning arrays, techniques for limited sector coverage, and antennas with dramatically increased pattern control features such as low sidelobe, adaptively controlled patterns. These new topics have substantially replaced large radar arrays in the literature and constitute a major change in the technology.

The paper presents a tutorial review of theoretical developments emphasizing techniques appropriate to finite arrays, but indicating parallel developments in infinite array theory, which has become the useful tool for analysis of large arrays. A brief review of the theory of ideal arrays is followed by a generalized formulation of array theory including mutual coupling effects, and is appropriate to finite or infinite arrays of arbitrary wire elements or apertures in the presence of a conducting ground screen. Some results of array tolerance theory are summarized from the literature and retained as reference throughout discussions of array component requirements and device tolerance for low sidelobe arrays.

Examples from present technology include conformal and hemispherical coverage arrays, lightweight printed circuit arrays, systems for use with reflectors and lenses in limited sector coverage applications, and wide-band array techniques.

I. INTRODUCTION AND CHARACTERISTICS OF IDEALIZED ARRAYS

A. Introduction

THE REVIEW paper by Stark [1] summarized developments in the theory and technology of phased arrays through 1974. In addition to a presentation of fundamental considerations in infinite array theory and the phenomenon called array "blindness," Stark's review included detailed descriptions of phasing circuits and array feed networks.

Major changes in array technology since 1974 might have been expected. Generally, it was not expected that emphasis throughout these intervening years would be on small, special-purpose arrays and not large ground-based radar arrays. It was also not generally expected that in 1982 array technology would face so many new challenges as to require theoretical and practical developments of a most fundamental kind.

Unfortunately, this greatly expanded need for array technology is not the result of past successes, for arrays have not been fielded in great numbers. This failure was the theme of a recent workshop sponsored by the Naval Research Laboratories [2] that sought to draw out new innovative array research with the goal of developing high performance, low cost radar arrays. The reason for this failure is that the cost of phased arrays has continued to be far in excess of the initial

optimistic prediction of an ultimate cost per array element of tens of dollars. Array cost estimates based upon existing technology [2], [3] show that arrays still cost hundreds of dollars per element, although there now appears to be some reason to hope for relief. Growth in array technology has been slowed primarily because of its cost.

The present needs for expanded array research, development, and production are due to increasing demands for higher performance systems. These include the need for agile beam tactical radars to acquire and track more targets than possible with reflector antennas, the need for using defense against military countermeasures, beam agility, deterministic and adaptive pattern control, and the need for conformal scanning antennas for high performance aircraft and missiles. Since arrays are expensive, it is a practical fact that they are selected only when conventional mechanical systems cannot adequately do the job; and this is true of each of the new applications. There is such an abundance of difficult requirements for ground-based aircraft and even satellite radar and communications, that one cannot help but imagine a revolution coming in the technology to fill these needs. One of the goals of this review is to summarize the present state of theory and technology, and to estimate how each must advance to serve this revolution.

Substantial advances have taken place since the early 1970's even though array cost has not declined. Major developments in theory include analytical studies of a wide variety of elements, solutions for large arrays, contributions to the understanding of edge effects and array "blindness," advances in synthesis and in adaptive optimization of patterns, and error analysis. Technological developments include great advances in components, phase shifters, and feed networks, and in broad-band subarraying. In addition, many new elements have been developed, most notably, microstrip and stripline elements for lightweight and conformal arrays. Finally, there have been dramatic strides in the implementation of adaptive control to optimize array signal-to-noise ratio for receive arrays, and in active transmit-receive module development.

Surely one can anticipate even greater advances throughout the 1980's. Monolithic thin and thick film technology is being developed today and should finally begin to bring about the cost reductions promised by automatic processes. These developments will include techniques for array and phase shifter manufacture, and also for fully active monolithic modules. Microprocessors have been proposed for use at each phased element to reduce cabling necessary for phase shifter settings. Time delay devices traditionally have been switched lines, but present research [4] points to coming availability of variable time delay control using magnetic delay lines. Fully digital array processing is now applicable to sonar systems [5] and

Manuscript received May 18, 1981; revised December 4, 1981.
The author is with Electromagnetic Sciences Division, Rome Air Development Center, Hanscom AFB, Hanscom, MA 01731.

to some narrow-band communication systems, but the advance of gigabit logic may make fully digital processing feasible for adaptive and deterministic control of large, wide-band arrays. Each of these advances brings its own promise, but each must operate within the constraints of a radiating electromagnetic system, and this is the reason for emphasizing fundamental electromagnetic bounds and limits throughout this paper.

In writing this paper the author has de-emphasized large array theory, partly because it was so thoroughly covered by Stark [1] and partly to highlight the large variety of array types and functions that will address future needs. In addition, there are a number of important topics only mentioned peripherally that deserve separate, detailed review. In this category are adaptive arrays and active transmit-receive modules.

One goal of this survey is to illustrate the vast collection of array types and the distinction between them, but the main goal is to emphasize those array parameters that control important characteristics required of future arrays. For example, to address the future need for dramatically lowered sidelobes and deep, wide-band pattern nulls, this paper addresses such fundamental issues as constrained null depths, feed network design and element pattern ripple to provide design data for system development. Fundamental limits to bandwidth, maximum scan angle, minimum number of control elements, and minimum sidelobe level are among the array parameters discussed and are necessary to the process of system selection.

The remainder of Section I deals with characteristics of idealized antenna arrays. It is tutorial in nature but outlines those properties and bounds that can be predicted by this simplest theory. The section covers collimation, pattern shape, beamwidth, directivity, grating lobes, pattern synthesis and null bounds, bandwidth and subarraying.

Section II introduces the more formal array theory, specifically applied to finite arrays, and outlines methods for solution of general classes of array problems. This section also discusses active element patterns for finite and infinite arrays and concludes with a discussion of the problems associated with scanning an array from zenith to end fire.

Section III discusses the practical aspects of array development, array errors, phase shifter quantization, selections of array elements, including new microstrip and stripline elements, and the choice of components for arrays including feed networks, polarizers, and phase shifters.

Section IV surveys current technology with emphasis on low sidelobes, conformal and low profile antennas, antennas for limited sector coverage, and wide-band array feeds. To aid designers, there is an attempt to give the performance limits of each system.

Many of the topics are necessarily treated in only a cursory manner, so it is fortunate that there is a vast literature of texts [6]-[17], journals, and topical symposia [18] that deal with aspects of array antennas. Several recent issues of journals deal with antenna arrays [19] and microstrip [20], conformal [21], and adaptive [22], [23] arrays. In addition, a recent PROCEEDINGS tutorial review paper [24] addresses the theory of adaptive arrays.

B. The Idealized Array

Many of the properties of practical array antennas are apparent from a detailed consideration of idealized arrays, or arrays whose elements are assumed electrically uncoupled from one another. For such an array of radiators, as shown in Fig. 1,

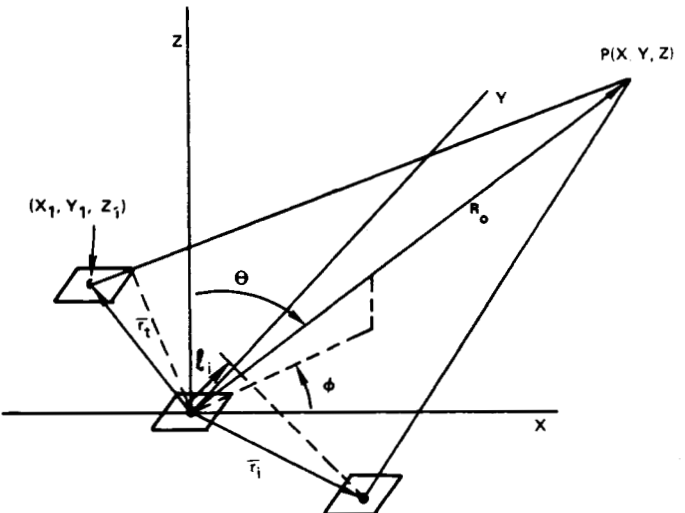


Fig. 1. Generalized array coordinates.

the electric field is given by the sum of radiated fields of each of the elements. Each element at position (x_i, y_i, z_i) is excited by a complex weighting a_i and radiates with a vector element pattern $\bar{f}_i(\theta, \phi)$ so that the total radiated field is given by

$$\bar{E}(\bar{r}) = K \sum_i \bar{f}_i(\theta, \phi) a_i \frac{e^{-jk|\bar{r}-\bar{r}_i|}}{|\bar{r}-\bar{r}_i|} \quad (1)$$

where

$$|\bar{r} - \bar{r}_i| = \sqrt{(x - x_i)^2 + (y - y_i)^2 + (z - z_i)^2}.$$

In the far field this term can be approximated by

$$|\bar{r} - \bar{r}_i| \approx R_0 - \bar{r}_i \cdot \hat{\rho} \quad (2)$$

where

$$\hat{\rho} = \hat{x}u + \hat{y}v + \hat{z}\cos\theta$$

$$\bar{r}_i = \hat{x}X_i + \hat{y}Y_i + \hat{z}Z_i$$

K is a complex constant, and

$$u = \sin\theta \cos\phi$$

$$v = \sin\theta \sin\phi$$

$$k = 2\pi/\lambda$$

are the direction cosines.

The total field is thus written

$$\bar{E}(\bar{r}) = K \frac{e^{-jkR_0}}{R_0} \sum_i a_i \bar{f}_i(\theta, \phi) e^{+j\bar{r}_i \cdot \hat{\rho} k}. \quad (3)$$

The vector element patterns \bar{f}_i are in general, different, even in an array of like elements. The difference is seldom planned, but usually results from the interaction between individual elements and the array edge. For purposes of this discussion we will assume that they are alike in an idealized array.

1) *Collimation:* The usual purpose of an array is to form a beam at some specific angle in space (θ_0, ϕ_0) . This can be done at all frequencies by choosing the excitation

$$a_i = |a_i| e^{-jkr_i \cdot \hat{\rho}_0} = |a_i| e^{-jkl_i} \quad (4)$$

with $\hat{\rho}_0$ given by (2) using θ_0 and ϕ_0 in the direction cosine expressions. At such a point, the fully collimated beam field strength is a simple vector summation of the element patterns

weighted by the amplitudes $|a_i|$

$$\bar{E}_0(\vec{r}) = K \frac{e^{-jkR_0}}{R_0} \sum_i \bar{f}_i(\theta_0, \phi_0) |a_i| \quad (5)$$

and if the element patterns \bar{f}_i are equal and isotropic ($|\bar{f}_i| = 1$) this is the largest possible value of the field $\bar{E}(\vec{r})$ for any given R_0 in the far field. Selection of the excitations of (4) is understood intuitively by considering that the projected distance to the observer at (R_0, θ_0, ϕ_0) is different for each array element by the length l_i in Fig. 1. Removal of this path length difference will cause the contributions from each element to add in-phase in the far field. The envelope of coefficients $|a_i|$ is the array illumination, and is the primary determinant of the radiated sidelobe levels, just as it is for aperture antennas.

Applying signals of the form of (4) is called time delay steering because the phase of the excitation signals exactly compensates for the time delay of a signal travelling the projected distances l_i . Time delay steering results in a fully collimated beam at all frequencies, but is extremely expensive, lossy, and bulky, for it depends upon switching relatively long delay lines. For this reason, true time delay is not often used at the array element level, but more commonly incorporated into the feed circuits of arrays divided into subarrays. Examples of subarray excitation are described in later sections.

Alternatively, at some fixed frequency f_0 , with wavelength λ_0 and wavenumber $k_0 = 2\pi/\lambda_0$, purely phase weighting can be substituted for the time delay steering. In such case the weighting factors a_i are

$$a_i = |a_i| e^{-jk_0 \vec{r}_i \cdot \hat{\rho}_0}$$

$$k_0 = 2\pi/\lambda_0$$

and

$$\bar{E}_0(r) \approx K \frac{e^{-jkR_0}}{R_0} \sum_i |a_i| f_i(\theta, \phi) e^{+j r_i \cdot (\mathbf{k} \hat{\rho} - \mathbf{k}_0 \hat{\rho}_0)} \quad (6)$$

which represents exact collimation only at fixed frequencies ($\lambda = \lambda_0$), and is called phase steering. Most arrays are phase steered, but when wide operating bandwidths are required it may be necessary to investigate options for time delay at the subarray level.

Several examples of array collimation are given below for the arrays of Fig. 2. Note m and n are half integers, $\pm \frac{1}{2}, \dots, \pm (N_x - 1)/2$ or $\pm (N_y - 1)/2$.

Periodic column array in one plane:

$$\vec{r}_m = \hat{x} X_m = \hat{x} m d_x; u_0 = \cos \theta_0.$$

Steering excitation:

$$a_m = |a_m| e^{-jk_0 m d_x u_0}.$$

Radiation pattern:

$$\bar{E}(\vec{r}) = \frac{K}{R_0} e^{-jkR_0} \sum_m \bar{f}_m(\theta, \phi) |a_m| e^{(j m d_x)(k u - k_0 u_0)}. \quad (7)$$

Periodic two-dimensional array:

$$\vec{r}_{mn} = \hat{x} m d_x + \hat{y} n d_y; \quad u_0 = \sin \theta_0 \cos \phi_0, v_0 = \sin \theta_0 \sin \phi_0.$$

Steering excitation:

$$a_{mn} = |a_{mn}| e^{-jk_0 (m d_x u_0 + n d_y v_0)}.$$

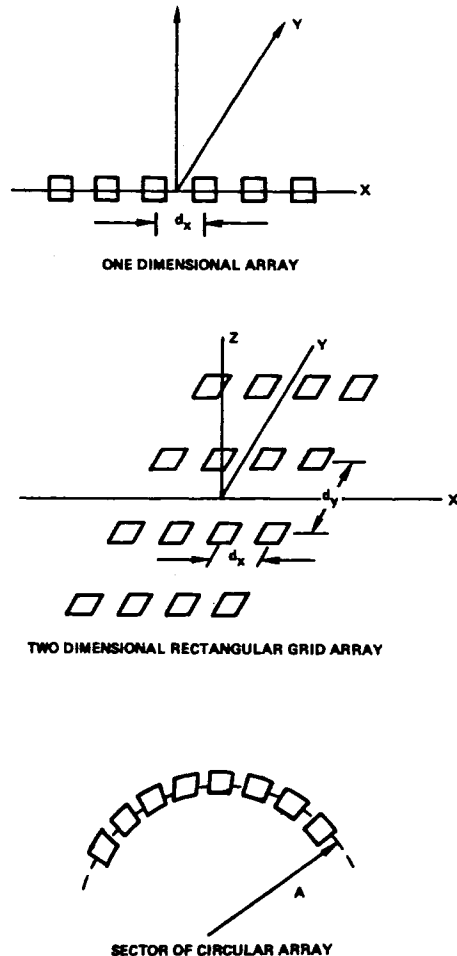


Fig. 2. Linear, planar, and circular arrays.

Radiation pattern:

$$\bar{E}(\vec{r}) = K \frac{e^{-jkR_0}}{R_0} \sum_{m,n} \bar{f}_{mn}(\theta, \phi) |a_{mn}| e^{j[m d_x (k u - k_0 u_0) + n d_y (k v - k_0 v_0)]}. \quad (8)$$

Circular array section: The circular array section of Fig. 2 is another characteristic array shape that requires a simple regular excitation vector to form a beam in the principal plane (θ, ϕ)

$$\vec{r}_m = \hat{x} a \cos \theta_m + \hat{y} a \sin \theta_m; \quad \hat{\rho} = \hat{x} \cos \theta + \hat{y} \sin \theta.$$

Steering excitation:

$$a_m = |a_m| e^{-jk_0 \cos(\theta_0 - \theta_m)}, \quad \theta_m = m \Delta \theta.$$

Radiation pattern:

$$\bar{E}(\vec{r}) = \frac{K}{R_0} e^{jkR_0} \sum_m \bar{f}_m(\theta) |a_m| e^{j a [k \cos(\theta - \theta_m) - k_0 \cos(\theta_0 - \theta_m)]}. \quad (9)$$

In each of the above cases the phase steered beam collimation is changed to time delayed collimation by substituting $k = 2\pi/\lambda$ for the phase steered term $k_0 = 2\pi/\lambda_0$.

2) Characteristics of Finite Planar Arrays: Pattern Shape, Beamwidth, Grating Lobes and Lattice Selection: The quality

of the beam formed by an array is measured by a number of factors. Chief among these are the directivity, beamwidth and sidelobe level of the array pattern, and the bandwidth over which satisfactory radiation characteristics can be obtained.

The directivity is the ratio of power density at the peak of the main beam ($\bar{r} = \bar{r}_0 = (R_0, \theta_0, \phi_0)$) to the average power density, or in terms of (1)

$$D = \frac{\bar{E}(\bar{r}_0) \bar{E}^*(\bar{r}_0)}{\frac{1}{4\pi} \int_0^\pi \int_0^{2\pi} \bar{E}(\bar{r}) \bar{E}^*(\bar{r}) \sin \theta d\theta d\phi}. \quad (10)$$

The integral over θ is often carried only to $\pi/2$ for most planar arrays with a ground screen, as it is assumed that radiation is negligible for $\theta > \pi/2$.

Equation (1) can be reduced to much simpler forms for linear and planar arrays. In [25, vol. 2, ch. 1], Elliott gives convenient formulas for the directivity of linear dipole arrays, and derives an especially simple form for arrays of isotropic elements with half wave spacing and currents a_m as in (7)

$$D = \frac{(\sum |a_m|)^2}{\sum |a_m|^2}. \quad (11)$$

This expression shows the directivity of a linear array to be independent of scan angle. As pointed out by Elliott, this behavior is peculiar to the linear array and results from the broad pattern perpendicular to the array axis. As the array is scanned toward end fire the area of this conical shape is reduced and the effect offsets the beam broadening in the plane of scan that tends to reduce gain.

Elliott gives a number of other very convenient formulas relating beamwidth and directivity for linear arrays with uniform and tapered illuminations, and for relating the directivity of planar arrays to linear arrays. In addition he obtains a formula relating beamwidth and directivity for a planar array

$$D = 32400/B \quad (12)$$

where

$$B = \theta x_3 \theta y_3 \sin \theta_0$$

and θx_3 and θy_3 are the 3-dB beamwidths of the pencil or elliptical beam at broadside. In this formula the beamwidths are in degrees.

This simple formula reveals the well-known cosine scan dependence exhibited by planar arrays. The formula is exact for uniform illumination, and a good approximation for other array illuminations for all θ_0 except very near endfire, where more detailed analysis is required. Scanning near endfire will be discussed in Section II-D.

The selection of array illuminations is described in many standard texts, but certain special cases are mentioned briefly in Section I-B5. The array illumination determines the beamwidth, sidelobes, and directivity. Equation (12) shows directivity as inversely proportional to the product of principal plane beamwidths. Uniform illumination ($|a_i| = 1$) produces the highest directivity and narrowest beam of any illumination (except for certain special "superdirective" illuminations associated with rapid phase fluctuations and closely spaced elements). The half power beamwidth of this radiation pattern for a linear array or in the principal planes of a rectangular

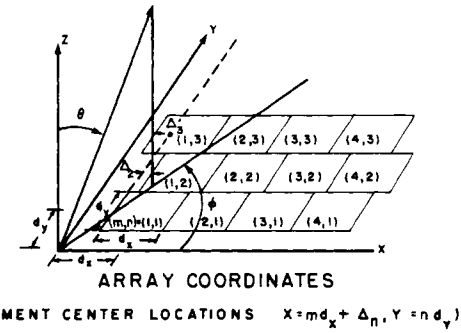


Fig. 3. Periodic two-dimensional array.

array at broadside is

$$\theta_3 = K_b \frac{\lambda}{L} \quad (13)$$

for $K_b = 0.886$. Uniform illumination also produces relatively high sidelobe patterns (about -13 dB). Selection of various tapered illuminations can result in much lower sidelobes, but is accompanied by wider beamwidths and lower directivity. As the array is scanned from broadside the beamwidth widens, again as second θ_0 , except near endfire.

A number of important characteristics of planar array patterns can be illustrated by considering an array with even numbers of rows and columns as shown in Fig. 3, and with each row displaced by some unspecified distance Δ_n , so that the element center locations are given by the coordinates

$$x = md_x + \Delta_n; y = nd_y$$

for

$$m = \pm \frac{1}{2}, \frac{3}{2}, \dots, \frac{N_x - 1}{2}$$

$$n = \pm \frac{1}{2}, \frac{3}{2}, \dots, \frac{N_y - 1}{2}.$$

It will be assumed that all element patterns are the same and have only one polarization.

The far zone electric field, normalized to unity, is given by

$$\bar{E}_n(\bar{r}) = \frac{\bar{f}(\theta, \phi)}{N} \sum_m \sum_n a_{mn} e^{jk(umd_x + \Delta_n u + vnd_y)}. \quad (14)$$

The excitation signals required to form a beam at (θ_0, ϕ_0) at some fixed frequency f_0 are

$$a_{mn} = |a_{mn}| e^{-jk_0(u_0 m d_x + u_0 \Delta_n + v_0 n d_y)}. \quad (15)$$

If the $|a_{mn}|$ amplitude illumination is a separable distribution in x and y so that $|a_{mn}| = |a_m^x| |a_n^y|$, and the element pattern is also separable, so that

$$\bar{f}(\theta, \phi) = \bar{f}_x(u) \bar{f}_y(v) \quad (16)$$

then the pattern can be written in the following form:

$$\begin{aligned} \bar{E}_n(\bar{r}) &= \frac{\bar{f}_x(u)}{N_x} \left\{ \sum_m |a_m^x| e^{j(ku - k_0 u_0)m d_x} \right\} \\ &\quad \cdot \frac{\bar{f}_y(v)}{N_y} \left\{ \sum_n |a_n^y| e^{j((kv - k_0 v_0)n d_y + \Delta_n(ku - k_0 u_0))} \right\} \\ &= E_x(u) E_y(v, v). \end{aligned} \quad (17)$$

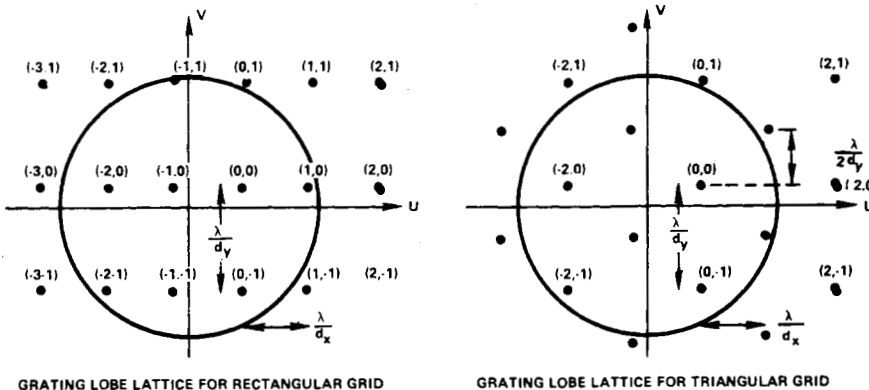


Fig. 4. Grating lobe lattices.

The pattern is not separable in general, but may be so for certain choices of Δ_n . This form of (17) will be useful in a later section for describing methods of lattice selection, but for the present it is convenient to set $\Delta_n = 0$ for all n . This is the familiar rectangular grid configuration, and in this case the field is fully separable.

If $\lambda = \lambda_0$, the factors E_x and E_y have their peak at $u = u_0$ and $v = v_0$ indicating that the row-column collimation produces a peak at the desired main beam position. These expressions can have principal maxima corresponding to other values of u and v however, and form high gain beams at direction cosines given by

$$u_p = \frac{\lambda}{\lambda_0} u_0 + p \frac{\lambda}{d_x}; v_q = \frac{\lambda}{\lambda_0} v_0 + q \frac{\lambda}{d_y} \quad (18)$$

where q and p are integers. Values of u and v corresponding to the discrete u_p, v_q parameters are called grating lobes, and are angular locations where the main beam is repeated. Not all values of q and p correspond to allowed angles of radiation however, for the direction of radiation θ measured from the array normal is given by

$$\cos \theta_{pq} = \sqrt{1 - u_p^2 - v_q^2} \quad (19)$$

and so real angles of radiation θ_{pq} require that the allowed values of u_p and v_q are constrained by the condition

$$u_p^2 + v_q^2 < 1. \quad (20)$$

These points are shown in (u, v) space as a regularly spaced grating lobe lattice about the main beam location (u_0, v_0) in Fig. 4(a). The circle with unity radius represents the bounds of the above inequality; all grating lobes within the circle represent those radiating into real space, and those outside do not radiate. The primary means of grating lobe avoidance is to select closely spaced elements so that none of the grating lobes lie in real space.

Equation (17) illustrates that in the ideal array the radiation pattern is the product of an element pattern $f(\theta, \phi)$ and an array factor that depends only upon the element position vectors and weighting. Fig. 5 demonstrates this property for for an array scanned in the principal plane $v = 0$. In this case the array element pattern, shown in Fig. 5(a), has zeros at $\sin \theta = \pm(p\lambda)/(d_x)$. Fig. 5(b) shows the array factor with a series of grating lobes in real space. Fig. 5(c) shows the combined pattern. The array is scanned off broadside, and because of the large interelement spacing d_x , there are numerous grating

lobes satisfying the inequality of (20). Careful element pattern selection can help to suppress grating lobes. For the particular case chosen all grating lobes would be suppressed for θ_0 broadside, because then all grating lobe peaks would be located at $p \lambda/d_x$, and would exactly correspond to the element pattern nulls. Grating lobe suppression through element pattern modification is a subject that will be treated in more detail in Section IV.

Grating lobe control can also be effected by the judicious selection of array lattices. The grating lobe positions indicated in Fig. 4(a) and (18) result from the selection of a rectangular grid of position vectors for the elements. That selection is not always optimum, and often there are advantages to choosing alternative grid shapes. Assume that the array is uniformly illuminated and that $\Delta_n = 0$. The normalized radiation pattern is then given by

$$\bar{E}_n(\vec{r}) = \bar{f}_x(u) \left\{ \frac{\sin \left[N_x \pi d_x \left(\frac{u}{\lambda} - \frac{u_0}{\lambda_0} \right) \right]}{N_x \sin \left[\pi d_x \left(\frac{u}{\lambda} - \frac{u_0}{\lambda_0} \right) \right]} \right\} \cdot \bar{f}_y(v) \left\{ \frac{\sin \left[N_y \pi d_y \left(\frac{v}{\lambda} - \frac{v_0}{\lambda_0} \right) \right]}{N_y \sin \left[\pi d_y \left(\frac{v}{\lambda} - \frac{v_0}{\lambda_0} \right) \right]} \right\} \quad (21)$$

It is obvious that the product of these two functions has principal maxima at each of the grating lobe positions of Fig. 4(a). The existence of grating lobes at these positions restricts the maximum scan angle for any given interelement spacing, or conversely, implies a maximum interelement spacing for a given scan volume. For example, one can show that for a large array the spacings must satisfy

$$\frac{d_x}{\lambda} < \frac{1}{u_0 + 1}; \frac{d_y}{\lambda} < \frac{1}{v_0 + 1}. \quad (22)$$

This criterion leads to the familiar condition that arrays scanning to endfire ($|u_0|$ or $|v_0| \rightarrow 1$) require spacings less than one-half wavelength.

The most common alternate choice of grating is called the triangular grid lattice, and consists of displacing every other row by $\Delta = dx/2$. This configuration introduces a different periodicity into the "v" plane, and the resulting function

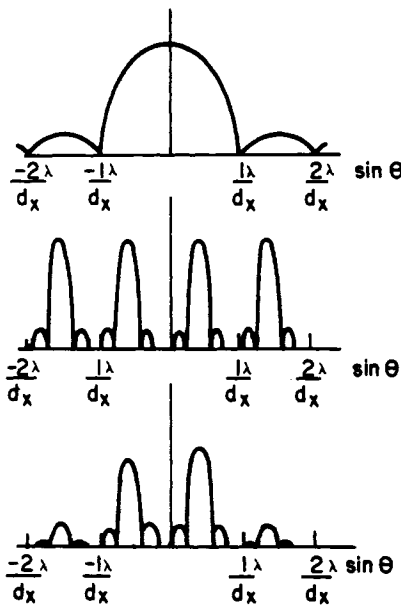


Fig. 5. Element pattern, array factor, and product.

$E_y(u, v)$ reduces to different expressions at the grating lobe positions $p = \pm 1, \pm 3$, and ± 5 vs the grating lobe positions $p = \pm 2, \pm 4$.

One obtains from (17) at the grating lobe positions $p = \pm 1, \pm 3, \pm 5$, and so on, the results (for N_y even)

$$E_y(u_p, v) = \frac{f_y(v)}{N_y} \frac{\sin [N_y \pi(v - v_0) dy/\lambda]}{\cos [\pi(v - v_0) dy/\lambda]} \quad (23)$$

This pattern has a zero at $v = v_0$, and an asymmetrical distribution in $(v - v_0)$ with principal maxima of unity at $[(v - v_0) dy/\lambda] = 0.5$. The grating lobes therefore are at $v = v_0 + (q + \frac{1}{2}) \lambda/dy$ as shown in Fig. 4(b).

At the grating lobes $p = 0, \pm 2, \pm 4, \dots$, the summation becomes

$$E_y(u_p, v) = \frac{f_y(v)}{N_y} \frac{\sin [N_y \pi(v - v_0) dy/\lambda]}{\sin [\pi(v - v_0) dy/\lambda]} \quad (24)$$

which again is the same distribution as for uniform illumination and $\Delta_n = 0$, and offers no grating lobe suppression.

The distribution chosen in the foregoing thus suppresses the odd grating lobes in one sector of space by splitting them each into two lobes and moving each out to a relatively wide angle, where they are reduced by the element pattern $e_y(v)$; the distribution does not alter the even grating lobes at all. This capability of selectively modifying a chosen grating lobe represents an additional degree of freedom that is useful in design, and in the triangular grid array it allows substantially wider interelement spacings and the use of fewer elements. For example, for a square grid array the maximum allowable area per element is $0.287 \lambda^2$, but for an equilateral triangular array the maximum area is $0.332 \lambda^2$ [6, p. 11-19].

It is possible to use more general, or even random row displacements Δ_n to suppress grating lobes in all but the plane of the main beam ($v = v_0$). One can demonstrate [26] however that such displacements alter peak grating lobe levels, but the average grating lobe power is independent of the Δ_n , and has an amplitude $1/N_y$ below the main beam (for unity element pattern). If the array had enough rows so that the grating lobe levels could be reduced everywhere to this average level (ex-

cept $v = v_0$) then the maximum available grating lobe suppression would be $1/N_y$, or about 9 dB for an eight row array, 12 dB for a 12 row array, and so on.

Radiation pattern distortion with scan angle is a well-known phenomenon, and is discussed by a number of authors including referenced works by Von Aulock [27] and others. In addition to lost gain, reduced resolution, and grating lobes, these authors describe beam coning effects that lead to substantial errors in array pointing accuracy.

Apart from these pattern shape characteristics of scanned arrays, there is also a severe bandwidth constraint imposed by scanning with phase shifters because the peak gain angle of a phase steered beam varies with frequency and does not occur at the established θ_0, ϕ_0 position except at $\lambda = \lambda_0$. For example, at center frequency the interelement phase shift ϕ_0 is given by

$$\phi_0 = k_0 d \sin \theta_0 \quad (25)$$

but the interelement phase required for this scan angle at some other frequency is

$$\phi = kd \sin \theta_0. \quad (26)$$

The net effect, beam pointing error referred to as beam squint, is that the beam scans away from the desired θ_0 . This is the most significant bandwidth limiting effect in array antennas.

Assuming an approximate half power beamwidth $(K_b \lambda s \theta)/L$ (note $K_b = 0.886$ for uniform illumination) one can solve for the array bandwidth under the assumption that the gain at each frequency limit is reduced to half power (that the squint is equal to a half beamwidth at each limit). The resulting fractional bandwidth is given by

$$\frac{\Delta f}{f_0} = \frac{\theta_3}{\sin \theta_0} \quad (27)$$

where θ_3 is the 3-dB beamwidth.

For small scan angles

$$\frac{\Delta f}{f_0} \sim \frac{1}{\eta_B} \quad (28)$$

where η_B is the number of beamwidths scanned.

3) *The Infinite Array:* Equation (1) gives the radiated field for any number of radiating elements in an array. Similar equations, given in Section II pertain to the array near field. Unfortunately the complex form of this expression makes it difficult to analyze arrays with large numbers of elements. In this case, for the purpose of calculating typical element patterns, it is customary to approximate the array structure by an infinite array because the majority of elements are far enough from the array edge so that their characteristics are similar to those of an element in an infinite array. Consider an array that has a rectangular grid lattice and is periodic in two dimensions. For an infinite array the summation in (1) can be transformed by the Poisson summation formula into a summation over wave modes as shown below

$$\begin{aligned} & \sum_{m=-\infty}^{\infty} \sum_{n=-\infty}^{\infty} \frac{e^{-jk\sqrt{(x-x'_m)^2+(y-y'_n)^2+z^2}} e^{-jk_0(u_0 m d_x + v_0 n d_y)}}{\sqrt{(x-x'_m)^2 + (y-y'_n)^2 + z^2}} \\ &= -j \frac{2\pi}{d_x d_y} \sum_p \sum_{q=-\infty}^{\infty} \frac{e^{-jk[u_p(x-x')+v_q(y-y')]-jk p q |z|}}{K_{pq}} \end{aligned} \quad (29)$$

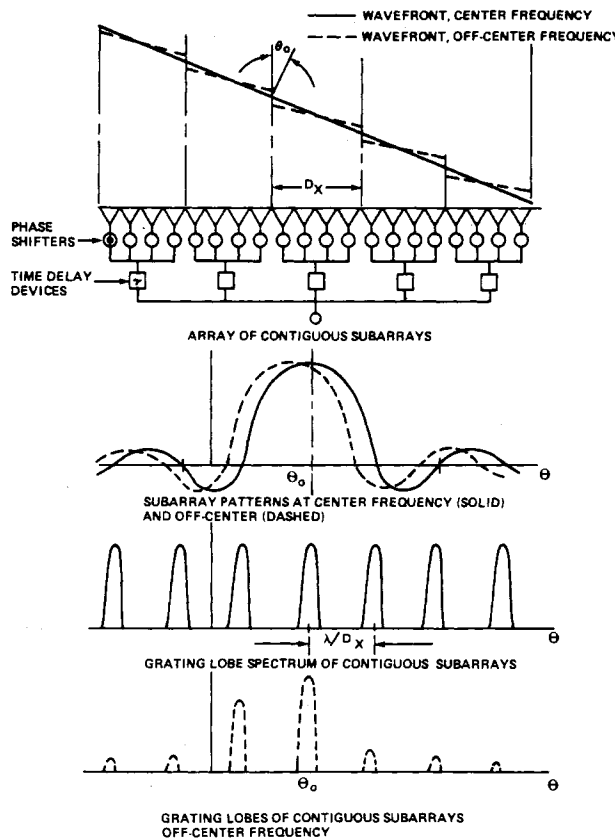


Fig. 6. Bandwidth properties of contiguous subarrays with time delay.

where

$$K_{pq} = k \sqrt{1 - u_p^2 - v_q^2}$$

and

$$x'_m = md_x + x', y'_n = nd_y + y'.$$

The u_p and v_q are the grating lobe locations as indicated in (18) and Fig. 4(a), and so this series is often referred to as the grating lobe series [28]. The expression illustrates some of the convenient properties of this most useful transformation, for the complicated square root function is replaced by much simpler exponential terms representing all the plane waves corresponding to points on the grating lobe lattice, some propagating and some evanescent. The propagating grating lobes, that is, those within the unit circle, are the only ones that represent true radiation and are used to compute far-field radiated power. For a linear infinite array one obtains

$$\sum_{m=-\infty}^{\infty} \frac{e^{-jk\sqrt{(x-x'_m)^2+y^2+z^2}}}{\sqrt{(x-x'_m)^2+y^2+z^2}} e^{-jk_0 u_0 m d_x} \\ = -\frac{j\pi}{d_x} \sum_{p=-\infty}^{\infty} e^{-jku_p(x-x')} H_0^{(2)} [K_p \sqrt{y^2 + z^2}] \quad (30)$$

where

$$K_p = k \sqrt{1 - u_p^2}. \quad (31)$$

The above expression also is an infinite set of waves and the coefficient for each wave is the Hankel function.

4) Subarrays for Wide-Band Operation: The bandwidth limitations implied by (27) are often reasonable for small

arrays, but are usually too restrictive for large arrays. For this reason it is common practice to combine phase and time delay steering by organizing the array into a relatively small number of subarrays and to use time delay devices at the subarray input ports and phase steering at all the array elements. The resulting array bandwidth is a compromise between the cost of providing time delay devices for a larger number of subarrays and the pattern deterioration and bandwidth limitations of dividing the array into too few subarrays.

The array of contiguous subarrays (Fig. 6) is conceptually simpler than other subarray approaches, and uses separate distribution networks to feed adjacent sections of the array. Phase shifters control the subarray pattern to produce a beam tilt and the time delay devices produce true time delay between the subarray centers.

To consider a specific example, assume a one-dimensional array of elements spaced d_x apart, with element pattern $f(u, v)$. The elements are grouped into subarrays of M elements. The entire array has \bar{N} equally spaced subarrays. Each of the subarrays has a subarray pattern that is the same as the bracketed term in (21), and when these subarrays are arrayed with time delay appropriate for beam collimation the complete field pattern is given by the expression

$$\bar{E}(\vec{r}) = \bar{f}(u, v) \cdot \left\{ \frac{\sin \left[M\pi d_x \left(\frac{u - u_0}{\lambda} - \frac{v}{\lambda_0} \right) \right]}{M \sin \left[\pi d_x \left(\frac{u - u_0}{\lambda} \right) \right]} \right. \\ \left. \cdot \left\{ \frac{\sin \left[\frac{\pi \lambda D_x}{\lambda} (u - u_0) \right]}{\bar{N} \sin \left[\frac{\pi D_x}{\lambda} (u - u_0) \right]} \right\} \right\} \quad (32)$$

where $D_x = Md_x$ is the subarray size.

This expression shows the total field as the product of element pattern, phase steered subarray pattern, and time delayed array factor. If the array were purely phase controlled, with $M \times \bar{N}$ elements each spaced d_x apart, its bandwidth given by (27) and (13) would be

$$BW = \frac{K_b \lambda_0}{M \bar{N} d_x \sin \theta_0 \cos \theta_0}. \quad (33)$$

In its present subarrayed form however, the time delayed array factor exactly collimates the subarray contributions at all frequencies, and the system gain bandwidth is essentially the same as the subarray bandwidth

$$BW = \frac{K_b \lambda_0}{Md_x \sin \theta_0 \cos \theta_0}. \quad (34)$$

For example, an array of 10 subarrays of 10 elements each has approximately 10 times the bandwidth of the phase steered array of 100 elements.

The above description emphasizes gain bandwidth, but, in fact, (32) shows that subarraying can introduce severe pattern degradation in the form of grating lobes that arise as frequency is changed. Fig. 6(b) illustrates that the subarray phase centers are appropriately delayed to form a beam at θ_0 , but each subarray has a phase squint that causes the peak of the subarray pattern to move off the position θ_0 . The result is the same as arraying very large elements. As shown schematically in Fig. 6(c) widely spaced subarrays have many grating lobes in

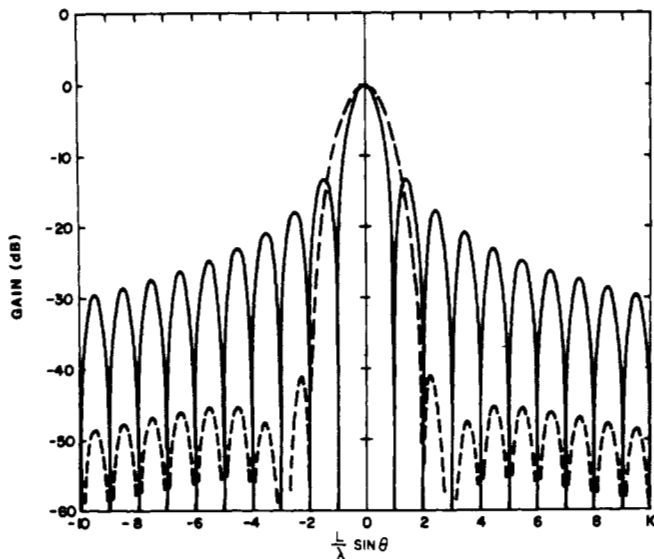


Fig. 7. Radiation patterns of uniform (solid) and cosine-squared-on-a-peDESTAL (dashed) illuminations.

real space. These are all suppressed by the subarray pattern zeros at $\lambda = \lambda_0$, but for other wavelengths the array grating lobes do not fall at the subarray pattern zero locations and in general constitute severe pattern deterioration.

One procedure for reducing these grating lobe peaks with contiguous subarrays is to make the subarrays of unequal sizes. This practice tends to reduce peak grating lobes by redistributing most of the energy into distributed sidelobe regions with lower peak levels but nearly the same average level.

Other techniques for producing wide-band subarrays and methods of grating lobe control will be discussed in later sections.

5) *Antenna Pattern Control:* There is no universally "best" antenna pattern. Instead it has been common practice to choose a pattern from one of a wide list of those already in the literature and to synthesize that pattern using directional coupler circuits in a constrained corporate feed circuit or to approximately synthesize it with a space fed array. The uniformly illuminated equiphase array has the highest gain except in the region of very close element spacing where a phenomenon called "super gain" can occur. The Dolph-Chebyshev [1], [29] weighting produces the narrowest beam for a given sidelobe level and is useful as a standard for comparison. Other illumination functions, such as the cosine squared on a pedestal and the Taylor [30], [31] illuminations offer advantages of simplicity in the selection of a power division network or appropriateness for large arrays. In addition to these analytic approaches to synthesis there have been a number of papers on synthesis by numerical methods. Examples of these procedures are the work of Strait and Hirasawa [32] and more recently of Elliott [33]. Array synthesis is described in a number of excellent references, among which are several texts [6], [12], [13]. Fig. 7 compares the radiation pattern of two well-known distribution functions and illustrates the tradeoff between beamwidth and sidelobe level. One of the important current topics in antenna theory is the use of array nulls to suppress interfering signals, notably jammers for the military application. Early work in this area dealt with pattern synthesis in idealized arrays but more recent efforts have included mutual coupling and realistic element patterns. The studies of Drane and McIlvenna [34] considered synthesis of optimal gain

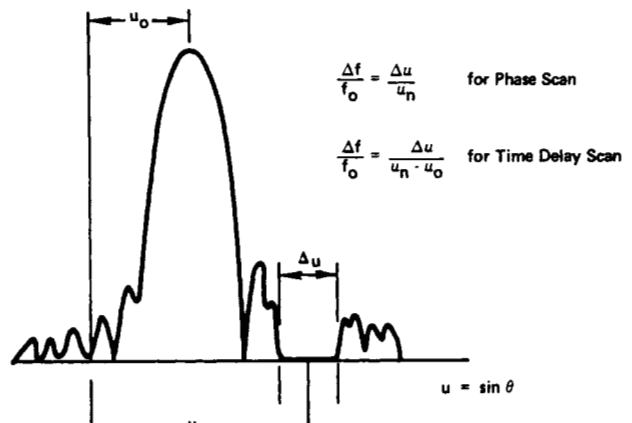


Fig. 8. Relations between bandwidth and angular null width.

patterns with constrained nulls with and without mutual coupling, and was based on expressing directivity as the ratio of quadratic forms, and solving this constrained maximization problem. The procedure for maximization has been used by a number of other authors [35]–[37] and is very lucidly described in the text [38] by Harrington.

Instead of using antenna synthesis to generate the complex weight for null forming there is a growing theory and technology of adaptive arrays that form these weights using analog circuits or digital processing. Most algorithms for array control are based on a number of pioneering studies by Applebaum [39], Howells [40], Widrow [41], and others, and are also implementations of the maximization of quadratic forms, but using the received signals at each port as parameters. Other procedures sense only a single array output signal and apply closed loop optimization procedures to suppress noise output or to optimize signal to noise.

Whether the weights are set adaptively or deterministically, there are fundamental limitations set by the array geometry. An N -element array can form only $N - 1$ nulls, and this is often referred to as the number of available degrees of freedom. In addition there are limitations to bandwidth and null depths, and research on these topics is of substantial current interest.

The following analysis will highlight some of these features. Consider a phase scanned antenna radiation pattern given by

$$S = \sum_{n=-(M-1/2)}^{M-1/2} A_n \exp \left[\left(j 2\pi n \frac{d_x}{\lambda_0} \left(\frac{\lambda_0}{\lambda} u - u_0 \right) \right) \right]. \quad (35)$$

Assume that the pattern has a notch in it and looks like the pattern of Fig. 8. At $\lambda = \lambda_0$ the notch location is defined by

$$u_l \leq u \leq u_h$$

and

$$\Delta u = u_h - u_l$$

is the width of the notch.

The feature of the wide notch is that it can provide a degree of wideband interference suppression, for one can show that if one could locate the notch around the interference so that for an interfering signal at u_n , at the highest interfering frequency

$$\left(\frac{\lambda_0}{\lambda} \right)_{\max} u_n = u_h$$

and at the lowest frequency

$$\left(\frac{\lambda_0}{\lambda}\right)_{\min} u_n = u_i$$

then one can show that the bandwidth over which good interference suppression will take place is given by

$$\frac{\Delta f}{f_0} = \frac{\Delta u}{u_n}. \quad (36)$$

Clearly one can increase the useful suppression bandwidth by creating a wide angular notched pattern.

For a time delay steered array one obtains (37) instead of (36)

$$\frac{\Delta f}{f_0} = \frac{\Delta u}{u_n - u_0} \quad (37)$$

which may or may not represent wider bandwidth suppression, depending upon how close the notched area is to the main beam direction.

These results lead to an approach to understanding wide-band array null steering through formation of wide notched patterns. Such patterns are usually formed by moving multiple nulls close together and this tends to use up the $N - 1$ degree of freedom very rapidly. An example of wide notch synthesis is the recent work of Gething *et al.* [42] and Tseng [43].

Equations (36) and (37) can also be used to estimate the bandwidth of simple nulls in antenna radiation patterns. For example, the array pattern of a uniformly illuminated aperture in one plane is

$$F(u) = \frac{\sin \left[M\pi \left(\frac{d_x}{\lambda_0} \right) \left(\frac{\lambda_0}{\lambda} u - u_0 \right) \right]}{M \sin \left[\frac{\pi d_x}{\lambda_0} \left(\frac{\lambda_0}{\lambda} u - u_0 \right) \right]} \quad (38)$$

a pattern which has multiple nulls and sidelobes. One can use (36) to estimate the bandwidth of one of these nulls at a level relative to the sidelobe level of adjacent sidelobes. Near any of these nulls, the normalized pattern amplitude is

$$F_n(u) = \sin \left[M\pi \left(\frac{d_x}{\lambda_0} \right) \delta u \right] \quad (39)$$

where $\delta u = u - u_0 - p\lambda_0/Md_x$, and is the distance from the center of the null in $u - u_0$ space.

The width of this null at a (power ratio) depth S below the local sidelobe level is computed from the above

$$\Delta u = \frac{2\sqrt{S}}{\pi L/\lambda_0} \quad (40)$$

where L is the length of the array.

Using (36) the bandwidth for a simple null is given by

$$\frac{\Delta f}{f_0} = \frac{2\sqrt{S}}{\left(\frac{\pi L}{\lambda_0} \right) u_n} \quad (41)$$

which is plotted in Fig. 9(a).

In this case the null is a simple zero in the pattern of a uniformly illuminated array, not a forced null as in an adaptive pattern. However, it is shown by Applebaum [38] that an adaptive system reacts to the presence of a single, monochromatic noise source by generating a canceller pattern with

the directivity of the array with its peak directed at the noise source. In this situation, if the adaptive array weights were fixed and noise bandwidth increased, the simple null bandwidth given above represents a worst case result. To obtain desired performance over a wider bandwidth without a tapped delay line network the adaptive array uses additional degrees of freedom to create a wide-band, wide angle null. Steyskal [44] has shown that for a least mean-square approximation to the desired, multiple nulled pattern the array uses its degrees of freedom to form sets of beams that act like sidelobe cancellers to produce nulls in the required directions at each required pattern null.

One can estimate the bandwidth of an array with broadened nulls as formed by multiple canceller patterns. In the most trivial case, we assume two canceller beams so close together that the quiescent pattern (the original pattern before adaptation) is nearly constant (note that this condition is unrealistic because the canceller beamwidths are on the order of the quiescent pattern sidelobe width). However, subject to this assumption the canceller pattern takes the form below, and is subtracted from the constant quiescent pattern

$$F_C = C \left[\frac{\sin \frac{M\pi d_x}{\lambda_0} (u - u_l)}{M \sin \frac{\pi d_x}{\lambda_0} (u - u_l)} + \frac{\sin \frac{M\pi d_x}{\lambda_0} (u - u_h)}{M \sin \frac{\pi d_x}{\lambda_0} (u - u_h)} \right] \quad (42)$$

with the constant C , chosen to produce the best pattern null.

After subtracting this pattern, the error, or the maximum pattern level between the two nulls, relative to the sidelobe envelope is found to be

$$\sqrt{S} = \frac{1}{48} \left(\frac{M\pi d_x}{\lambda_0} \right)^2 \Delta u^2 \quad (43)$$

and, by (36), the bandwidth for a given sidelobe level is

$$\frac{\Delta f}{f_0} = \frac{\Delta u}{u_n} = 2.2 \frac{\lambda_0}{L u_n} S^{1/4} \quad (44)$$

which is plotted in Fig. 9(b).

Thus the use of two degrees of freedom can cancel a quiescent pattern over a given area and so be commensurate with wide-band nulling. The use of more cancellers should broaden the nulled width and hence increase bandwidth. Extension of the above analysis can give some estimate as to the available nulled bandwidth and sidelobe level as a function of available degrees of freedom in this idealized case.

II. ARRAY ANALYSIS

A. Integral Equation Formulation of Array Radiation

The analysis of Section I gives the field of an array of radiators with known currents or aperture fields. Implicit in that formulation are three assumptions: that the current or fields are proportional to applied excitations; that the distribution of current or aperture field is the same for each radiator; and that the distribution does not change as the array is scanned. A primary challenge to modern array theory is that, in general, none of these statements are true. In a finite array all of the currents and fields differ from element to element in magnitude, phase, and distribution, and the forms of these distributions vary as a function of frequency and array scan angle. The radiated field can be written as generalized integrals that include current and charge distributions over the surface

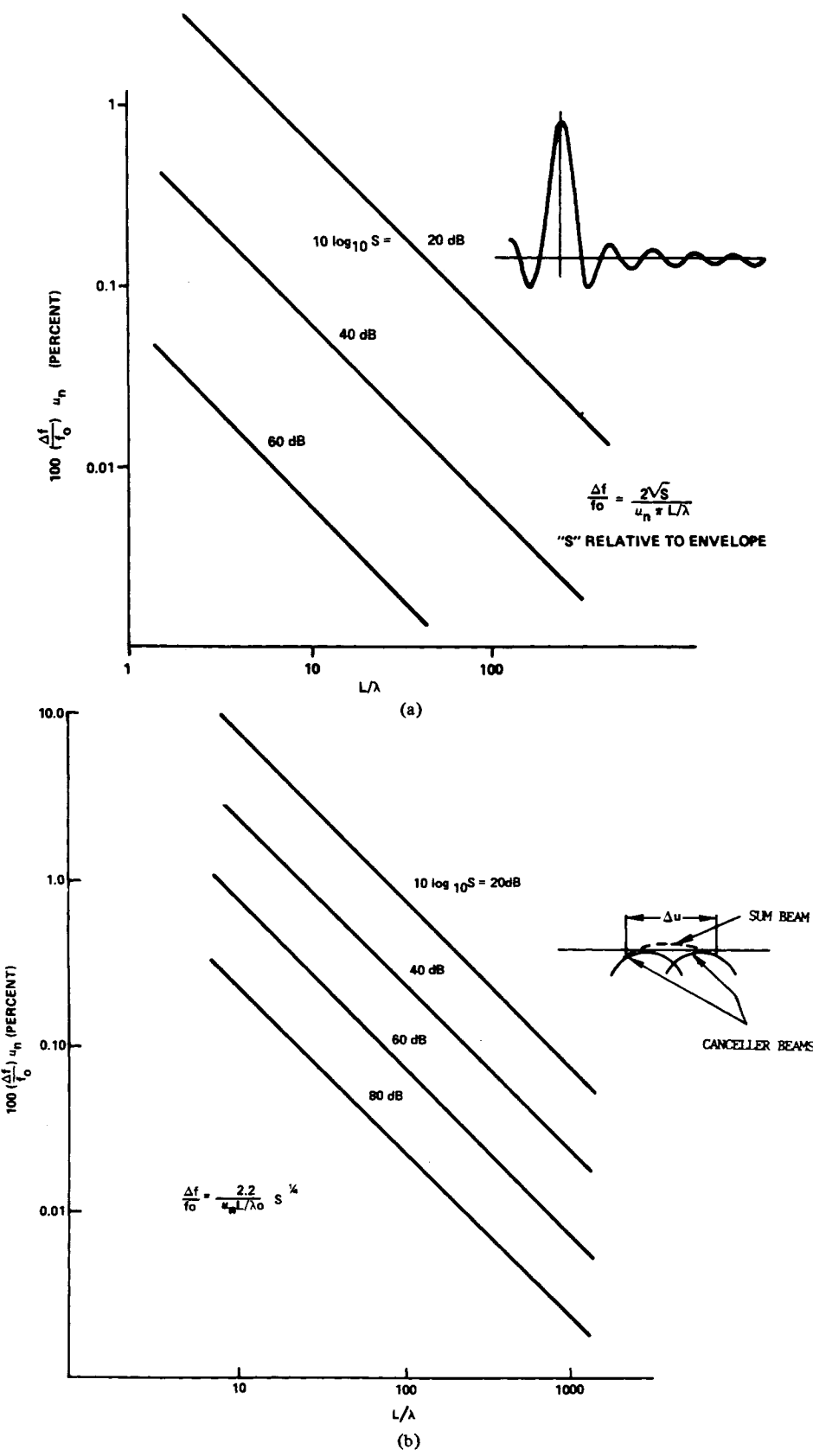


Fig. 9. (a) Bandwidth of single null (uniform illumination). (b) Bandwidth of nulled region formed by two degrees of freedom.

of the radiating antennas and nearby diffracting bodies. The same integral expressions can be used to require satisfaction of boundary conditions at each radiator and each diffracting

body, and so to evaluate the relevant currents and charges. This procedure usually results in a multiplicity of simultaneous integral or integrodifferential equations, and has not been

solved exactly except in the special case of infinite waveguide arrays in an infinite ground screen [45], [46].

The free-space electromagnetic field can be written using the dyadic Greens function notation of (45)

$$\begin{aligned} \bar{E} &= -j\omega\mu \int \bar{\Gamma}_0(\bar{r}, \bar{r}') \cdot \bar{J}(\bar{r}') dV' \\ &\quad - \int \nabla G(\bar{r}, \bar{r}') \times \bar{J}_m(\bar{r}') dV' \quad (45) \\ \bar{B} &= -j\omega\epsilon\mu \int \bar{\Gamma}_0(\bar{r}, \bar{r}') \cdot \bar{J}_m(\bar{r}') dV' \\ &\quad + \mu \int \nabla G(\bar{r}, \bar{r}') \times \bar{J}(\bar{r}') dV' \end{aligned}$$

where

$$G(\bar{r}, \bar{r}') = \frac{e^{-jk|\bar{r}-\bar{r}'|}}{4\pi|\bar{r}-\bar{r}'|}$$

and

$$\bar{\Gamma}_0(\bar{r}, \bar{r}') = \left(\bar{U} + \frac{1}{k^2} \nabla \nabla \right) G(\bar{r}, \bar{r}').$$

Here $G(\bar{r}, \bar{r}')$ is the free-space scalar Greens function and $\bar{\Gamma}_0(\bar{r}, \bar{r}')$ is the free-space dyadic Green function. The unit dyad \bar{U} is $(\hat{x}\hat{x} + \hat{y}\hat{y} + \hat{z}\hat{z})$ in rectangular coordinates. In this familiar form the integrals satisfy Maxwell's equations and are proper except within a region occupied by the source. The electric and magnetic currents \bar{J} and \bar{J}_m are in general unknown, and are evaluated by solving a set of integrodifferential equations.

When the sources are in the presence of an infinite perfectly conducting ground plane it is convenient to choose a combination of solutions of the above form to satisfy the boundary condition at the conducting plane. This has been done for the general case by Levine and Schwinger [47], but for most array problems the only magnetic current sources are the tangential electric fields in the ground plane at $z = 0$. In this case the fields in the half space $z > 0$ are given by

$$\begin{aligned} \bar{E} &= -j\omega\mu \int_V \bar{\Gamma}'(\bar{r}, \bar{r}') \cdot \bar{J}(\bar{r}') dV' \\ &\quad - 2 \int_S \nabla G(\bar{r}, \bar{r}') \times \bar{J}_m(\bar{r}') dS' \\ \bar{B} &= -2j\omega\epsilon\mu \int_S \bar{\Gamma}_0(\bar{r}, \bar{r}') \cdot \bar{J}_m(\bar{r}') dS' \\ &\quad + \mu \int [\nabla G(\bar{r}, \bar{r}') \times \bar{J}(\bar{r}') - \nabla G(\bar{r}, \bar{r}') \times (\bar{U} - 2\hat{z}\hat{z}) \cdot \bar{J}(\bar{r}')] dS' \quad (46) \end{aligned}$$

where

$$\bar{\Gamma}' = \bar{\Gamma}_0(\bar{r}, \bar{r}') - \bar{\Gamma}_0(\bar{r}, \bar{r}' - 2\hat{z}\hat{z} \cdot \bar{r}') \cdot (\bar{U} - 2\hat{z}\hat{z})$$

and

$$\bar{J}_m = -\hat{n} \times \bar{E}.$$

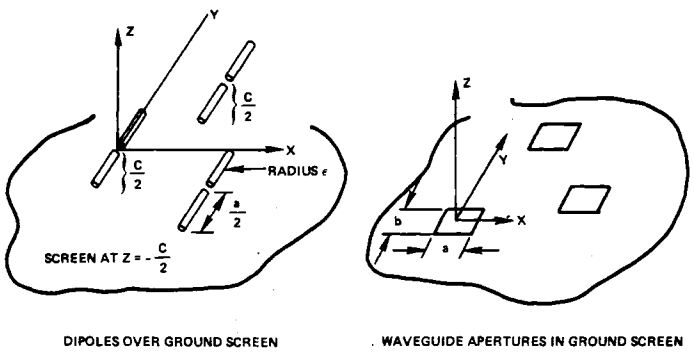


Fig. 10. Dipole and waveguide array geometries.

This form is of particular importance to the consideration of apertures in the conducting plane, for then the magnetic current contributions \bar{J}_m are surface integrals over the tangential electric field in the apertures, and the electric current contributions are readily recognized as corresponding to the electric sources in the region $z > 0$ and their images that appear to originate as sources in the half plane $z < 0$.

Often it is convenient to rewrite these equations using magnetic and electric potential functions (the electric potential is often called the vector potential). In this form they become

$$\begin{aligned} \bar{\pi}_m &= j \frac{2}{\omega} \sum_m \int_{S_m} (\hat{z} \times \bar{E}(r')) G(r, r') dS_m; \\ \bar{A} &= \mu \int \bar{J}(r') \cdot \bar{\mathcal{G}}(\bar{r}, \bar{r}') dV' \\ \bar{E} &= -j\omega\nabla \times \bar{\pi}_m - j \frac{\omega}{k^2} [\nabla(\nabla \cdot \bar{A}) + k^2 \bar{A}] \\ \bar{B} &= \nabla(\nabla \cdot \bar{\pi}_m) + k^2 \bar{\pi}_m + \nabla \times \bar{A} \quad (47) \end{aligned}$$

where

$$\bar{\mathcal{G}}(\bar{r}, \bar{r}') = [\bar{U}G(\bar{r}, \bar{r}') - (\bar{U} - 2\hat{z}\hat{z})G(\bar{r}, \bar{r}' - 2\hat{z}\hat{z})].$$

1) *Dipoles Over a Ground Plane:* The advantage of using potential functions is the convenience in recognizing scalar expansions. For example, the fields of an array of thin dipole antennas, shown in Fig. 10(a), with their axes along the y direction can be derived in terms of a single term of the vector potential $\bar{A} = \hat{y}Ay$. For thin dipoles, it has become accepted practice [48], [49] to write the current distributions as if the entire current were concentrated at the dipole axis, and so to reduce the volume integral to an integral in one dimension (along the y axis), and to use this approximation even at the dipole surface. In the case of a collection of dipoles located a distance $c/2$ above a ground plane and oriented as above, with half lengths $a/2$ and dipole radius ϵ , (47) gives the fields in the upper half space with

$$G(\bar{r}, \bar{r}') = \frac{1}{4\pi} \frac{e^{-jk\sqrt{(x-x_n')^2 + (y-y_n')^2 + (z-c/2)^2}}}{\sqrt{(x-x_n')^2 + (y-y_n')^2 + (z-c/2)^2}}. \quad (48)$$

If there are no apertures in the conducting ground plane, it is assumed that the \bar{J}_m are null, and the entire field is expanded in this single component vector potential. Treatment of dipole arrays implies the consideration of an assumed source distribution within the half-space. For thin dipoles this is usually

formulated as a delta function of electric field in the center of the dipole, resulting in an integrable potential difference across the infinitesimal source point of the dipole center ($y = 0$ for the n th dipole in the Fig. 10(a)). In this case one writes the equation for $E_y \equiv 0$ at the surface of the dipole, neglecting the boundary conditions on other E -fields, and neglecting any radial variation of field around the dipole because of the "thin" dipole approximation. The resulting integrodifferential equation is

$$E_y = V^n \delta(y) = -j \frac{\omega}{k^2} \left[\frac{\partial^2 A_y}{\partial y^2} + k^2 A_y \right] - h \leq y \leq h \quad (49)$$

where

$$A_y = \mu \sum_m \int_{V_m} I_m(y') \hat{y} \cdot \bar{\mathcal{G}}(r, r') dy' \quad (50)$$

for applied potential $V^n \delta_n(y)$; and Dirac delta function $\delta_n(y)$. At the n th dipole the above is integrated to obtain

$$\begin{aligned} A_y &= C_1^n \cos ky + C_2^n \sin ky + jk \frac{V^n}{\omega} \sin ky \quad 0 \leq y \leq h \\ &= C_3^n \cos ky + C_4^n \sin ky \quad -h \leq y \leq 0 \end{aligned} \quad (51)$$

where the term with V^n is obtained from the particular integral over the source, assumed to occupy the infinitesimal region $0 \leq y \leq \epsilon$. Evaluation of the discontinuity in the derivative of the potential function yields the relationship $C_2^n = C_4^n$.

The above is reduced to a matrix equation by expanding the current in a series

$$I_m(y') = \sum_{p=1}^P a_{p,m} i_p(y'). \quad (52)$$

Imposing (52) at $P+3$ points on each dipole allows the coefficients $a_{p,m}$, C_1^n , C_2^n , and C_3^n to be determined for each term in the current expansion.

Other authors have used alternative means of solving dipole equations. Harrington [38, ch. 4], for example, uses vector and scalar potential functions and not the integral equations used above. Moreover, the method of solution used above is just one means of solving the given equation. Another is to use a numerical procedure in which one expands $I(y)$ as a sum of suitably weighted values either constant or varying over small segments " Δ " of the element. For example, with constant values I_n defined over the dipole, one would write

$$I(y) = I_n(y); y_n - \Delta/2 < y < y_n + \Delta/2. \quad (53)$$

This approximation leads to a matrix equation that can be solved by a variety of procedures. Examples in the literature include the work of Harrington [49] and many others [50] for dipole antennas or other wire antenna configurations.

2) Waveguide Slot Arrays: Waveguide and slot array problems are also readily formulated using potential functions, but for waveguide radiators there are no actual electric current sources in the half space $z \geq 0$, and the only equivalent sources needed are the magnetic current sources as represented by the tangential aperture fields. In this case there is no single vector component that serves to completely represent the fields except for special two-dimensional cases. In general, however, for a finite waveguide aperture the solution is vector, and is formulated by expanding the aperture field in a set of functions and matching fields in the waveguides and free space.

For open-ended waveguides it is convenient to choose as basis functions the waveguide normal mode fields, and for unloaded rectangular waveguides one can choose the orthogonally polarized transverse electric fields. The transverse electric field for the waveguide at the origin of the coordinate system of Fig. 10(b) is

$$\bar{E}_T = \bar{e}_0(x, y) e^{-jk_z(0)z} + \sum_n V_n \bar{e}_n(x, y) e^{-jk_z(n)z} \quad (54)$$

where the $\bar{e}_n(x, y)$ are the transverse mode functions for the two possible polarizations, the $k_z(n)$ are the modal propagation constants and V_n are undetermined modal amplitude coefficients. This expression represents a single incident mode in the waveguide, and an infinite series of reflected modes. Typically all but the $k_z(0)$ propagation constants are imaginary, indicating that they are beyond waveguide cutoff, but they enter into the solution to match boundary conditions. The solution is obtained by expansion of the transverse magnetic waveguide fields in terms of these and writing the half space fields ($z > 0$) as the aperture field. Construction of the free-space Greens function assures that the tangential E field is continuous, and imposed continuity of the magnetic field components results in a vector integrodifferential equation using continuity of tangential magnetic fields at all the apertures.

$$\hat{z} \times \bar{B}(z = 0^-) = \hat{z} \times \bar{B}(z = 0^+)$$

$$= j2\omega\epsilon \hat{z} \times \sum \int_{S_p} \bar{\mathcal{F}}^0(r, r') \cdot (\hat{z} \times \bar{E}) dS'. \quad (55)$$

The magnetic fields for $z = 0$ can be obtained from (54) using waveguide modal admittances. Equation (55) can then be reduced to a matrix equation by following Galerkin's [37] procedure and solving for aperture fields. The details of this procedure will not be carried further, but are described in a number of available references [14], [18].

These two problems illustrate formulation of integral equations for the most fundamental array geometries. Similar analytical approaches are used for more complex geometries.

Tai [51] lists dyadic Green's functions for a number of other geometries, and it is possible to write field expressions for arrays of apertures in many of the basic geometric shapes such as spheres, infinite cylinders, and cones, and to obtain approximate field expressions for more general shapes using the Geometrical Theory of Diffraction. Some of these approximate techniques will be discussed in Section IV.

Finite array formulations become more difficult numerically as more elements are added to the array. One solution to this dilemma has been to study very large arrays using infinite array theory. This type of formulation is discussed in the next section.

B. Active Element Patterns and Mutual Coupling in an Infinite Array

Equations (29) and (30) in Section I-B3 are key to developing the theory of infinite arrays. Assuming periodic incident fields or applied sources such that for an infinite array of apertures with elements at $(x_m, y_n) = (md_x, nd_y)$ (rectangular grid)

$$a_{mn} = |a_{mn}| e^{-j(2\pi/\lambda_0)(u_0 md_x + v_0 nd_y)}. \quad (56)$$

Equation (47) can be converted by the Poisson Summation

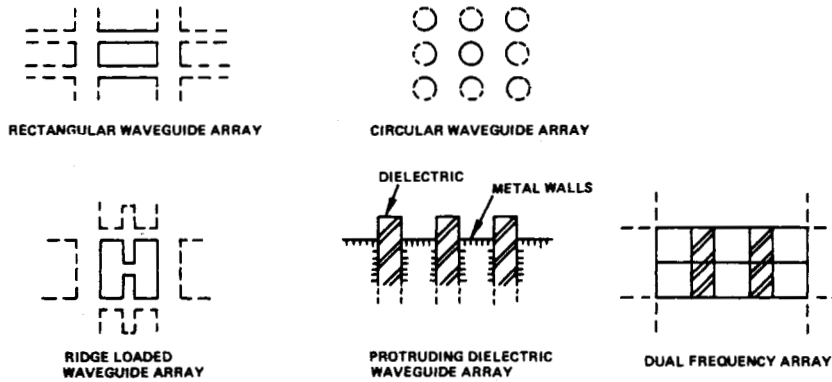


Fig. 11. Several configurations with existing infinite array solutions.

formula to the form given in (29), and written

$$\bar{\pi}_m(\bar{r}) = \frac{1}{\omega d_x d_y} \sum_{p=-\infty}^{\infty} \sum_{q=-\infty}^{\infty} \frac{e^{-jk(u_p x + v_q y) - jK_{pq}|z|}}{K_{pq}} \cdot \int_S dS' e^{jk(u_p x' + v_q y')} [\hat{z} \times \bar{E}(x', y')] \quad (57)$$

from which one can write \bar{E} and \bar{B} fields. In this circumstance the array boundary value problem is solved by assuring that all boundary conditions are satisfied throughout a single spatial period which is often called a unit cell.

An alternate method is to begin with the recognition of periodicity and expand the fields from periodic functions at the outset. This procedure is mathematically equivalent to the use of the Poisson Summation formula for periodic fields in a periodic lattice. A coherent exposition of the use of this approach is in the work of Oliner and Malech [52].

Infinite array theory offers direct insight into the concepts of active element patterns and grating lobes. For example, in a rectangular grid array with periodic excitation, the electric field can be written from (47) and (57) in terms of the tangential aperture field E_T as

$$\bar{E}(\bar{r}) = \frac{k}{d_x d_y} \sum_{p=-\infty}^{\infty} \sum_{q=-\infty}^{\infty} \frac{e^{-jk(u_p x + v_q y) - jK_{pq}|z|}}{K_{pq}} \cdot \bar{f}_{pq}(\theta, \phi) \quad (58)$$

where

$$\bar{f}_{pq}(\theta, \phi) = \int_S dS' e^{jk(u_p x' + v_q y')} \cdot [\cos \theta_{pq} \bar{E}_T(x', y') - \hat{z} \hat{\rho}_{pq} \cdot \bar{E}_T(x', y')] \quad (59)$$

and

$$\hat{\rho}_{pq} = \hat{x} u_p + \hat{y} v_q + \hat{z} \cos \theta_{pq}.$$

In this expression the element pattern $\bar{f}(\theta, \phi)$ is vector, and is common to all elements of the array. The exponential term $\exp(-jK_{pq}|z|)$ represents a traveling wave only for grating lobes within the unit circle as indicated in Section I-B3. Thus, in the region far from the array (z large), only one term of the series exists in the absence of grating lobes. The pattern $f(\theta, \phi)$ is sampled at those points (u_p, v_q) corresponding to the grating lobe lattice and the infinite array radiates only in

those distinct directions. The element pattern includes mutual coupling between all the elements of the array because the tangential component $\bar{E}_T(x', y')$ is evaluated by the solution of a boundary value problem like that of Section II-B.

Radiated power from the infinite array is evaluated by integrating the dot product of the Poynting vector across a unit cell. By conservation of energy it is simply shown that the normalized power radiated from an infinite array is given by $[(1 - |\Gamma|^2) \cos \theta_{00}]$ when no grating lobe radiates, and so the field pattern of (58) also defines the amplitude of the array reflection coefficient. It is accepted practice to measure the element pattern in an array and infer the reflection coefficient from this data. The normalized element pattern of (58), evaluated at the peak of the main beam is thus $[(1 - |\Gamma|^2)(\cos \theta_{00})]^{1/2}$ for the driven infinite array without grating lobes, and it would also be the measured pattern resulting from exciting one element of a very large array.

Rigorous infinite array solutions have been obtained for a large number of array types. Fig. 11 shows a few of the basic array configurations for which infinite array solutions are published. Included in the figure are flush mounted arrays of rectangular [53] and circular [54] elements, ridge loaded elements [55]–[57], protruding dielectric (TEM solution) [58], and a dual frequency dielectric loaded configuration [59]. Among other published solutions are numerous interlaced multiple frequency configurations [60], examples of dielectric loading [61], iris loading [62], and fence [63] or corrugated plate [64] loadings for impedance match, as well as several very wide-band configurations for waveguide [65] and stripline [66]. In addition there have been a number of infinite dipole array solutions published [67]–[69].

Among the more important phenomena uncovered through infinite array theory is the description of the so-called blindness phenomenon. This behavior was described in great detail in the tutorial review paper by Stark [1], and so will not be treated here. Fig. 12 shows the basic phenomenon as discovered by Farrell and Kuhn [45], [46] in the first published analytical work on the subject. This figure shows a measured deep null in an element pattern and compares the data with results computed using a single mode grating lobe series and a full modal array solution. The null is due to the cumulative effects of a mutual coupling and can be related to surface wave type behavior at the array face [25], [69]. In many cases the existence of the null is understood as a cancellation process involving waveguide higher order modes, and this is why the single mode grating lobe solution bears no correlation to the

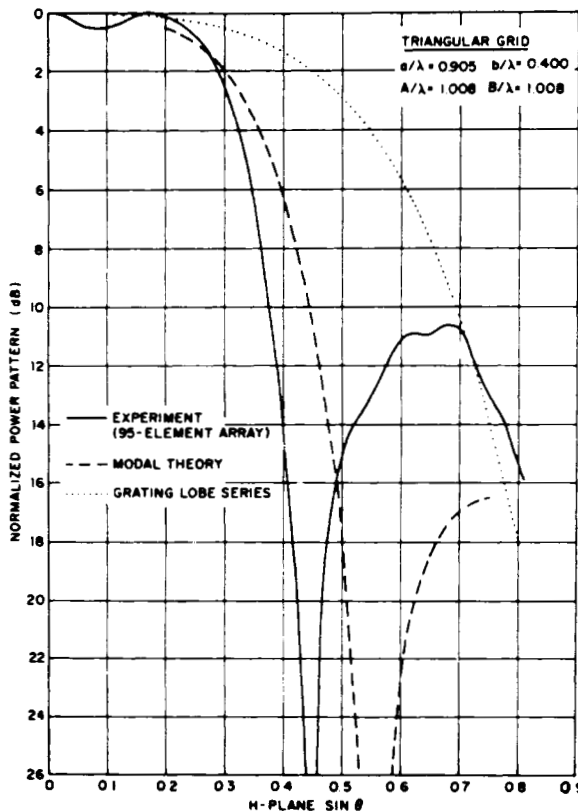


Fig. 12. Array element power pattern showing array blindness (after Farrell and Kuhn [46]).

data in Fig. 12. In the years since this initial discovery these blindspots have been found in most waveguide array configurations and in some dipole and strip-line arrays [70]. In many cases the problem can be reduced or eliminated by keeping the element lattice dimensions d_x and d_y small enough so that grating lobes are well beyond the maximum scan angle throughout the operating frequency range [69].

Blindspots reported in dipole arrays seem to be related to the presence of dipole supports. Analytical studies of infinite dipole arrays [67] without supports do not exhibit array blindness. A forthcoming publication by Mayer and Hessel [71] analyzes a strip line dipole structure and shows that for practical spacings the balanced stripline dipole feed structure supports a propagating TM mode in addition to two TEM modes. The TM mode propagation constant is scan dependent and for certain parameter selections it occurs before the onset of the grating lobe. It is conjectured that this mode might be the cause of blindness in dipole arrays.

C. The Element Pattern in a Finite Array of Apertures

The subject matter of this paper is more closely allied to moderate size than very large arrays, and although an infinite array has a unique element pattern, in a finite array the active element pattern is different for each element. This fact does not reduce the utility of the concept however, because the element pattern is a useful bridge between theory and measurements. For a finite array of apertures one can obtain a far-field expression directly from (74) using

$$|\bar{r} - \bar{r}'| \approx R_0 - \bar{r}' \cdot \hat{\rho} \quad (59)$$

where R_0 is measured from the coordinate origin in the aper-

ture to the given point in space at R_0, θ, ϕ and

$$\begin{aligned} \bar{r}' &= \hat{x}x' + \hat{y}y' \\ \hat{\rho} &= \hat{x}u + \hat{y}v + \hat{z} \cos \theta. \end{aligned} \quad (60)$$

The Green's function of (45) can then be written in the form

$$G(\bar{r}, \bar{r}') \approx \frac{e^{-jkR_0} e^{jk(\bar{r}' \cdot \hat{\rho})}}{4\pi R_0}. \quad (61)$$

Evaluation of (47) for apertures in the plane $z = 0$, but otherwise arbitrarily located yields [14]

$$\begin{aligned} \bar{E}(\bar{r}) = \frac{jk}{2\pi} \frac{e^{-jkR_0}}{R_0} \sum_m \int_{S_m} dS'_m [\cos \theta \bar{E}_T(x'_m, y'_m) \\ - \hat{z} \hat{\rho} \cdot \bar{E}_T(x'_m, y'_m)] e^{jk\bar{r}' \cdot \hat{\rho}} \end{aligned} \quad (62)$$

where \bar{E}_T is the tangential field in each aperture, as obtained from the solution of a set of integral equations as described in Section II-A. One can express the E -field in terms of a scattering matrix including a term proportional to the incident field (incident and orthogonal polarization) and all induced contributions from other elements. For an array of waveguide elements, and for simplicity neglecting cross-polarized and higher mode components, the total field of the m th waveguide can be written using the scattering matrix of the array junctions using the expression below

$$\bar{E}_T = \left(a_m + \sum_{n=1}^M S_{mn} a_n \right) \hat{y} e_{10}(x', y') \quad (63)$$

where the a_n is the incident field in each n th aperture, and S_{mn} is the conventional scattering matrix. Then

$$\begin{aligned} \bar{E}(\bar{r}) = \frac{jk}{2\pi} \frac{e^{-jkR_0}}{R_0} [\hat{y} \cos \theta - \hat{z} v] c_0 \\ \cdot \sum_{m=1}^M g(m) \left(a_m + \sum_{n=1}^M S_{mn} a_n \right) \end{aligned} \quad (64)$$

where

$$g(m) = e^{jk\bar{r}'_m \cdot \hat{\rho}}$$

and

$$c_0 = \int_{S_m} e_{10}(x', y') e^{+jk(ux' + vy')} dS'_m.$$

This expression can be written

$$\begin{aligned} \bar{E}(\bar{r}) = \frac{jk}{2\pi} \frac{e^{-jkR_0}}{R_0} [\hat{y} \cos \theta - \hat{z} v] c_0 \\ \cdot \sum_{m=1}^M a_m g_m \left[1 + \sum_{n=1}^M S_{nm} \frac{g_n}{g_m} \right] \\ = \frac{jk}{2\pi} \frac{e^{-jkR_0}}{R_0} c_0 \sum_{m=1}^M a_m g_m \bar{f}_m(\theta, \phi). \end{aligned} \quad (65)$$

For simplicity, this derivation was carried out for linearly polarized single mode radiators, but the result can be generalized to any array and reveals what is implied by the concept of element patterns in a finite array. The expression shows the far field written as the sum of element excitation coefficients

a_m multiplied by the time delay factor g_m and an element pattern $\tilde{f}_m(\theta, \phi)$ which is now different for each element. The element pattern includes mutual coupling from other elements, which all radiate from different phase centers, hence the term g_n/g_m , multiplying the scattering coefficient $S_{n,m}$. Since some of the mutually coupled terms can have phase centers which may be quite far from any given element (m), the mutually coupled terms can produce very angle sensitive changes to the element patterns resulting in rippled [15] and distorted patterns that have strong frequency dependence. This effect is discussed in Section IV for cylindrical arrays.

Apart from these insights into element pattern distortion, (65) reveals that array element patterns are measured just as is a scattering matrix—by loading all elements but the driven one and measuring the radiated element pattern. This procedure is one of the most useful diagnostics in array practice, and illustrates the importance of element patterns in finite array technology.

D. Scanning from Broadside to Endfire with a Planar Array

Among the requirements stimulating advanced phased array developments is the need for obtaining extremely wide angle and even hemispheric coverage from a single array antenna. This capability is important for a number of applications, including ground-based radars but it is nowhere more important than for airborne arrays for satellite communication.

Aircraft Satcom systems often require coverage from the zenith to the horizon, usually with circular polarization. The obvious advantage of a hemispherically scanned array for this application is that a single array could perform the whole communication function that would require a multiplicity of arrays scanning over normal ($\pm 60^\circ$) limits.

In an infinite two-dimensional array the pattern directivity for a perfectly matched aperture varies as $\cos \theta$. If the array mismatch is not corrected as a function of scan angle the gain will be further reduced according to the expression

$$[1 - |\Gamma|^2] \cos \theta. \quad (66)$$

Because of the cosine factor, the infinite two-dimensional array has zero gain at the horizon.

Column arrays of omnidirectional elements scanned in the direction of the column's axis have no decrease in directivity with scan angle as mentioned in Section I-D2, but in practice both two-dimensional and linear array scanning performance are dominated by mutual coupling, or equivalently, by the inability to achieve broad element patterns in an array.

For finite arrays the beamwidth in the plane of scan varies much like $\sec \theta$ except near endfire. At the horizon the elevation beamwidth of a column of two dimensional arrays in free space is given approximately by Walter [10] and Elliott [25]

$$\delta = \sqrt{\frac{4\pi}{C} \left(\frac{\lambda}{L_1} \right)} \quad (67)$$

where L_1 is the length of the array in the endfire direction and C is a constant which varies between 3.5 and 7 depending upon phase velocity and the array distribution. Assuming an azimuthal beamwidth of approximately λ/L_2 , where L_2 is the array dimension perpendicular to the plane of scan, the directive gain at endfire is

$$D \approx \sqrt{4\pi C} \left(\frac{L_2}{\lambda} \right) \sqrt{\frac{L_1}{\lambda}}. \quad (68)$$

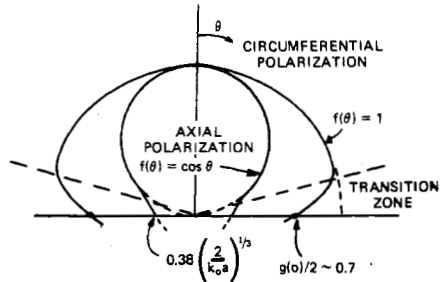


Fig. 13. Roll plane patterns of circumferentially and axially polarized slots on a cylinder of radius "a."

This result is consistent with that obtained by Elliott [25] if the factor $C = 3.546$ is used. The directivity is multiplied by 4 for the array over a perfect ground plane (and the beamwidth of (67) is halved).

The ratio of directive gain at endfire to directive gain at broadside (with perfectly conducting ground) is

$$\frac{D}{D_0} = \sqrt{\frac{C}{\pi}} \sqrt{\frac{\lambda}{L_1}}. \quad (69)$$

This equation shows that for any given broadside directive gain (D_0) it is most advantageous to decrease L_1 (the array projection in the endfire direction) as much as possible, for this minimizes the scan loss. It also indicates that larger arrays suffer increased scan loss. For example, a square array with 20 dB gain at broadside should exhibit a directivity degradation of 1 dB at endfire, but for a 30 dB square array, 4.5 dB falloff is expected.

Unfortunately this decrease in directivity is only one of the factors tending to make scanning to endfire inefficient. Other major factors are diffraction and scattering due to the vehicle on which the array is mounted, element pattern narrowing and array mismatch due to mutual coupling.

Fig. 13 shows the geometry of a cylinder which is taken as having a constant radius "a." For simplicity, consider radiation only in the $x-y$ plane (perpendicular to the cylinder axis). For a large cylinder one can disregard edge effects in the array so that each element pattern is approximately the same, and compute the radiation pattern as the product of the array factor and element pattern.

Pathak and Kouyoumjian [72] give a convenient expression for the fields of infinitesimal aperture mounted on generalized perfectly conducting structures using the geometrical theory of diffraction. The application of this result to an aperture mounted on the top of a perfectly conducting cylinder is described in [73]. Using the results one can express the radiation pattern of elementary slots or arrays on cylinders in terms of the radiation into three distinct regions depending upon whether the point of observation is in the upper hemisphere (called the illuminated region), the lower hemisphere (called the shadow region), or in the vicinity of the horizon (called the transition region). The angular extent of the transition region is of the order of $(k_0 a)^{-1/3}$ on each side of the shadow boundary for a cylinder of radius "a." Fig. 13 illustrates that within the illuminated region the axially polarized radiation for an infinitesimal element has a $\cos \theta$ element pattern. Moreover, within the important transition region these patterns are modified so that the circumferentially polarized component does not remain constant, but drops to a value of about 0.7 in field strength, or -3.2 dB as compared with its value at the zenith, while for axial polarization the horizon radiation is not

zero, but approximately

$$0.38 \left(\frac{2}{k_0 a} \right)^{1/3} \quad (70)$$

Thus, for a thin slot with circumferential polarization the horizon gain is independent of the size of the cylinder, but for an axially polarized slot the horizon gain varies directly as a function of $(k_0 a)^{-1/3}$. For cylinders of radius "a" approaching 50λ , the horizon field is thus approximately 23 dB below zenith gain.

These results are important to aircraft antenna design for Satcom communication because such systems emphasize high gain coverage very close to the horizon. The above pattern levels indicate 3.2 dB loss for the circumferential polarization, but so much more loss for axial polarization that for an aircraft with a fuselage radius of many wavelengths there is virtually no hope of substantial horizon gain in that polarization. Since most satellites are circularly polarized this means for a circularly polarized array that the one way gain to a satellite is reduced by approximately 9.2 dB even before considering array effects.

The remaining factor tending to reduce enfire gain is array mutual coupling. This important phenomenon will be discussed in Section IV in connection with several specific examples of conformal arrays.

III. PRACTICAL PHASED ARRAYS

The discussion of scanning behavior in the previous section was intended to outline the more important phenomena that occur in all types of arrays. The need to avoid array resonances (or blindness), and to perform detailed tradeoffs of scanned impedance matching are among the most important considerations facing the array designer.

Many other subtle phenomena influence array design and ultimate performance. Practical arrays may be conformal to an aircraft or missile or mounted above the earth but in general they are never free from significant interaction with some external structure. Small arrays may have each element pattern substantially different because of mutual coupling and edge effects. Another factor setting a bound on ultimate performance is the amplitude and phase accuracy of the network exciting the array. This topic is considered in Section III-A. Many other considerations influence the designer's choice of elements and feed network, and often play a dominant role in making the final selection. Among these are the need to reduce array weight, cost, or size, to make the array conformal to some surface, or to obtain very precise or variable pattern control. Such considerations result in a continual increase in the variety of array elements, feed designs and phasing devices, and often lead the designer to select a technology whose behavior is not well established or predictable. This section outlines some of the choices available to array designers and the factors influencing selection of a specific geometry.

A. Array Errors and Phase Quantization

The ability of an array to create a desired antenna pattern in space is limited by diffraction effects resulting from finite antenna size, by the fact that the array can only approximate a continuous current or aperture distribution by a discrete function, and by random or correlated errors in the array illumination. Random errors in antennas have been treated by a number of authors, and some of the results are quoted here in order to follow their implication in selection of phase con-

trols and power distribution networks. Element pattern ripple also contributes to phase and amplitude errors in an array but the extent to which that error can be treated as random may depend upon the particulars of the configuration.

In an array with random phase and amplitude errors, and including randomly failed elements, the average sidelobe level (power) far from the beam peak is given by [13], [15]

$$\sigma^2 = \frac{\epsilon^2}{P_e N \eta} = \frac{[(1 - P_e) + \bar{\Delta}^2 + P_e \bar{\delta}^2]}{P_e N \eta} \quad (71)$$

where

$\bar{\Delta}^2$ amplitude error variance normalized to unity

$\bar{\delta}^2$ phase error variance

P_e probability of survival for any element in the array

η array efficiency

N total number of elements.

This equation gives the normalized sidelobe level relative to the average array gain. The failed elements in the array are assumed to be randomly located, and the average value of the phase and amplitude errors is assumed to be zero. The sidelobe level above should be considered the average of a number of antenna patterns, not the average level of any one antenna.

The reduction in directivity due to these errors is given by

$$\frac{D}{D_0} = \frac{P_e}{1 + \bar{\Delta}^2 + \bar{\delta}^2}. \quad (72)$$

Peak sidelobe levels are also given in the literature. A convenient result is obtained when the errors are sufficiently large compared to sidelobes or null depths that structured minor lobe radiation is negligible and the statistics of the field intensity pattern are described by a Rayleigh density function. In this case the probability that a particular sidelobe level v_0 is exceeded at any point is [13]

$$\text{Prob}(v > v_0) = \exp \left[\frac{-v_0^2}{\sigma^2} \right] \quad (73)$$

where σ^2 is the average sidelobe level of (71).

Starting with the expression above, valid at a particular point, Allen [15] derives the following rule of thumb for the error ϵ^2 allowable for an array with gain G , far sidelobe level $1/R$ and using element lattice areas 0.5λ on a side

$$\epsilon^2 \leq \frac{1}{10 \pi} \frac{G}{R} \quad (74)$$

which results in an allowable phase error of about 10° when the sidelobe level is numerically equal to the gain, and assuming 99 percent probability that all sidelobes lie below the value $(1/R)$.

This important relationship explains why it is fairly easy to design arrays with sidelobes at the isotropic level, but to maintain sidelobes of 20 dB below the isotropic level would require 1° phase error, an extremely difficult goal and one barely within the present state of the art.

A digitally controlled "p" bit phase shifter has 2^p phase states separated by phase steps of $2\pi/(2^p)$. Miller [74] has analyzed the resulting peak and rms sidelobe levels for this staircase approximation to the desired linear phase progression and has shown the loss in array gain due to the triangular error distribution [dS]

$$\Delta G = \frac{1}{3} \frac{\pi^2}{2^{2p}} \quad (75)$$

which is on the order of 0.23 for a three-bit phase shifter and 0.06 for a four-bit phase shifter. More significant are the average sidelobe levels which, based upon an average array loss of 2 dB to account for illumination taper and scan degradation are:

$$\text{rms Sidelobes} \approx \frac{5}{(2^p N)} \quad (76)$$

where N is the number of elements in the array. For a one dimensionally scanned array N is the number of phase controls, and the rms sidelobe level above is measured in the plane of scan. The net result is to require extreme precision for unidimensional scanned arrays. References [6] and [74] give curves showing this sidelobe level for various phase shifter bits "p" and N up to 10 000 elements. For -50 dB rms sidelobes an array of 1000 elements requires five-bit phase shifters, but an array of 10 000 elements can maintain 50 dB sidelobes with only three-phase bits.

Of greater significance to antenna design is that the phase errors have a periodic variation across the array and tend to collimate as individual sidelobes, called phase quantization sidelobes, which are much larger than the rms levels. A detailed discussion of this phenomenon is given in [6, pp. 14-42], along with simple formulas for evaluating the resulting lobes. A perfectly triangular quantization error causes a quantization lobe level of $1/2^p$, which gives -30 dB for five-bit phase shifters. Ref. [6] shows that for discrete phase shifters the error is not triangular, and Brown [75] shows that the maximum quantization lobe can be substantially larger.

One solution to the peak quantization lobe problem as suggested by Miller and in a more recent paper by Buck [76] is to decorrelate the phase shifter errors. Decorrelation occurs naturally in space fed arrays, where the phase shifters collimate the beam as well as steer it. In such arrays the phase error is distorted from the triangular shape and the quantization lobe is substantially reduced.

Alternatively, in an array with in-phase power division one can introduce a phase error into each path and then program the phase shifter to remove the error in addition to steering the beam. Optimizing this error can reduce the peak sidelobes very close to the rms sidelobe level, but this consideration must be carefully accounted for in the array design.

An entirely different solution to the quantization lobe problem is often achieved at the system level by recycling all the phase shifters between consecutive radar pulses or between transmit and receive. This process, called beam dithering [7], consists of adding a fixed phase shift to the phase command and re-computing phase shifts. The net result is to change all the phase states so that the quantization is made differently for each pulse (or between transmit and receive). If this procedure is compatible with other radar processing, one can use simple row-column steering but introduce randomness into the quantization steps to reduce the peak quantization lobes.

B. Array Elements

Array elements usually fall into one of the categories described in Section II-B. They are some form of dipole or slot, whether excited by a waveguide or transmission line. Waveguide arrays, though heavy, tend to have low loss, good bandwidth and relatively graceful scan degradation. They also have been the subject of numerous design studies, and so their behavior is well documented and predictable. Examples of specific waveguide element design are the studies of Wheeler [77], [78], wherein matching networks were derived using

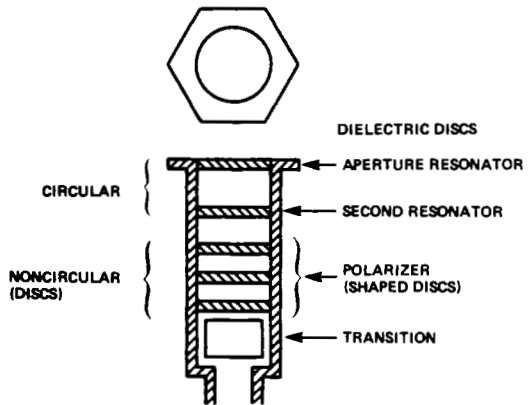


Fig. 14. Circular element for triangular grid array (after Wheeler [78]).

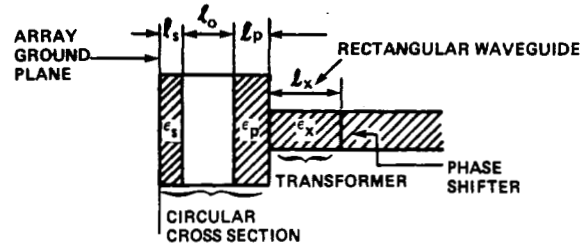


Fig. 15. Doubly tuned waveguide array element (after Lewis *et al.* [79]).

waveguide transmission circuits like that shown in Fig. 14 consisting of dielectric slabs mounted in and above the waveguide. The later studies of McGill and Wheeler [79] introduced the use of a dielectric sheet, often called a WAIM (wide angle impedance matching) sheet to produce a susceptance variation with scan angle that partially cancels the scan mismatch of the array face. These early studies were based upon the grating lobe series approximation (and assumed only a single waveguide mode) and so did not properly account for array blindness effects, but were nevertheless very useful for design optimization. Another significant influence in waveguide array design was the work of Knittel [69], described in more detail in Section II, who showed that at any operating frequency one could always reduce the interelement spacing to avoid a blindness condition. This does not mean that all waveguide elements can be made to scan equally well by reducing spacing, for in fact certain structures are much more subject to nulling problems, and so incur severe mismatch problems at much smaller scan angles than others at any given spacing. Examples of this are structures with external loading, heavy dielectric loading or baffles or protruding dielectric elements. In addition to WAIM dielectric sheets, the work of Lee and Jones [62] showed that waveguide irises can also be used to produce good scan match over very wide angles and can even eliminate an array blindness that was present in the unloaded waveguide array. By far the most common practice to date has been to use relatively standard waveguide elements, and to devote a substantial effort to frequency and scan matching the elements using conventional microwave networks within the waveguides. There are numerous computer codes for evaluating scan variation of these basic elements, and indeed some for simplifying the scan matching.

One significant recent development in impedance matching of waveguide arrays is the synthesis of double tuned response characteristics achieved using dielectric loading and a cutoff waveguide section. Fig. 15 shows a cross section of the

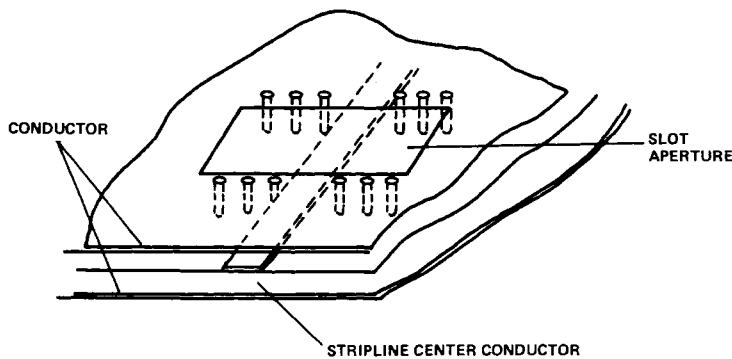


Fig. 16. Stripline slot radiator.

geometry synthesized by this procedure [80] including a loaded rectangular waveguide (phase shifter), a transformer to circular guide, two dielectric disks, and an unloaded section of guide that is below cutoff [81] at the operating frequencies.

Dipole arrays have also received substantial attention, and have generally graceful scan properties when properly designed. The survey article by Stark [82] summarizes much of the early data on dipole arrays including studies at Lincoln Laboratory of a 10×10 array of slot-fed dipoles and the development of several thicker dipole elements.

Apart from coaxially fed dipole arrays and open-ended waveguide arrays, there are a number of other elements, each designed to suit some special application. Among these is a large class of stripline and microstrip radiating elements. Stripline elements can be developed with bandwidth up to an octave, and can be combined with precision circuitry for low sidelobe pattern control. Microstrip elements have far less bandwidth, but with low-cost, lightweight designs can have good pattern characteristics. A recent report by Hall and James [83] describes a variety of low profile array elements. Fig. 16 shows one means of exciting flush mounted stripline slot antennas. Often these elements are isolated from the rest of the stripline medium by plated-through holes or rivets that form a cavity as shown in the figure, and which serve to suppress higher order modes.

Fig. 17(a) shows one common type of stripline printed dipole. This design, due to Wilkinson [84], uses a metallization on two sides of a microstrip line to produce a complete dipole fed by a two-wire line in the plane of the dipoles. This dipole and printed circuit distribution network is fabricated by two photographic exposures using a two-sided printed circuit board, and so is an example of low cost technology. The array was mounted a quarter wavelength above a ground plane and uniformly illuminated by a reactive power divider to form a pencil beam.

Another convenient circuit for dipole design, shown in Fig. 17(b), is described in a report by Hanley and Perini [85] and is a printed stripline folded dipole with a Schiffman balun. One major advantage of this element is that it is printed in a single process, all on one side of a circuit board and is relatively inexpensive to produce.

Several very broad-band elements have been described in the literature. Among these, the broadest band is the flared notch antenna (Fig. 18) studied by Lewis *et al.* [58] which exhibits up to octave band when used in an array, but needs careful design for any given array configuration because of the possibility of array blindness effects for critical frequencies and scan angles.

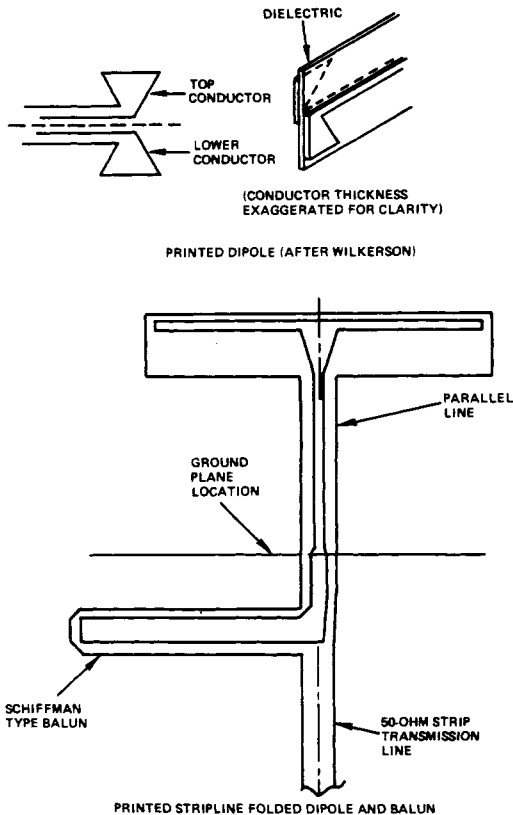


Fig. 17. Printed circuit dipole configurations.

One of the continuing needs of future array technology is the development of truly low cost, lightweight arrays, but the task of lowering array cost has proven far more than an exercise in efficient production techniques. It now seems that such arrays will only be practical when elements, phase shifters, and transmission lines can all be assembled automatically. A dramatic stride in this direction is the microstrip array and associated feed networks. Fig. 19 shows a sketch of the basic microstrip "patch" element, a rectangular sheet of conducting metal suspended in close proximity to a metallic ground plane, and usually formed by etching the copper from one side of the printed circuit board. The conducting patch is excited by a microstrip transmission line as shown in the figure or by a coaxial line. The basic patch element [86] has been analyzed by a number of authors and its radiation model depicted in Fig. 19 assumes the element to radiate as two slots separated by a half wavelength in the dielectric medium. This and other varieties of microstrip element have been the subject of many

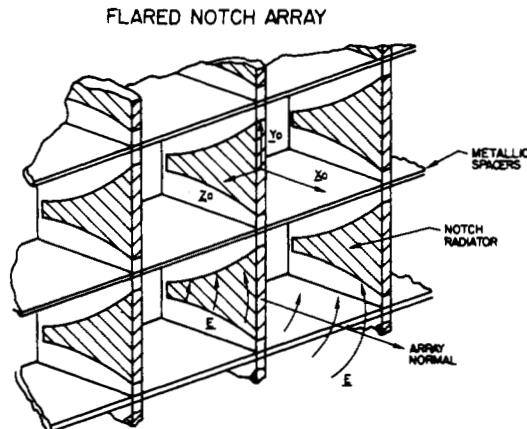
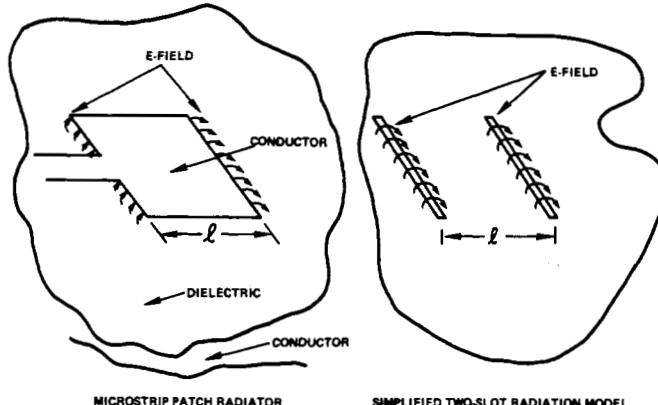
Fig. 18. Flared notch array elements (after Lewis *et al.* [66]).

Fig. 19. Microstrip patch radiator (after Munson [87]).

detailed theoretical investigations. Circuit models of varying degrees of complexity have been developed by Lo [87], Carver [88], and Derneryd [89] while integral equation and moment method analysis have been proposed by a number of other authors [90], [91].

The primary reasons for using microstrip radiators are to take advantage of the low fabrication cost achieved by etching elements and transmission lines, and to produce very low profile array elements. Measured against these criteria the patch element is unexcelled. Unfortunately, the basic patch is narrow band, with percentage bandwidth given approximately by

$$100 \frac{\Delta f}{f_0} = 5t f_0 \quad (77)$$

where t is the thickness (in centimeters), for the air-loaded patch. In addition, the element has a directive element pattern because it is a half wavelength long and so is not suited to wide-angle scan. A number of very creative microstrip elements have been developed to address some of these needs. Fig. 20 shows a square patch design for radiating circular polarization, a shorted rectangular patch for producing a much wider element pattern in the scan plane, and a combination of shorted patches that radiates circular polarization and is the microstrip equivalent of crossed slot radiators [92]. Many other microstrip radiators have found practical application. Of these, the most significant is the circular disk radiator of Howell [93] (Fig. 20(d)) which can be excited by a microstrip line but

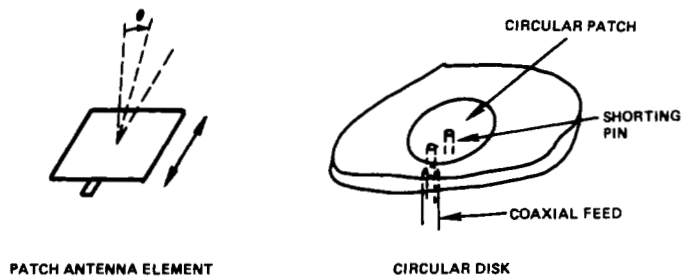


Fig. 20. Useful microstrip radiator types.

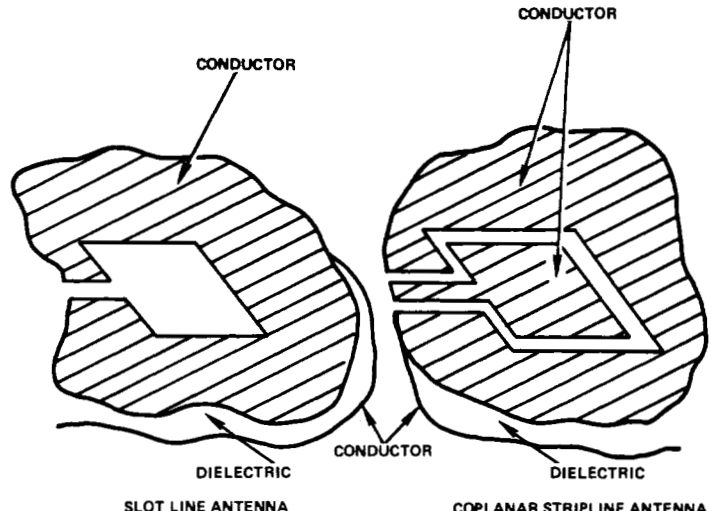


Fig. 21. Two printed circuit radiators.

which also is very suitably excited from below the ground plane, as shown in the figure. Still other transmission line media offer advantages for array use in a variety of applications. Fig. 21 shows examples of slotline and coplanar stripline antenna elements referenced by Greizer [94].

C. Passive Components for Arrays: Polarizers and Feed Networks

The trends toward greater flexibility, more accurate pattern controls and light weight compact array structures are also affecting the type of components used in arrays. This section lists some of the passive components used to control radiated polarization and to provide power distribution networks for precise pattern synthesis.

Waveguide polarizers using a probe or obstacle to excite both polarizations and some variation of a quarter wave plate to produce the requisite $\pm 90^\circ$ delay for circular polarization have long been used as phased array components. Recent advances in this direction have stressed broad-band perfor-

mance and polarization flexibility. A dual frequency waveguide polarizer, recently developed by Crone *et al.* [95] for a reflector feed, which provides good circular polarization over two 500-MHz bands with lower frequencies of 12 and 14 GHz, typifies the advanced state of this art, although is too large for array use. Other waveguide polarizers in current use include the tapered septum polarizer [96] for converting linear to circular polarization which operates over about a 2 to 5 percent bandwidth and the stepped-septum polarizer of Chen and Tsandoulas, a three-port device that allows polarization agility over at least 20 percent bandwidth with isolation greater than 26 dB [97].

Often it is less expensive to insert a polarizer in front of the whole array, and this is a customary solution for nonscanned arrays. The earliest polarizer of that type is a grid of quarter wave plates, but a much more popular recent solution is the use of meander line polarizers following the work of Matthai *et al.* [98].

Power divider networks for array feeds must be extremely precise to synthesize low sidelobe radiation patterns. Other requirements often impose extreme high power specifications, and still others demand very lightweight or compact construction practices. Waveguide and coaxial line corporate feed networks are most often used for high-power arrays but the increasing ease and quality of stripline construction has made stripline the medium of choice for many new array developments. Often it is convenient to produce hybrid combinations of waveguide, coaxial line, and stripline to take advantage of inexpensive stripline network techniques for lower power sections of the array while using waveguide or coaxial line at the high power regions of the feed network.

Precise feed synthesis requires both equal and unequal power dividers. The most commonly used stripline components are reactive tee power dividers, branch line couplers, parallel coupled line, and in-line power dividers. Although simplest and least expensive to construct, reactive tee power divider networks have no isolated port and hence offer serious mismatch and isolation problems when used to feed mismatched elements. Reactive corporate feed networks are therefore useful mainly for fixed beam arrays or for power division in the unscanned plane of arrays with one plane of scan. Single section [99] branch line couplers occupy an area approximately $\lambda/4$ square and are most useful for coupling ranges from 3 to 9 dB. These couplers are easily fabricated using a conventional stripline by machining or etching the center conductor. Parallel coupled stripline power dividers for loose coupling (>10 dB) can also be designed from conventional stripline using side coupled parallel lines, but tighter coupling requires the use of three-layer stripline for broadside coupled lines (3 to 6 dB coupling) or variable overlap couplers for intermediate values. Single section parallel coupled power dividers are $\lambda/4$ long but occupy less area than branch line hybrids. Another likely choice for array feed networks is the Wilkinson [99] in-line power divider or its impedance compensated derivative, the split tee power divider [100]. Single section Wilkinson power dividers are $\lambda/4$ long for equal power division and $\lambda/2$ long for unequal power division. Split tee power dividers have an extra stage of impedance matching and so are longer by approximately $\lambda/4$, although they have the advantage of wider bandwidth.

In-line power dividers have excellent broad-band characteristics in comparison with branch and coupled line hybrids because the coupling ratio is determined exclusively by relative

impedance ratios, not line length. Similarly, in-line hybrids are in-phase power dividers and so there is little phase error introduced with frequency change. The output ports of branch and coupled line hybrids have substantially different phases ($\pi/4$ for equal power division) and, although this can be compensated at center frequency, networks of these hybrids tend to be very narrow band relative to in-line hybrids. Typical bandwidths for individual in-line hybrids can reach an octave. The selection of power division networks is critical to array design and the choice can vary substantially with the application. The following two developments illustrate this point.

An example of a modern stripline array feed design is the dual shaped beam column array synthesis by Hanley and Perini [85]. The requirements for this array was to form two independent, shaped, elevation beams, a lower pencil beam and an upper beam with an approximate csc^2 pattern. The network forms the lower beam using a combination of two orthogonal beams and the upper beam using a weighted combination of six other orthogonal beams. Beam orthogonality allows the proper array weighting to be accomplished with lossless networks. The resulting column network, shown in Fig. 22, is composed of two- and three-branch stripline power dividers, some with interchanged output lines to give a wide range of coupling values. Branch-line couplers were chosen in preference to coupled-line devices because of the convenience of using two-layer stripline board for fabrication while maintaining a wide enough range of coupling values. Three-branch couplers were used for coupling values up to 6.7 dB because of their wide-band performance, but for higher coupling values, two-branch couplers were used to avoid etching very fine stripline conductors. The series feed network required 43 different coupler designs ranging from 3.4 to 12 dB. Another practical innovation incorporated into this circuit comes from the recognition that the effective electrical length of a branch line coupler is equal to its physical length only at design frequency. The slope of the insertion phase of a coupler is greater than that of an uncoupled line, and the greater the coupling the greater the slope. Thus the bandwidth of this series fed branch line coupler network was broadened by adding line lengths before each element that did not simply equate total path length, but approximately equated the total slope of the phase frequency curve at each element. This network formed the requisite beams with less than 1.05 dB loss over 15 percent bandwidth at 1.3 GHz.

A second illustration of modern feed technology is the corporate stripline feed for a low sidelobe fixed beam array at L-band [101], [102]. This study reported the development of a split tee stripline coupler power divider network for a very large L-band array operating over the frequency range from 800 to 1400 MHz, and consisting of 8 rows of 36 elements each. The corporate feeds were constructed of stripline with the center conductor machined by a computer controlled milling machine to produce a -55-dB Chebyshev "taper" (including the effects of mutual coupling). To achieve such accurate pattern control over a wide frequency range the design used split tee power dividers and relatively low coupling values throughout the feed. Toward this end, Winchell compared binary and nonbinary networks for producing the severe taper. Two of the networks are shown in Fig. 23, with coupling values for the lossless couplers indicated on the figure. The binary network leads to necessarily high coupling values (and thus to relatively narrow-band couplers with faster

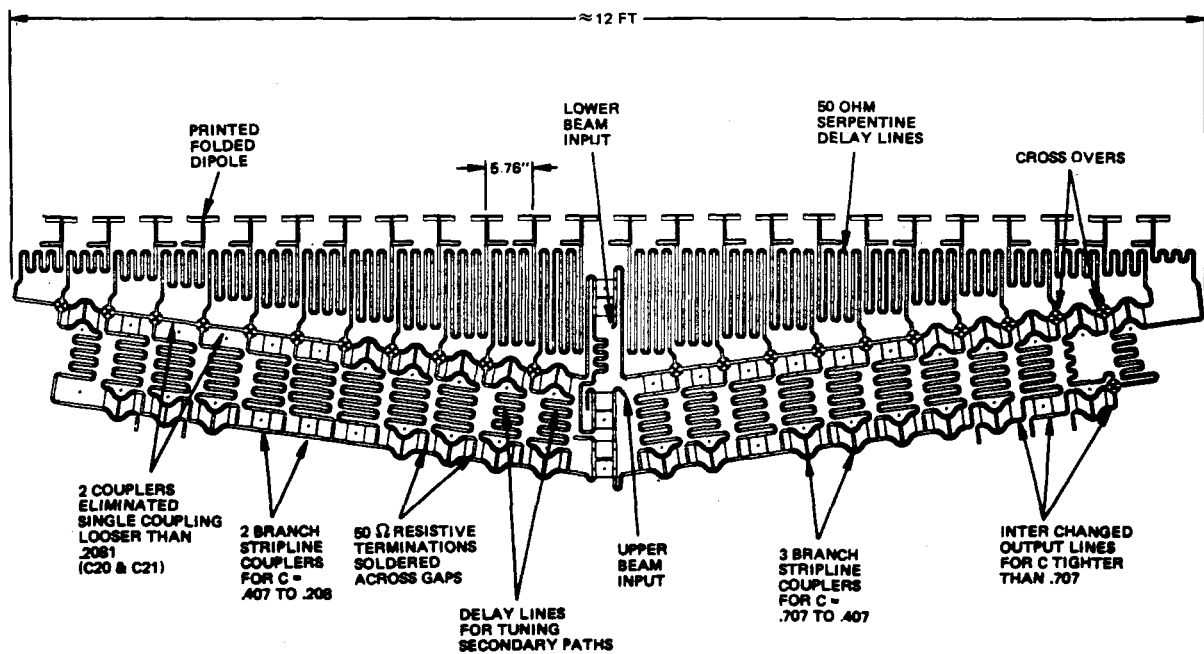


Fig. 22. Strip line column array (after Hanley and Perini [85]).

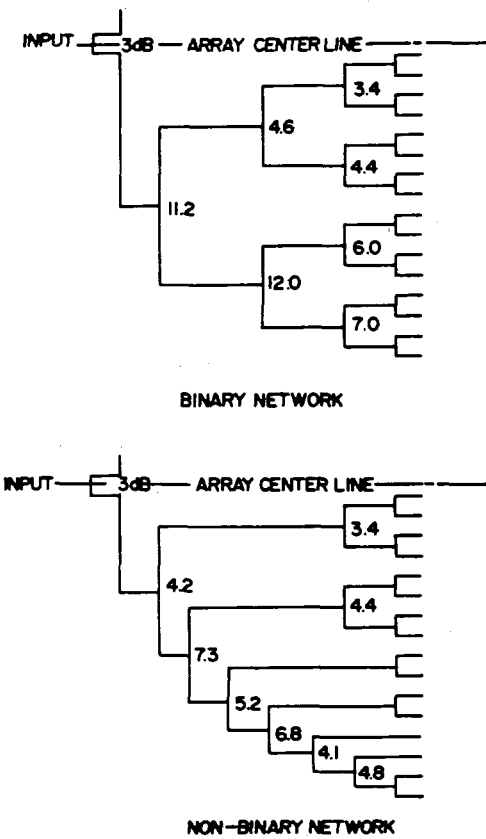


Fig. 23. Effect of network structure on coupling values (after Winchell [101]).

phase slopes). Couplers with less than 4 dB coupling have phase and amplitude differences within ± 0.03 dB and $\pm 0.15^\circ$ over the 55 percent bandwidth, and 5 dB couplers have differences within ± 0.1 dB amplitude and ± 0.5 phase. Couplers with higher coupling values had much poorer broad-band performance. Nonbinary networks, or partially binary (such as the one in Fig. 23(b)) can have lower coupler values, but

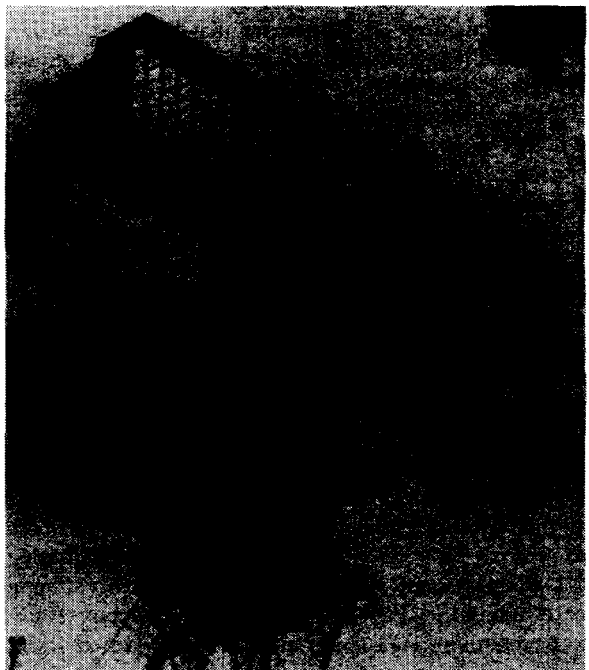


Fig. 24. L-Band low sidelobe array (courtesy of Westinghouse Corporation).

they have significantly unequal path lengths which must be equalized by additional compensating lines to improve the broad-band response. The final design had all couplers less than 4.4 dB with the exception of 5.1 dB couplers feeding the outer six elements on each side of the array. The completed array shown in Fig. 24 demonstrated better than -36 dB peak and -48 dB rms sidelobes over about 45 percent bandwidth. The author has computed the results of several minor modifications to the distribution network, and indicates that these would result in an improvement in performance approaching 45 dB peak and 55 dB rms sidelobes over the same bandwidth.

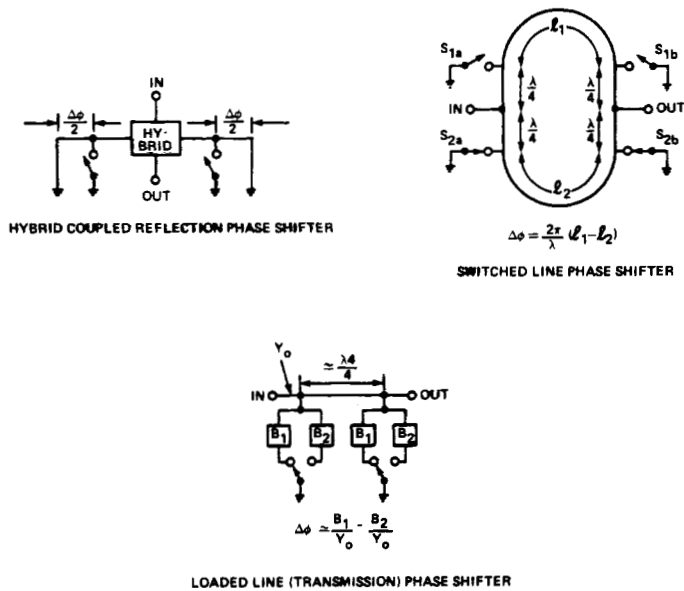


Fig. 25. Diode phase shifter circuits.

D. Array Phase Control

A number of recent references have described array phasing devices and phase shifter networks in great detail. Therefore, this subject will be treated only briefly here. In addition, the topic of time delay devices for arrays is omitted because the primary components used to date are switched transmission lines and governed by the same critical characteristics as phase shifters.

Phasing networks are most often implemented at the RF operating frequency because this is usually the most efficient process. Notable exceptions use phase shifters at intermediate frequencies and up-convert to RF [103], [104] with amplifiers to improve efficiency. In addition many ingenious intermediate frequency phase scanning systems have used harmonically derived phase shifts or frequency displaced signals across an array to produce time varying beam positions (see [105]). Systems of this type are described in the literature and their operation is beyond the scope of this paper. There are also new system concepts that utilize optical fibers, phase locked oscillators [106], or spatial frequency components [107] to synthesize radiation patterns. RF phase shifters have also been described in substantial detail in other references [108]–[112] and so are only treated here to outline the choices open to the design engineer. In general, diode phase shifters dominate the frequency range below 2 GHz and ferrites are usually selected above 5 GHz. Diode phase shifters are compact and very light in weight compared to ferrite devices and so are gaining popularity in lightweight array configurations through 15 GHz, often in combination with low cost monolithic microstrip antenna circuits.

At present the most popular types of diode phase shifter designs for arrays are the hybrid coupled, switched line, and loaded line phase shifters using p-i-n diodes. These three fundamental networks are shown in Fig. 25. Hybrid and loaded line (transmission) phase shifters require two diodes per bit, and switched line phase shifters require four per bit. Switched line hybrids also have greater insertion loss and an undesirable phase dependence with frequency that usually makes them unsuitable for low sidelobe array control. However, they do possess distinct advantages in weight and com-

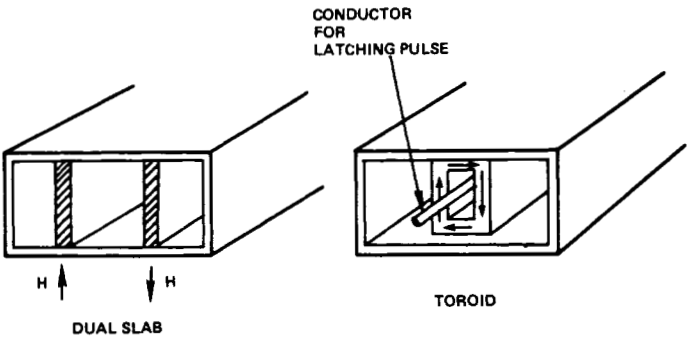


Fig. 26. Dual slab and toroid ferrite phase shifters.

pactness, and have been used successfully in monolithic microstrip antennas for many years. Hybrid and transmission phase shifters have lower loss and better bandwidth performance. An S-band stripline hybrid phase shifter is reported by White [110] to have an average phase error of only 3° over 20 percent bandwidth. This device had about 0.8 dB average loss from 3.0 to 3.5 GHz and was tested to high power burn-out at 4 kW peak with 0.1 ms pulses and 0.05 duty cycle. Insertion loss for X-band and Ku-band phase shifters was about 2 and 3 dB, respectively.

Broad-band, low sidelobe array designs are possible using Schiffman phase shifters because this phase shifter produces nearly constant phase shift over extremely wide frequency ranges. White [110] gives data for a 90° bit over a frequency ratio of 2.27:1.

A precise, low sidelobe array developed by Tsandoulas [113] used six-bit diode phase shifters developed by Microwave Associates and achieved phase tolerance limits of less than 0.9° rms for the 90 and 180° bits, 0.4° for 45°, 22.5°, and 11.25° bits, and 0.2° for the 5.625° bit. These remarkable results were achieved in a practical testbed array described in Section IV.

Ferrite phase shifters have been built to operate up to 60 GHz and possess excellent characteristics for many phased array applications. Several recent survey articles and an annotated bibliography [114]–[116] summarize progress in this field and list numerous references to devices and to the fundamental theory of ferrite phasor operation. Nonreciprocal ferrite phase shifters include early twin slab designs (Fig. 26(a)) that require a transverse switched external magnetic field and the well known toroid designs (Fig. 26(b)) that use a longitudinal wire to drive the ferrite magnetization to saturation as in a latching phase shifter, or to various points on the magnetization curve with flux drive circuitry. Typical digital latching phase shifters can have bandwidth in excess of 10 percent and insertion loss between 0.5 and 1 dB. Power levels can vary from 1 kW to as much as 150 kW peak and average power levels to 400 W. Latching phase shifters have switching times on the order of one microsecond and have become standard throughout the industry. Flux drive circuits with toroidal phase shifters allow for analog phase settings, and so need not be restricted to specific phase bit values. The major disadvantage of these nonreciprocal phase shifters is the need to reset them between transmit and receive functions for radar application.

Among several varieties of reciprocal ferrite phase shifters the dual-mode phase shifters have replaced Reggia-Spencer phase shifters which have been found to have low values of

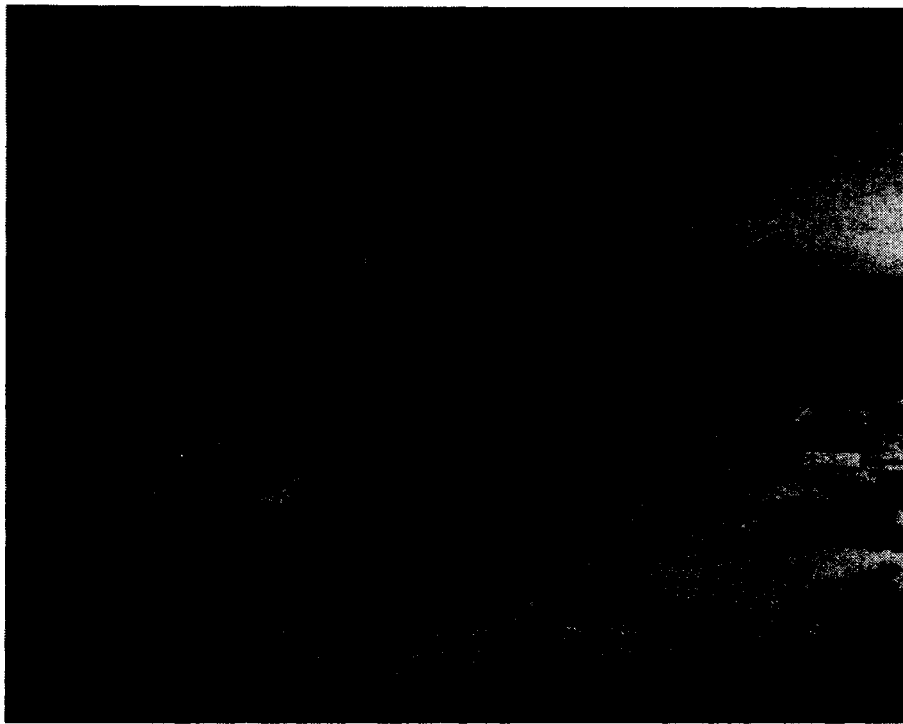


Fig. 27. Pave paws array (courtesy of Raytheon Company).

phase shift per wavelength. Dual mode phasors are Faraday rotation devices that convert a linearly polarized incident waveguide mode to circularly polarized energy using a non-reciprocal ferrite quarter wave plate, phase shift the energy by Faraday rotation, and then convert it back to linear polarization. A signal from the opposite direction is converted to circular polarization of the opposite sense but since the direction of propagation and polarization are both opposite it incurs the same reciprocal phase shift. Dual mode phase shifters are very competitive with toroid phase shifters and have average power levels up to 1.5 kW at S-band and peak powers to 150 kW. Insertion loss can be 0.6 dB through X-band. Switching speed can be on the order of tens of microseconds for a latched design depending on the application. The reference by Ince [112] compares specific phasor examples for S-band through Ka band.

One other important reciprocal phase shifter which is very competitive for a restricted set of applications is the analog rotary-field phase shifter of Boyd [117]. This phase shifter is based on the principle of the commercial rotary-vane phase shifters after Fox [118], and uses a ferrite rod of circular cross section fitted with a slotted stator in which are wound two sets of coils that each generate a four-pole field. In comparison to the well known rotating half wave plate of the Fox phase shifter, the stator windings produce a rotating four-pole field distribution, with the orientation of the principal axes proportional to the coil driving current values. The dc distribution in the ferrite serves to rotate a virtual half wave plate that is converted to a phase shift just as is the mechanical half wave plate rotation of the Fox phase shifter. This circuit has the disadvantages of requiring watts of drive power per phase shifter and having relatively long switching times (200–500 μ s). Its advantage for many applications far outweigh these disadvantages because it has nearly dispersionless phase shift that can be maintained within a degree or two over substantial bandwidths, has insertion loss well under 1 dB, and can handle

very high peak and average power levels. An S-band model operates at 90 kW peak, 3 kW average power, 0.5 dB insertion loss, and phase tracking within $\pm 1.5^\circ$ over about 9 percent bandwidth.

THE VARIETY OF ARRAY CONCEPTS AND TECHNOLOGY

The survey by Stark [1] emphasized large ground-based arrays for surveillance radar systems. These systems have not become less important, but this is a period of such dramatic growth in smaller arrays designed to satisfy special requirements that the properties of larger arrays have been deemphasized in this summary. This section describes techniques for a number of important requirements, including very low side-lobe arrays, conformal arrays and arrays for hemispherical coverage, hybrid array-reflector and array-lens techniques for limited sector coverage, various lightweight antenna techniques, and ultra-wide-band technology for large arrays.

The arrays described in this section are all quite different in their design, function, and characteristics. Hybrid array-reflector antennas in general perform no function that cannot be performed better by conventional phased arrays, but they satisfy their requirements for the lowest possible cost. Printed circuit array antennas, microstrip, strip line, or other media such as coplanar stripline have inherently no better performance than waveguide arrays, have more serious tolerance requirements because of space limitations and the state-of-component development, and fundamentally lower power transmitting capabilities: but again are much cheaper and also lighter weight than waveguide arrays and therefore suit many applications that are not satisfied by conventional waveguide or coaxial arrays. Use of these new transmission media implies a relatively important change in the technology, for it impacts bandwidth, scanning performance, and other array characteristics, including even the way phase controls are designed and fabricated. Hemispherical coverage and wide-band arrays both require markedly different techniques than conventional

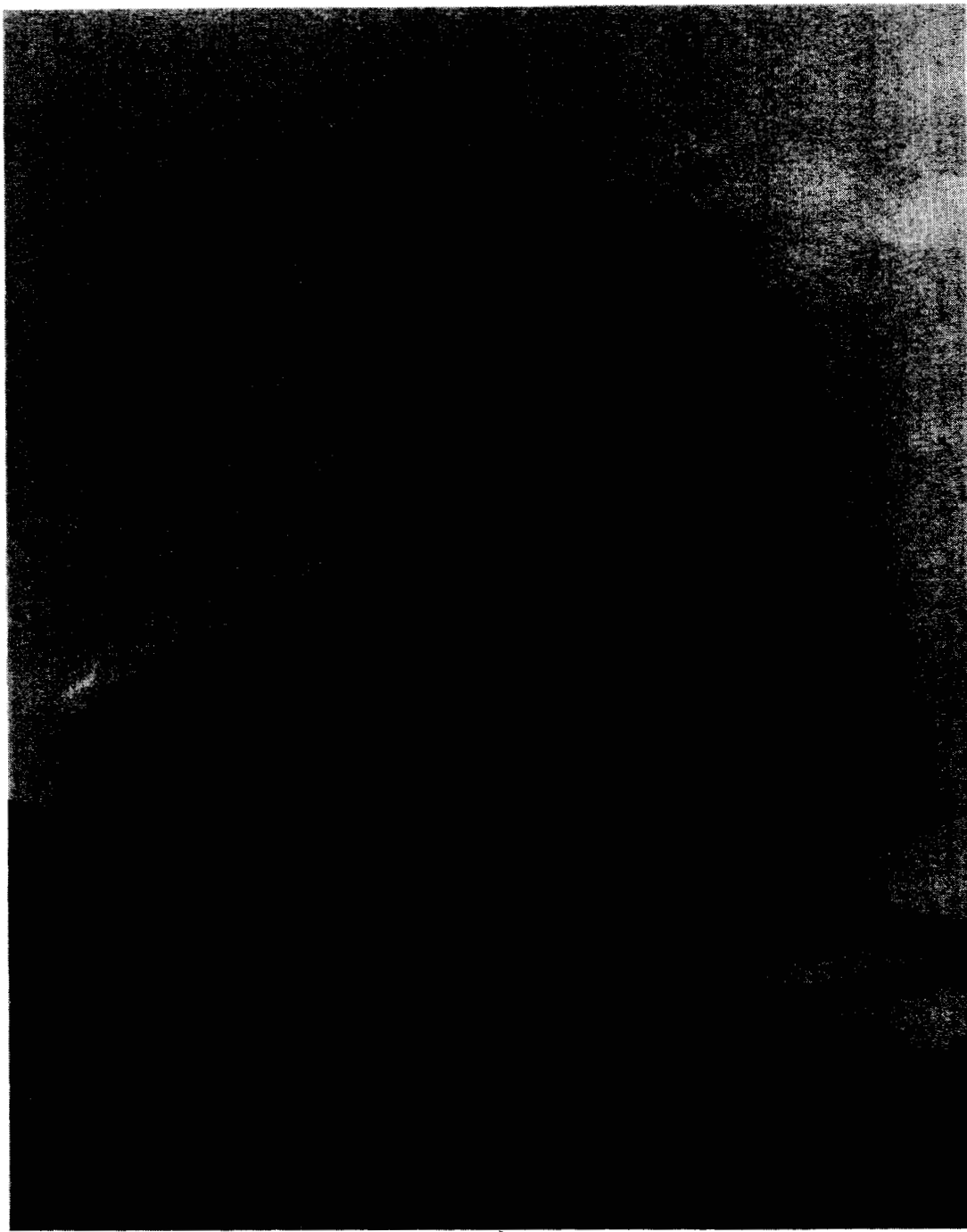


Fig. 28. Patriot array (courtesy of Raytheon Company).

planar arrays. Finally there is a whole class of arrays designed for extremely fine pattern control. It is this area that is perhaps the most important new technological requirement to be met by future array systems, and one that is not well addressed by present day technology. The development of arrays with deterministic or adaptive control of very deep, broad-band pattern nulls or extremely low sidelobes over wide bandwidths will require advances well beyond the techniques described in this survey, and will be a major stimulus to array technology for a number of years.

A. Current Technology for Radar Arrays

Antenna arrays for strategic radars have reached an advanced state of maturity. For example, the Pave Paws radar

system has a solid-state UHF array shown under construction in Fig. 27. Each of the two array faces contains 2677 antenna elements, with 1792 active elements and 885 dummy elements occupying the filled aperture of approximately 72.5 ft diameter. Each face transmits 585 kW peak and 145 kW average power.

Tactical radars face the more severe demands implied by transportability and performance in a hostile environment, and yet they must be inexpensive, because of the need to field a relatively large number of each type. One example of current tactical radar technology is the Patriot array (Fig. 28), a space fed C-band array of 5161 elements that has separate transmit and receive pencil beam feeds [7], [119]. The radar is a mobile multifunction radar developed by Raytheon Corporation.

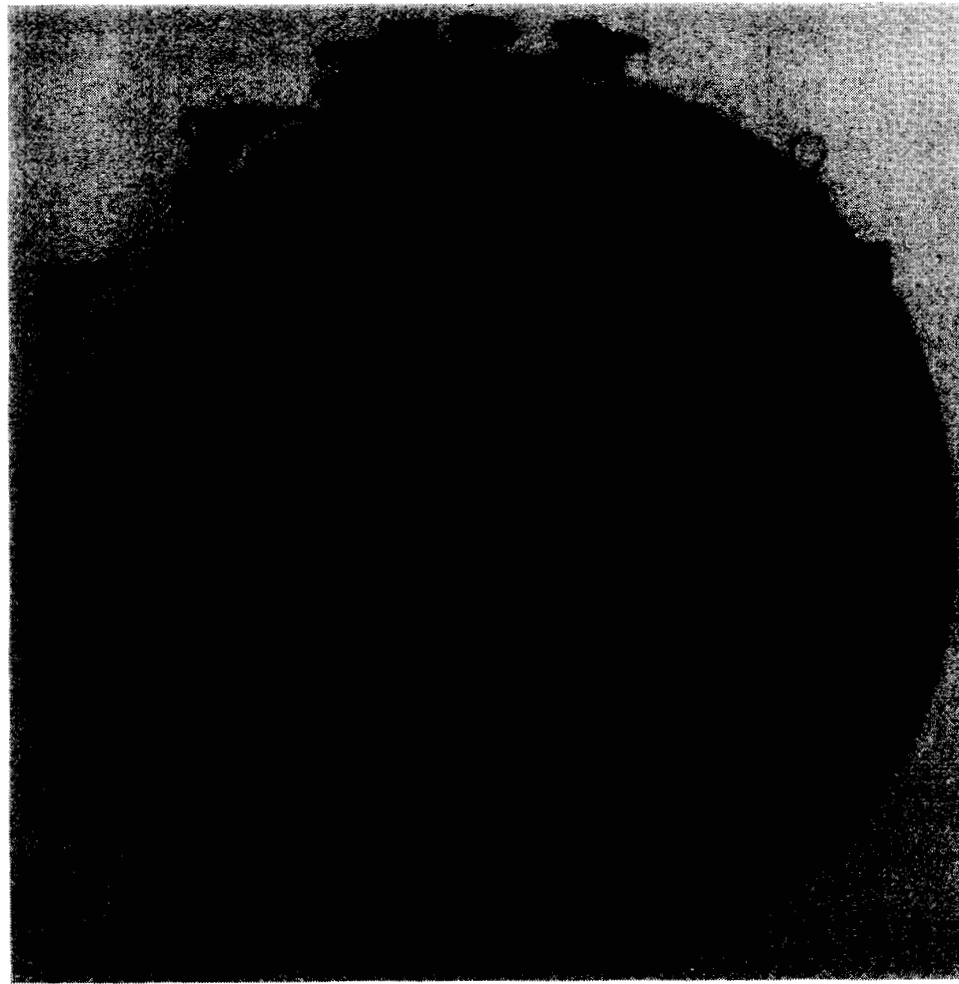


Fig. 29. Electronically agile radar array (courtesy of Westinghouse Corporation).

In addition to the main array radar, the system also includes five sidelobe canceller arrays.

The Firefinder system developed by Hughes Aircraft Co. includes the AN/TPQ-37 artillery locating radar and the smaller AN/TPQ-36 mortar locating radar. Both radars scan 90° sectors in the azimuth plane. The AN/TPQ-36 tracks in azimuth and elevation by sequential lobing using ferrite phase shifters for azimuth scan and frequency dispersive slot arrays for a few degrees of elevation scan. The AN/TPQ-37 uses monopulse tracking with diode phase controls for scan in azimuth and a few degrees of elevation.

The electronically agile radar (EAR) array (Fig. 29) is a multifunction airborne radar antenna developed by Westinghouse Corporation. The EAR antenna has 1818 phase shifters and was developed as a constrained fed array with azimuth and elevation beam steering via the phase shifters and drivers which are integrated into the radiating element.

The AN/TPS-59 is a solid-state array radar developed by General Electric Co. with a planar array of 54 row feed networks to form a pencil beam that is steered in elevation (Fig. 30). The array is rotated in the azimuth plane to provide azimuth and elevation coverage. Fifty-four solid-state transmitters and receivers are housed behind the array, one for each row. The entire elevation range is scanned in less than 0.1 s. Each row is fed by 20 transistorized power amplifier modules operating in parallel to achieve a peak output of nearly 35 kW for the entire array. Electronic control allows

the vertical beamwidth to be varied as a function of elevation angle, while azimuth rotation is at 6 and 12 rpm. The row feed is a lightweight single layer stripline circuit. The antenna is 30 by 15 ft, has a transmit gain of 38.9 dB, an average duty cycle of 18 percent, and sidelobe levels less than -25 dB.

A major antenna development for shipboard radar is the Navy's Aegis program with its AN/SPY-1A radar, a four-faced C-band phased array system developed by RCA. Each array has 4480 elements fed by a waveguide power divider system. Transmitting and receiving functions utilize different array illuminations and subarrays. The illumination is uniform on transmit. A modified circular Taylor distribution is used on receive for the monopulse reference channel with a modified Bayliss for azimuth and elevation error channels. The array is divided into basic modules, each containing 32 radiating elements. Two modules constitute a receiving subarray, and four modules make up a transmitting subarray. The extensive use of subarraying is for the purpose of array organization, fabrication, and to accommodate high power amplifiers in the transmit network. Phase shifters are used at element and array level and there are no time delay units.

The demands imposed by electronic countermeasures in military systems are leading to antenna systems with much lower sidelobes. The Air Force AWACS antenna system, an early warning surveillance system, was the first development to address this need. In addition, the ultra-low sidelobe antenna (ULSA) system for the TPS-43 Search Radar (Fig. 31) and the

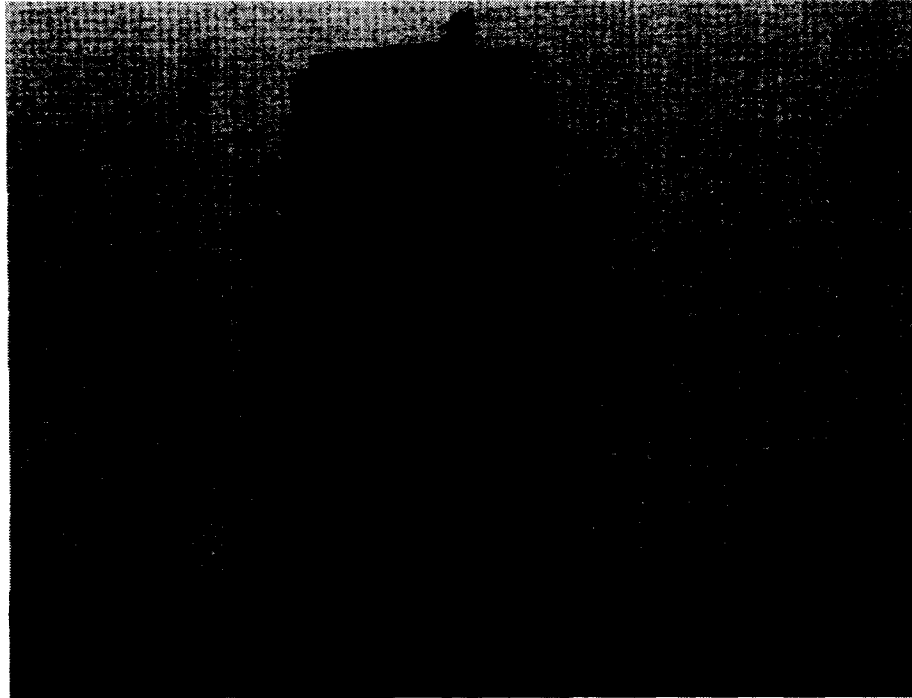


Fig. 30. TPS-59 array (courtesy of General Electric Company).

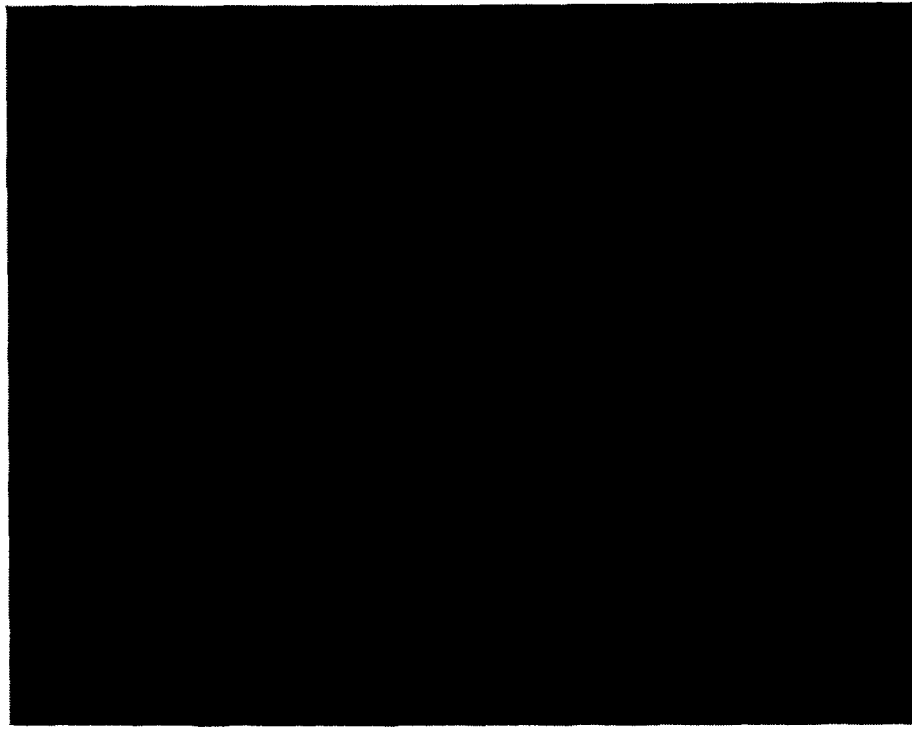


Fig. 31. Ultra-low sidelobe array.

Army Hawk antenna system are all examples of antennas that scan in the vertical plane and maintain extremely low sidelobes in the azimuth plane. Designed by Westinghouse Corporation, these arrays use slotted waveguide row radiators and have multiple or scanned elevation beams.

Other low sidelobe arrays have been developed using precision stripline feeds for wider band performance [101], [102], [120]. Like the slot array geometries, these antennas

are mechanically rotated in the azimuth plane and rely on ultra precise row distribution networks and stacking of uncorrelated rows for low azimuth sidelobes. Elevation coverage is provided electronically, but with substantially higher elevation plane sidelobes.

A recent paper by Tsandoulas [113] describes the development of an array of 252 waveguide elements arranged in 42 vertical columns and scanned in the azimuth plane. Through

careful tolerance control in the power division network and extremely accurate phase shifters (see Section III) the array achieved azimuth scan patterns with all but the first sidelobe below -42 dB. This significant development represents the lowest scan plane sidelobes achieved to date.

B. Conformal and Hemispherical Coverage Arrays

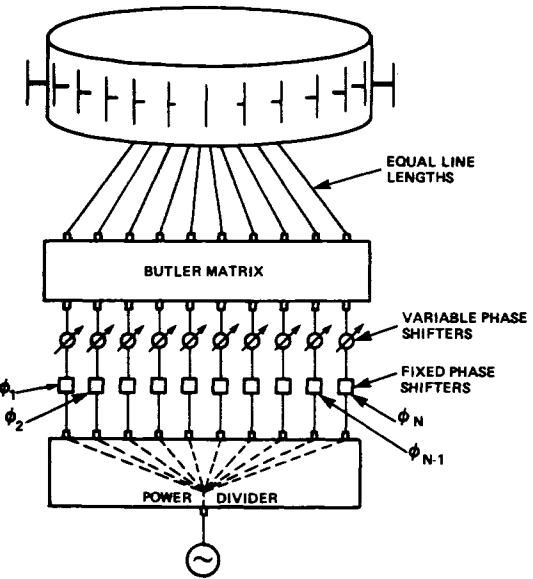
The need for conformal or low profile arrays for aircraft and missile applications, and for ground-based arrays with 360° azimuth coverage or hemispherical coverage, has grown continually with requirements that emphasize maximum utilization of available space and minimum cost.

The earliest and continuing stimulus for cylindrical and circular array development is the need for inexpensive systems with mechanical or electronic scanning having constant gain throughout the 360° coverage sector. There are also a number of spacecraft and aircraft applications requiring low profile or conformal arrays. Cylindrical conformal arrays have been built for despun radiation from spinning missiles, and for omnidirectional coverage in the plane perpendicular to the missile axis. Major developments have been made in arrays conformal to missile and aircraft nose cones. Requirements for flush-mounted or low profile aircraft antennas for satellite communication have been a new stimulus for the development of arrays that scan over very wide angles to provide coverages from zenith to horizon. These and other applications have produced a body of work that was the primary subject of two conferences, numerous sessions at technical symposiums and a Special Issue of *IEEE TRANSACTIONS ON ANTENNAS AND PROPAGATION* [21].

Several editorial references and surveys that summarized the state of the art as of 1974 pointed out directions for ongoing research. Kummer [21] listed significant features that distinguish the scanning behavior of conformal and planar arrays.

Array elements on curved bodies point in different directions, and so it is unusually necessary to turn off those elements that radiate primarily away from the desired direction of radiation. Moreover, one cannot factor an element pattern out of the total radiation pattern and so conformal array synthesis is very difficult. Mutual coupling problems can be severe and difficult to analyze because of the extreme asymmetry of structures such as cones and because of multiple coupling paths between elements (for example the clockwise and counterclockwise paths between two elements on a cylinder). Cross-polarization effects arise because of the different pointing directions for elements on curved surfaces causing the polarization vector projections to be nonaligned. In addition there is a need to use different collimating phase shifts in the azimuth plane of a cylindrical array scanned in elevation due to the fact that steering in azimuth and elevation planes is not separate. Another phenomenon related to mutual coupling is the evidence of ripples on the element patterns of cylindrical arrays. This phenomenon can be explained in terms of creeping wave contributions.

There is a vast literature and history of circular and cylindrical array developments, many of which are described in standard texts [121], and so will not be detailed here. Provencher [122] lists a number of techniques for feeding circular arrays including mechanical or electronic switching, lens-switch combinations, and hybrid matrix phase shifter combinations. Electronic switching schemes use a bank of switches to bring a given illumination taper to one sector of the array (usually a 90 to 120° arc), and a set of switches to provide fine beam steering between those characteristic positions determined by the sector switching network.



SCHEMATIC DIAGRAM OF A SCANNING MULTIMODE ARRAY.

Fig. 32. Schematic diagram of a scanning multimode array network (after Sheleg [123]).

Several more sophisticated types of electronic switches for circular arrays are based on a concept originally proposed by Shelton [123] and developed by Sheleg [124] that uses a matrix fed circular array with fixed phase shifters to excite current modes around the array, while variable phase shifters provide continuous scanning of the radiated beam over 360°. The geometry is shown in Fig. 32. A more recent extension of this technique proposed by Skahil and White [125] excites only that part of the circular array that contributes to formation of the desired radiation pattern. The array is divided into a number of equal sectors and each sector is excited by a Butler matrix and phase shifters. With either of these circuits, sidelobe levels can be lowered by weighting the input excitations to the Butler matrix. The technique of Skahil and White was demonstrated by using an 8 X 8 Butler matrix and 8 phase shifters to feed four 8-element sectors of a 32-element array. The design sidelobes were -24 dB and measured data showed sidelobes below -22 dB.

The radiating properties of circular arrays have also been the subject of more detailed studies than other conformal arrays. It has been known for a long time that cylindrical array problems can be analyzed by use of the symmetry properties of the array. By this means one can avoid the solution of N simultaneous integral equations for an N -element circular array and instead solve N independent integral equations, one for each of the solutions with periodicity $2\pi/N$. Superposition of these N solutions yields the complete array solution for any given excitation. This method has been used by Tillman [121] and Mack [126] for dipole and monopole arrays, and more recently by Borgiotti [127] for waveguide arrays with active elements covering a sector on an infinite cylinder. The results of these and other [128], [129] theoretical studies have revealed distinct differences between the element patterns of radiators in cylindrical and planar arrays. The main distinction is the existence of potentially severe ripples in cylindrical array element patterns as shown in Fig. 33. Sureau and Hessel [130] have used asymptotic methods to show that the actual radiated pattern can be considered the superposition of a space wave contribution and several creeping waves which propagate around the cylinder and radiate away from the cylinder in the forward direction. The space wave and actual

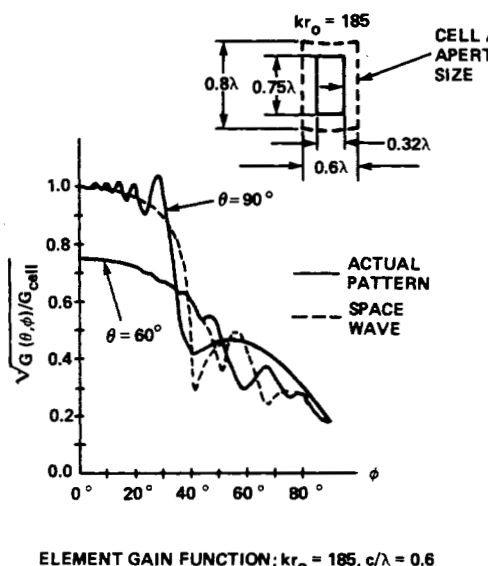


Fig. 33. Element gain function for array on a cylinder (after Sureau and Hessel [130]).

patterns are shown in the figure for radiation at two different angles θ measured from the cylinder axis. These ripples tend to decrease with cylinder radius and to increase with frequency. This feature may ultimately limit the synthesis possibilities with cylindrical arrays, and may also reduce the potential for broadband null steering with adaptive systems. Recent work [131] has shown that smoother element patterns can be obtained by limiting element spacing to less than $\lambda/2$.

Elements on more generally shaped structures including cones [132], [133] and spheres [134] have been analyzed by a number of authors, and the use of asymptotic techniques like the Geometric Theory of Diffraction have made it possible to analyze fully generalized surfaces [132], [135]. The recent development of a ray technique [136], [137] called the Periodic Structure Ray Method has shown promise in the analysis of mutual coupling effects in large concave arrays.

One of the more persistent problems is the need for flush-mounted or low profile aircraft arrays for satellite communication. Military requirements for such arrays at SHF and EHF frequencies dictate high array gain and unusually large coverage regions including the entire upper hemisphere for some applications.

Fig. 34 shows several of the array configurations that have been considered for this application. The most obvious solution is to simply use a single planar array at the top of the aircraft fuselage, but this requires the antenna to scan to endfire and hence to incur losses as described in Section II. Equation (69) gives the ratio of endfire array gain to broadside gain for an array of isotropic radiators. This gain is modified to account for the element patterns of the basic radiators. For circularly polarized radiation there is an additional 6 dB loss near the horizon due to polarization mismatch, and additional loss due to mutual coupling effects. Gain reductions exceeding 10 dB at the horizon are not uncommon for this design. One of the first studies of scan matching is the development by Borgiotti and Balzano [128], which gives analytical results for an array of circular apertures on a cylinder. The array length is infinite along the cylinder axis, and the array elements are disposed completely around the circumference of the cylinder, but only the elements occupying a given sector of the cylinder are excited.

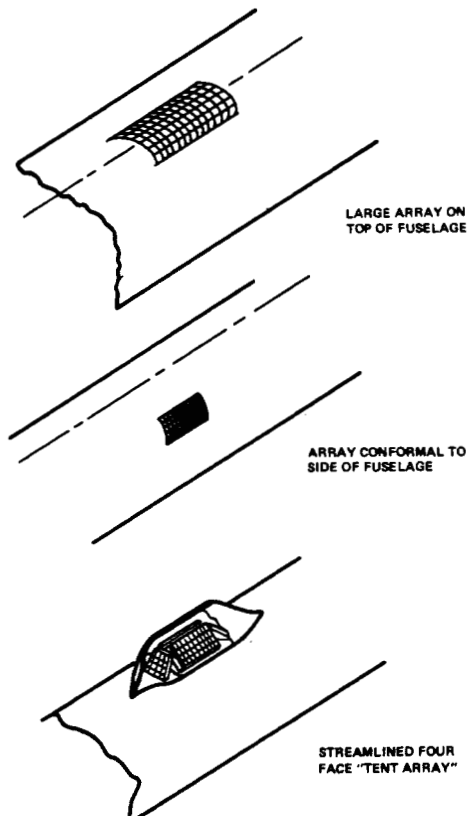


Fig. 34. Configuration for SHF airborne Satcom terminal arrays.

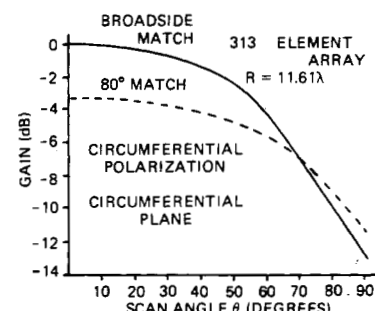


Fig. 35. Gain versus scan contour for array on cylinder (after Borgiotti and Balzano [128]).

Borgiotti and Balzano describe the phenomenon of scanning on a cylinder, and present results for the array matched at 80° from zenith. Their circumferential plane data shows that axial polarization gain degradation at the horizon is so large that virtually no amount of scan matching can improve it. The circumferential polarization radiation in the circumferential plane shows approximately 13 dB horizon gain reduction for standard equiphase matching of the array, but matching the array at 80° can increase the horizon gain about 2 dB, while reducing the zenith gain by 2 to 3 dB as compared with the unmatched case. The result of this scan matching procedure is to produce more uniform coverage over the hemisphere, yet it does not greatly improve array efficiency.

Fig. 35 shows the scan data for an array of 313 elements on a cylinder of radius 11.6λ . The graph indicates that the best scan conditions for this array give 3 dB loss at zenith, and a total of 11 dB loss at the horizon. These theoretical data were confirmed in a later experimental study by Balzano [138].



Fig. 36. Low profile array for mechanical/electronic hemispheric scan (courtesy of Hazeltine Corporation).

using a similar array geometry. The predicted bandwidth for the technique is 10 percent.

The low profile array subsystem (Fig. 36) developed by Hazeltine Corporation provides hemispherical coverage for an airborne satellite communication terminal, the Small SHF/EHF Airborne Satcom Terminal (SESAST) by a combination of mechanical rotation in azimuth and electronic scanning in elevation.

Since the array is only scanned electronically in elevation, it uses only a fraction of the phase shifters required in a fully phased array. It is therefore more cost effective than a fully phased array.

The array provides full duplex operation over the SHF terminal bands of 7.25 to 7.75 GHz (receive) and 7.90 to 8.40 GHz (transmit). It consists of 21 rows which are individually phased to steer the beam in elevation. Each row comprises 32 slots, providing a narrow azimuth beam. Key features of this design are

- a dielectric sheet above the aperture to provide wide-angle impedance matching;
- delay progression along the aperture to delay steer the quiescent beam to 60° above the horizon; this results in minimal frequency scan losses at the scan extremes (0° and 90°);
- independent ferrite phase shifters for receive and transmit;
- compact low-loss radial power dividers to provide the 21-way power split;
- a computer-designated fairing to minimize diffraction loss at the horizon.

Two other configurations using fixed arrays have also been the subject of recent studies. Fig. 34(b) shows a conformal microstrip array mounted on the side of an aircraft fuselage, and Fig. 34(c) shows four array faces mounted at the top of the aircraft fuselage in a streamlined "tent" configuration. These two configurations have application to the satellite com-

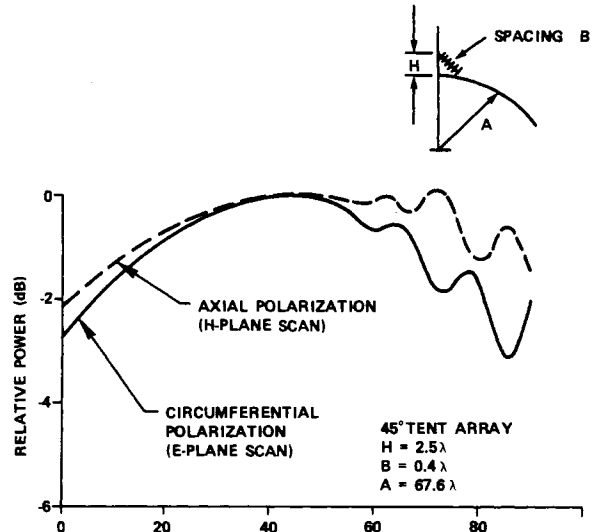


Fig. 37. Multipath effects on four face array over cylinder.

munication problem, and are the subject of current development programs to evaluate their utility. In both cases, the array is tilted to gain some projection in the vertical dimension. If the two side arrays were tilted 45° from the vertical and could be perfectly matched they would illuminate most of the upper hemisphere with gain within -6 dB of peak except for an area where the gain drops to about -7.5 dB near the cylinder axis. Additional factors that further reduce this coverage are the loss of the axial polarization near the cylinder axis and mutual coupling buildup.

Adding front and rear faces, perhaps with less gain and a more nearly vertical orientation as shown, can provide good pattern coverage with circular polarization over the hemisphere in the "tent" configuration while maintaining a streamlined profile. Detailed pattern calculations for an array of this type

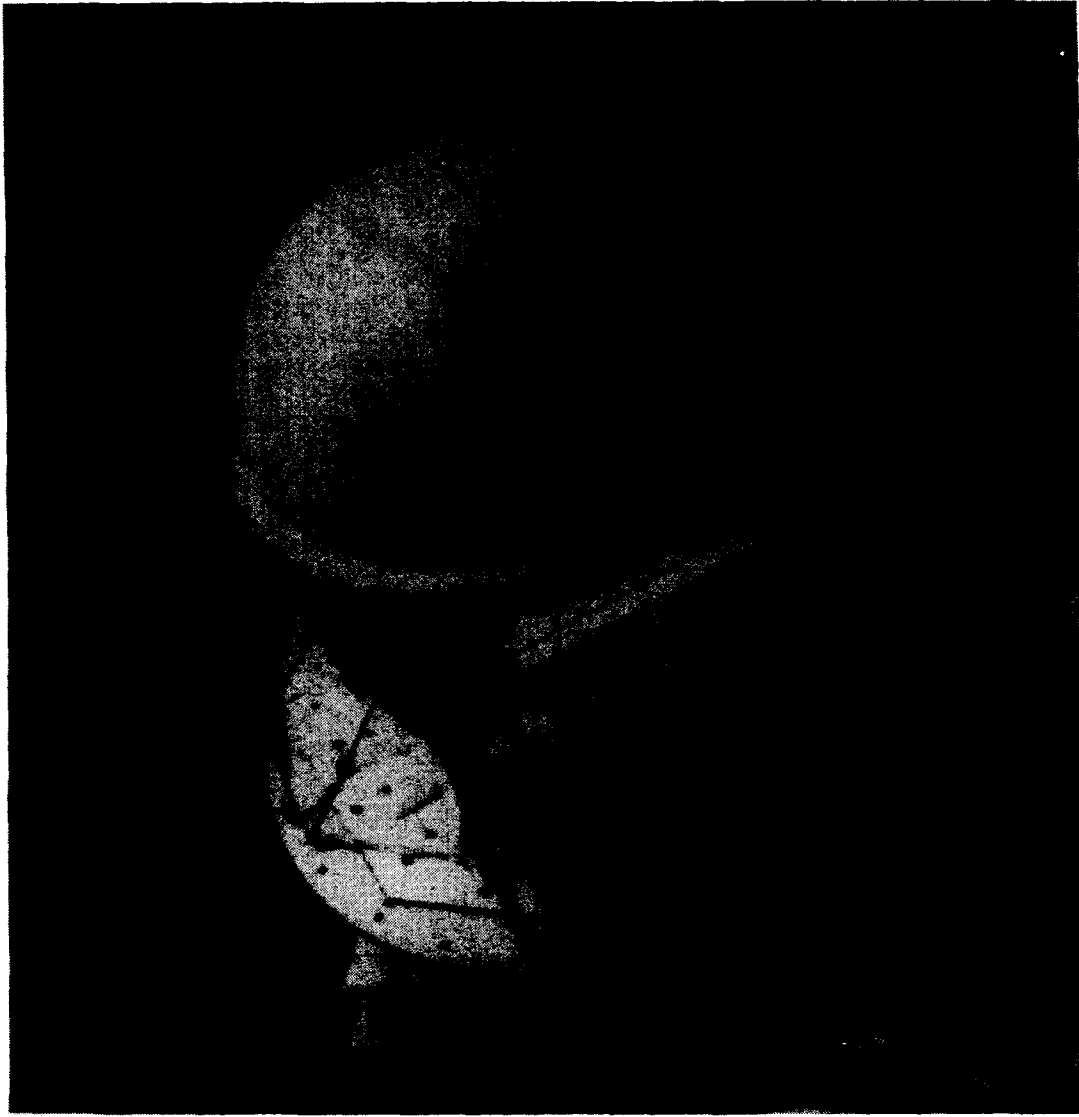


Fig. 38. The dome antenna array (courtesy of Sperry Corporation).

have been carried out using geometrical optics [139] following the work of Kouyoumjian and Pathak [140]. Fig. 37 shows the computed peak gain for both polarizations using a small tent-shaped array mounted at 45° on the top of a large cylinder. The indicated pattern ripples are the result of specular multipath from the cylinder surface, and the figure shows that these do not materially alter the elevation plane coverage of the array.

One of the more promising recent innovations in wide angle scanning is the Dome antenna [141]. This novel structure uses the vertical projection of the dome to achieve increased gain at low angles of elevation. The basic antenna, shown in Fig. 38, has a passive spherical lens made up of fixed phase shifters, and a conventional planar phased array. As shown in Fig. 39, the array steers an illuminated spot to various portions of the lens, and the fixed phase delays of the lens are computed so as to convert the array scan directions θ into a factor K times that angle and so to obtain scan in excess of the planar array scan angle.

Analysis of the dome and phase shifter settings are done by ray tracing. The array phase shifter settings are determined to form the nonlinear phase progression required to scan the

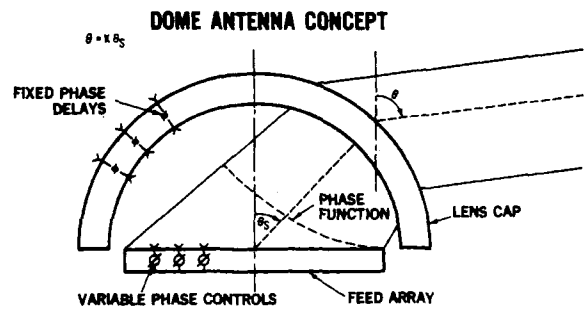


Fig. 39. Collimation by dome array.

searchlight type beam to various spots on the lens. Although the radiated beamwidth varies with scan angle, the Dome can achieve scanning over sectors larger than a hemisphere, and in fact has achieved scan to ± 120 degrees from zenith. Steyskal [142] gives equations for the gain limits of a given cylindrical dome based upon allowable scan angles for the feed array, and shows that the ratio of the average gain to the broadside feed array gain is bounded by a parameter that depends upon the feed array scan limit.

Depending upon specific design criteria, it is possible to select a lens/array configuration that emphasizes endfire radiation. Schwartzman and Stangel [141] illustrate several possible gain/scan profiles for a dome lens. One design measured at 5.4 GHz has about 20 dB gain at zenith, peak gain in excess of 26 dB at 65° from zenith, and 24 dB at the horizon. These data highlight the possibility of obtaining substantial gain at the horizon. The array feed for this lens has a diameter of 40 in, and so the array broadside directivity is approximately 35 dB. There is substantial penalty associated with the improvement of coverage at 90° and beyond, but the penalty is not nearly as severe as would be incurred for a conventional array scanned to endfire.

C. Arrays and Hybrid Scan Antennas for Limited Sector Scanning

A great many applications require electronic beam scanning over small scan sectors, typically ± 7 to 10° . These applications include fire control systems, weapons locators, air traffic control radars, microwave landing systems, and synchronous satellite communications antenna. A major requirement for each is the need for high gain coupled with rapid electronic scanning. Since the cost of a large conventional array would be prohibitive for most of these systems, there has developed a new class of antenna technology, called limited scan antennas. These antennas compromise wide angle scan capability for reduced system cost. Often these systems involve other compromises, for they have few controls as compared with conventional arrays, and are limited in the quality of pattern that can be maintained as a function of scan. Thus sidelobe degradation, gain falloff, and narrow bandwidth are also likely consequences of scanning this class of antenna; but with all these limitations, the cost advantages of limited scan antennas has made them a fruitful and growing area of array technology.

A special class of limited scan antennas is called "hybrid scan" systems and consists of an electronically scanned array combined with a radiating aperture, a reflector or lens, which will be referred to as the objective aperture. The hybrid system may also include another structure, perhaps a second lens, multiple beam matrix, or sub-reflector. Systems of arrays with mechanically scanned reflectors or lenses are excluded from this description.

A number of research and development programs have investigated antennas for limited sector scan, and have developed guidelines for design and means of comparing various antenna types. Some of the parameters that can be determined from the gain and scan sector are the size of the radiating aperture, the number of required control elements, and the bandwidth. This section will describe principles that determine these system characteristics.

For any array or hybrid system there is a minimum number of controls required for scan over a given scan volume, and that number is approximately the number of beamwidths within the scan volume. Awareness of this criterion allows the designer to optimize various antenna parameters, to minimize system cost or the size of the array or final aperture, or to reduce the radiated sidelobes. A measure of the minimum number of array elements is contained in the definition of a parameter introduced by Patton [143] and called "element use factor." This parameter is N/N_{\min} where N is the actual number of phase shifters in the control array, and N_{\min} is the minimum number of control elements. Patton defined this minimum for an array scanning in one plane as one of the fac-

tors in the expression below. The expression given is for a rectangular array with a rectangular scan sector.

$$N_{\min} = \left(\frac{\sin \theta_{\max}^{(1)}}{\sin \left[\frac{\theta_3^{(1)}}{2} \right]} \quad \frac{\sin \theta_{\max}}{\sin \left[\frac{\theta_3^{(2)}}{2} \right]} \right). \quad (78)$$

$\theta_{\max}^{(1)}$ and $\theta_{\max}^{(2)}$ are the maximum scan angles in the two planes measured at the peak of each beam and $\theta_3^{(1)}$ and $\theta_3^{(2)}$ are the half-power beamwidths in these planes.

Several authors have given derivations of similar minimum criteria, notably Stangel [144] and Borgiotti [145]. The analysis given here is intended only to develop some insight into the condition and its implications.

If one considers an aperture in one plane with overall length D and chooses to develop a method for synthesizing a desired radiation pattern within the angular sector $-u_{\max} < u < u_{\max}$, one can achieve that synthesis by constructing the pattern from a finite sequence of orthogonal beams. If the array of length D , consisting of N elements spaced d_x apart has its n th element excited by the coefficient

$$a_n = e^{-j(2\pi/\lambda)d_x u_i n} \quad (79)$$

corresponding to a point u_i in $\cos \theta$ space, the resulting far field pattern is given by

$$g_i(u) = N g_e(u) \frac{\sin \left[\frac{N\pi d_x}{\lambda} (u - u_i) \right]}{N \sin \left[\frac{\pi d_x}{\lambda} (u - u_i) \right]} \quad (80)$$

where $g_e(u)$ is the element pattern.

This radiation pattern has the special characteristic that it is one of an orthogonal set of pencil beams ($g_i g_m^* = \delta_{im}$) if the interbeam spacing u_i is chosen such that

$$u_i = \frac{\lambda}{D} i = \frac{1}{N} \frac{\lambda}{d_x} i$$

and

$$i, n = \pm \frac{1}{2}, \pm \frac{(N-1)}{2}. \quad (81)$$

In addition to orthogonality, the beams have the characteristic that the beam with index i has its maximum at u_i , and has zero at any other value, u_j for j within the set defined above. Thus it is possible to synthesize a shaped beam pattern

$$g(u) = \sum_i g_i(u_i) a_i \quad (82)$$

by matching the value of the i th beam to the desired pattern at the angle denoted by $u_i = \sin \theta_i$. Since only one beam has a nonzero value for a particular choice of i , the synthesis is performed by exactly matching the required pattern at N points, with N constituent beams of the orthogonal set. This type of synthesis was developed by Woodward and Lawson [146], and is described in some detail in a number of texts [147]. For an aperture of electrical length D/λ , N beams will fill a sector of width $(N-1)\lambda/D$ in $\sin \theta$ space. A given shaped pattern within this sector can thus be matched at N points by N separate controls, assuming a network that can switch between the various beams. Thus the minimum number of con-

trols required to form or scan a beam within the given sector is equal to the number of pencil beams within the sector, which is essentially a restatement of (78).

Another convenient form of (78) that is particularly applicable to arrays of large elements or subarrays is derived below.

The outermost beam of the set has its peak value at:

$$u \frac{N-1}{2} = \frac{\lambda}{2d_x} \frac{N-1}{N} = \sin \theta_{\max} \quad (83)$$

and the phase progression between elements for this beam is

$$\Delta = \pi \left(1 - \frac{1}{N} \right). \quad (84)$$

There can be no beam with $\sin \theta$ larger than this, because if there were it would have a grating lobe that would be of significant size and would contribute to a loss of gain and pattern ambiguity. Equation (84) also implies a minimum number of control elements necessary for an array by stating that the array can be scanned to one half a beamwidth of the angle of grating lobe onset. For N large, the array has the scan limit

$$\frac{d_x}{\lambda} \sin \theta_{\max} = 0.5 \left(1 - \frac{1}{N} \right) \approx 0.5 \quad (85)$$

and the minimum number of controls for large N is

$$N_{\min} = \frac{N(d_x/\lambda) \sin \theta_{\max}}{0.5}. \quad (86)$$

This equation is equivalent to the condition in a one-dimensional version of (78) upon assuming an approximate beamwidth λ/Nd_x .

For narrow beams and a rectangular scan sector, the element use factor can be written in the form

$$\frac{N}{N_{\min}} = \frac{0.25 \lambda^2}{(d_1 \sin \theta_{\max}^{(1)}) (d_2 \sin \theta_{\max}^{(2)})}. \quad (87)$$

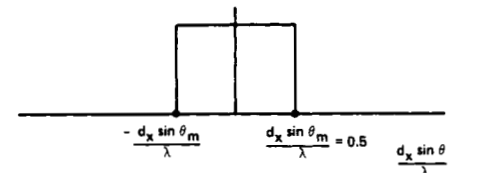
The nature of the controls implied by the above criterion has not been stated. However one could imagine various sorts of switching networks to access ports of a network that excites individual orthogonal beams. The most obvious type of limited scan antenna is obtained by simply using oversize antenna elements or subarrays as shown in Fig. 40, and scanning these as far as possible. Unfortunately, the use of large elements implies the existence of many grating lobes in real space, and these may represent significant sidelobe energy unless some action is taken to suppress the sidelobes. Patton [143] and Manwarren [148] have used randomized element locations for this purpose and Mailloux [149] has investigated the use of higher order aperture modes for grating lobe cancellation. Another approach is to attempt to synthesize element patterns that approach the "ideal" pattern shape of Fig. 40(b). This pattern shape is chosen to have a constant gain function over the desired scan range (the $\cos \theta$ factor is neglected because of the scan angle limitation), and zero gain outside of the scan range for grating lobe suppression. For scan to the maximum angle $\theta_{\max} > 0$, the nearest grating lobe is at

$$\sin \theta = \sin \theta_{\max} - \frac{\lambda}{d_x}$$

and so the maximum width of the ideal element pattern that still gives perfect grating lobe suppression is chosen so that for



Oversize Elements or Subarrays for Limited Sector Scan



"IDEAL" ELEMENT PATTERN FOR LIMITED SCAN SYSTEM
($\cos \theta$ SUPPRESSED)

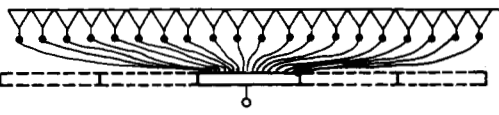
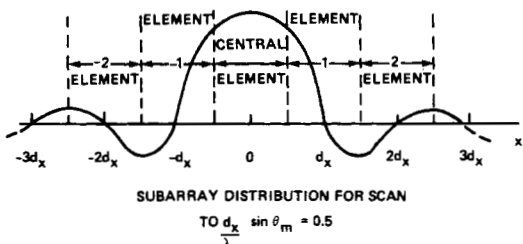


Fig. 40. Ideal subarray pattern for limited sector coverage.

a very large array

$$\frac{d_x}{\lambda} \sin \theta_{\max} = 0.5. \quad (88)$$

This condition is identical to (85), although that expression was related to the limitations of the set of orthogonal beams.

Unfortunately it is not possible to synthesize this ideal element pattern with an element of width d_x , for one can show that the ideal pattern requires an amplitude distribution (Fig. 40(c)) that extends over a large number of elements, and has the form

$$\frac{\sin(\pi x/d_x)}{\pi x/d_x}.$$

One can try to approach synthesis of an ideal element pattern only by building a network that connects each input port with a subarray of many elements. Since this is so for each input port the subarrays overlap and can approximate the complex distribution of Fig. 40(c). The most successful examples of overlapped subarray synthesis to date have been achieved using space fed subarrays [150], and will be described later in this section and in Section IV-B, where they are referred to as dual transform systems. The concept is described in the review article by Tang [150], who addresses mainly the application of overlapped subarrays to broad-band scanning arrays. Among the several references to synthesis of overlapped subarray networks, there is a generalized analytical study by Dufort [151] and a specialized development by Mailloux [152] of a network for forming an overlapped sub-

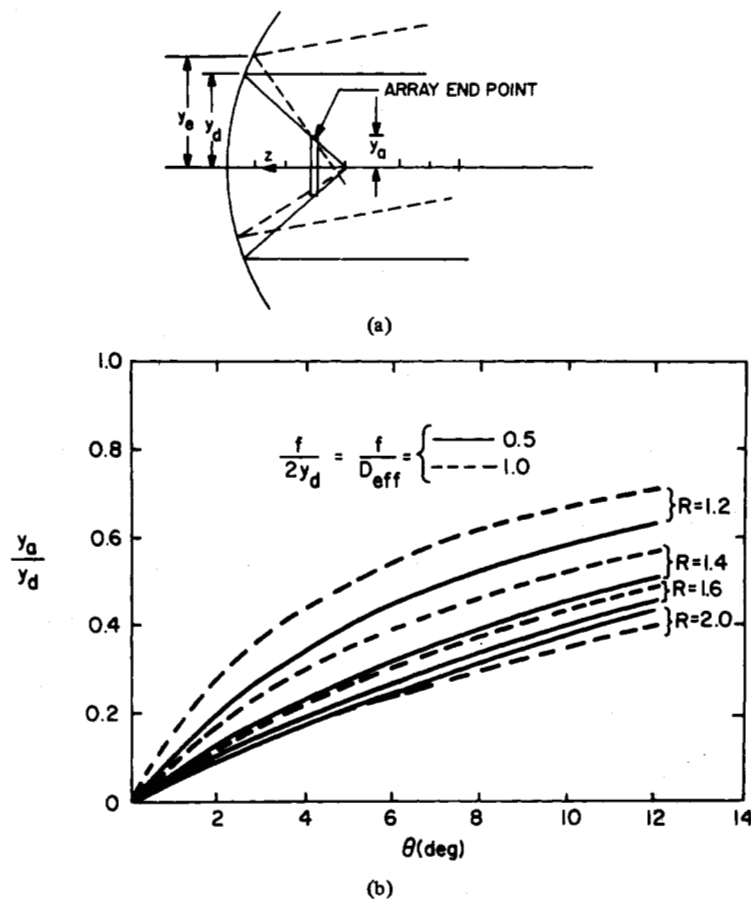


Fig. 41. (a) Off-axis parameters of array-reflector limited scan system (array-reflector geometry and ray trajectories at scan limit). (b) Off-axis parameters of array-reflector limited scan system (normalized array size versus scan angle).

array for oversize apertures excited with higher order modes for limited sector scanning.

One of the earliest forms of limited scan hybrid systems consists of an array used as a transverse feed for a reflector (or lens) antenna. The array is located a distance less than the focal length from the reflector and so the objective aperture serves to project the incoming received wavefront onto the array face, but does not focus it at the array. The system converts the incident wavefront to a converging wavefront at the array, and a tapered array distribution transforms it to a more or less equally tapered aperture illumination. A key feature of such systems is that the objective must be large because the scanned array illuminates a spot that moves across the main aperture as a function of scan. Design is usually based upon the criterion that the array aperture illumination be the complex conjugate of the received field distribution for an incident plane wave (see Assaly and Ricardi [153] and Winter [154]). This places a minimum limit on the size of the array because the usual requirement to scan with phase only requires that the array must be outside of the region of nonuniform fields near the focus. Beginning in the early 1960's, the use of such a transverse feed was investigated by a number of authors, and has proven to be one of the more effective means of providing limited sector scanning of reflector antennas.

Winter [154] described a flat array feed for a parabola similar to that shown in Fig. 41(a) and achieved 7 beamwidths of scan with *E*-plane sidelobes approximately -15 dB relative to

the main beam in the *E*-plane, and approximately -10 dB in the *H*-plane. A more recent study is described by Tang [155] and Howell [156]. Array size, location, and approximate phasing are usually computed by geometrical optics. Tang gives an equation for the percentage of blockage as a function of reflector size, illuminated diameter scan angle, and focal length, and points out that sidelobe ratios on the order of -18 dB for a design of this type can be achieved with reasonable size reflectors, but if one insists on sidelobes lower than -20 dB a much larger main reflector must be chosen.

The relevant geometric constraints are shown in Fig. 41(a) for a symmetrical (parabolic) reflector with focal length f and an array feed of size $2y_a$. Two rays cross at the top of the array. The lower ray at an incident angle θ is reflected at y_d , and passes through the focus. The second ray is incident at an angle θ , and after reflection crosses the first ray path at the array edge. The condition for determining array size is to choose the array so that it intercepts all the reflected rays that come from the active region on the reflector for all up to the maximum scan angle. The figure shows that the illuminated region must be allowed to move, to fully utilize the array for all scan angles. Choice of a large y_e tends to make the array smaller. The resulting array size $2y_a$ is given in terms of the other reflector parameters and the given scan angles as

$$\frac{y_a}{y_d} = 1 + K_1 \quad (89)$$



Fig. 42. Precision approach radar antenna AN/TPN-19 (courtesy of Raytheon Corporation).

where

$$K_1 = \left\{ \frac{g_2(y_e, \theta) \left(\frac{y_e - y_d}{f} \right) + g_1(y_e, \theta) \left[\left(\frac{y_e}{2f} \right)^2 - \left(\frac{y_d}{2f} \right)^2 \right]}{g_2(y_e, \theta) y_d + g_1(y_e, \theta) \left[\left(\frac{y_d}{2f} \right)^2 - 1 \right]} \right\} \quad (90)$$

and where

$$g_1(y, \theta) = \left[\left(\frac{y}{2f} \right)^2 - 1 \right] \sin \theta - y \cos \theta$$

$$g_2(y, \theta) = \left[\left(\frac{y}{2f} \right)^2 - 1 \right] \cos \theta + y \sin \theta.$$

Fig. 41(b) shows the resulting normalized array size as a function of maximum scan angle θ for two effective focal length ratios, $f/2y_d = 0.5$ and 1.0, and several values of the allowable spot motion ratio $R = y_e/y_d$.

This result, equivalent to that derived by Tang [55] can be used to estimate reflector and array size and location for a given coverage sector and hence to evaluate gain reduction and sidelobes due to blockage. In addition, it leads directly to an estimate of the element use factor. A reflector scanning a rectangular angular sector $\theta_1 \times \theta_2$ radians, using effective aperture sizes y_{d_1} and y_{d_2} , and array element spacings a_1 and a_2 has an element use factor (78) of:

$$\frac{N}{N_{\min}} = \frac{0.25}{\theta_1 \theta_2} \frac{y_{a_1}}{y_{d_1}} \frac{y_{a_2}}{y_{d_2}} \frac{\lambda^2}{a_1 a_2}. \quad (91)$$

For example, a square 10° scan sector and a square section of a parabola with $f/2y_d = 1$ has $y_a/y_d = 0.44$ (for $R = 1.6$), and with 0.7λ array element spacing in both planes the resulting element use factor is 3.28. The above analysis serves as a

rough guide to estimate array size and system performance, and demonstrates that single reflector and array hybrid systems require a relatively large array and an oversize reflector. Hence, if they are designed with on-axis feeds they suffer blockage that ultimately limits their sidelobe ratio.

The need for improved pattern performance has led to offset array structures with reduced aperture blockage and lower sidelobes. Notable among these is the Precision Approach Radar antenna of the TPN-19 GCA system shown in Fig. 42. The antenna has 1.4° azimuth beamwidth and 0.75° elevation beamwidth, and scans ± 9.5 beamwidths in elevation and ± 6.65 beamwidths in azimuth. The array uses 824 phase shifters, and so has an element use factor of approximately 3.25. The first sidelobes are at the -20 dB level throughout most of the scan sector, rising to -18 at the limits. The system operates over a 2 percent bandwidth at X-band, and has a realized gain of approximately 39 dB at the scan limits. Since the main reflector size is about 3×3.8 m this corresponds to an aperture efficiency of approximately 30 percent. The low aperture efficiency is the result of the illuminated spot moving across the oversize reflector as a function of scan.

Equation (87) also reveals that if one uses an objective lens or reflector for magnification, then the element factor for the feed array itself can still be unity if the array elements scan to their limit $d/\lambda \sin \theta = 0.5$ in both planes. The maximum scan angle of the array example discussed earlier is approximately

$$\theta_{\max} = \tan^{-1} \left\{ \left(\frac{y_d}{f} \right) \frac{\left(\frac{y_e}{y_d} - 1 \right)}{\left(1 - \frac{y_a}{y_d} \right)} \right\} \quad (92)$$

which is 24.5° for the example previously considered. Assuming a rectangular scan sector and rectangular reflector, and 0.7λ spacing for the array elements, the element use factor is

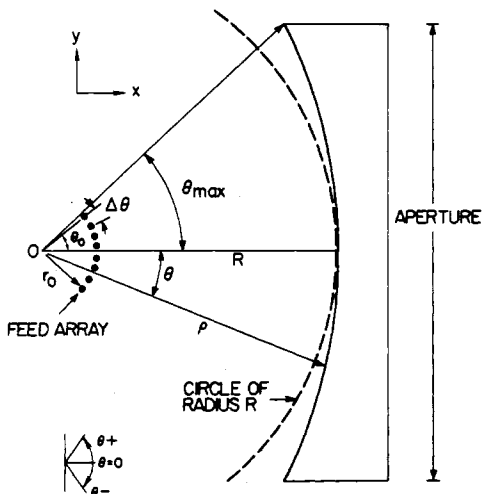


Fig. 43. Scan corrected lens antenna (after McGahan [158]).

computed by (92) and (87) to be 2.98, which is relatively close to the exact number evaluated from (91). This result is obtained without considering any details of the reflector surface, and is based only upon the array scan limits, but it illustrates how dominant a part is played by these purely geometric constraints.

Thus the reflector-array hybrid system needs a relatively large number of phase controls because one cannot scan over the extremely wide sector ($\pm 45^\circ$ for 0.7λ array spacing in the example above) to obtain a low element use factor. Attempts to scan that wide a range would necessarily mean inefficient use of the main objective.

Further advances with reflectors of this type could result from the use of special limited scan array feed techniques designed to have an element use factor nearer unity for the narrow scan ranges required to steer a reflector.

In addition to transverse fed reflector systems, it is possible to develop advanced scanning systems with array fed lens structures. One such concept has been proposed by Schell [157] and recently implemented by McGahan [158]. The antenna uses an array disposed around a cylinder to scan a reflector or lens surface that is contoured according to an optimum scan condition, rather than a focusing condition. The reflector is then stepped or the lens phase corrected to achieve focusing. In one plane of scan the technique achieves an element use factor of about unity, while using an oversize final aperture to allow motion of the illuminated spot. Typical aperture efficiency is 20–25 percent.

Fig. 43 shows a schematic view of an array-lens implementation of this concept. The array element currents are equal in amplitude and have a progressive phase given by $\beta n \Delta\theta$. The reflector surface (or lens back face) is chosen to transform this phase variation into a linear wavefront normal to the beam direction.

In addition to requiring few phase controls, this geometry can have very low sidelobes since the amplitude distribution on the array is transferred very simply onto the inner lens surface. Theoretical results indicate that with perfect phase and amplitude control this structure can have sidelobes below -40 dB.

Most single reflector or lens structures with a phased array feed are simple but require a relatively large number of phase controls and oversize apertures. Dual reflector systems have been developed for scanning over wider angles with small, high efficiency primary apertures. Several of the more signifi-

cant of these studies were conducted by Fitzgerald [159], [160] who investigated the scanning properties of near field Cassegranian (Fig. 44(a)) and offset fed Gregorian (Fig. 44(b)) confocal paraboloid configurations. Both geometries could scan many beamwidths with good efficiency but the off-axis configuration exhibited better sidelobe performance because of reduced blockage, and required fewer phase shifters for equivalent scan with an element use factor of about 2.5. Optimizing the main and subreflector contours can improve the scan characteristics of this system and reduce the element use factor to about 2.

More recent studies have sought to increase the aperture efficiency by allowing movement of an illuminated zone on a subaperture and to decrease element use factors by maximizing the phased array scan. McNee *et al.* [161] performed a theoretical and experimental study of a limited scan system consisting of a main reflector, a multiple beam forming system, and a phased array. Shown schematically in Fig. 44(c), this concept has its earliest roots in the subarraying systems to be described in Section IV-F, but the geometry is very similar to the Gregorian subreflector antenna of Fitzgerald. The element use factor is much smaller than that of Fitzgerald because the array is made to scan over a wide angle in accordance with the principle of (91). The additional scan is possible because the feed lens is made very large (approximately 0.65 the size of the main reflector) compared to the subreflectors of Fitzgerald (0.25 to 0.350) and so the structure is considerably more bulky. Analytical results for a spherical lens feed system indicate that a 1° beam can be scanned over a $\pm 10^\circ$ sector with sidelobes at -20 dB and with an element use factor approximately 1.4.

More recent examples of dual reflector technology relate to satellite antennas with limited sector coverage corresponding to the earth's subtended angle at synchronous altitude. Bird *et al.* [162] describe a dual reflector offset Cassegrain system using an array of circular waveguides as a feed. The array is excited in clusters so as to match the complex distributions required for reducing cross-polarized components of radiation while maintaining good aperture efficiency. This theoretical study addressed the problem of forming individual beams for a satellite system with polarization isolation between beams. Dragone and Gans [163] studied several multiple reflector systems for satellite communication including a Gregorian arrangement of offset confocal paraboloids with a small phased array, and a three-reflector offset system consisting of a paraboloid objective, a hyperboloid subreflector, a second paraboloid subreflector, and an array feed. The three-reflector system was then adapted to use a quasi-optical frequency diplexer and so permit two separate array feeds to excite the structure at 12 and 14 GHz. These and other new efforts addressing the needs of satellite systems show that there remains substantial room for innovative use of array reflector hybrid systems.

Several dual-lens configurations show promise of providing high quality performance over limited angular sectors. The first is the structure shown in Fig. 44(d), which was investigated by Tang and Winter [164] using a computer simulation. The array focuses a small spot on the elliptical rear face of a lens which transfers the spot to a region of the focal arc of a final lens with spherical backface. Sidelobes are at approximately the -16 dB level for $\pm 10^\circ$ scan. The aperture efficiency is about 60 percent, the element use factor is 1.5, and although the L/D ratio is at least 1.7, the main aperture diameter D is small because of its efficient illumination. The intermediate lens is about 0.7 the size of the final lens.

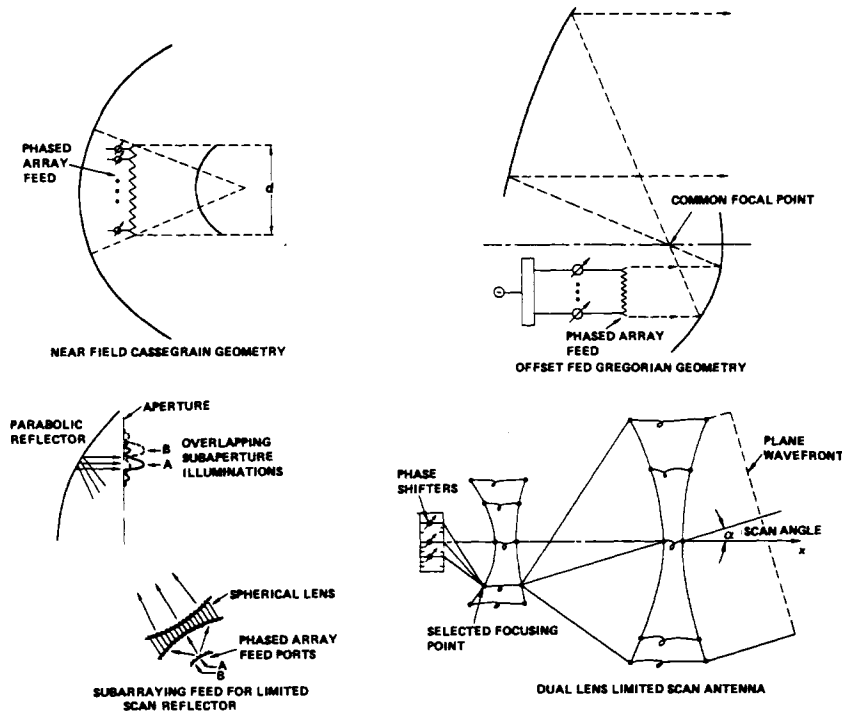
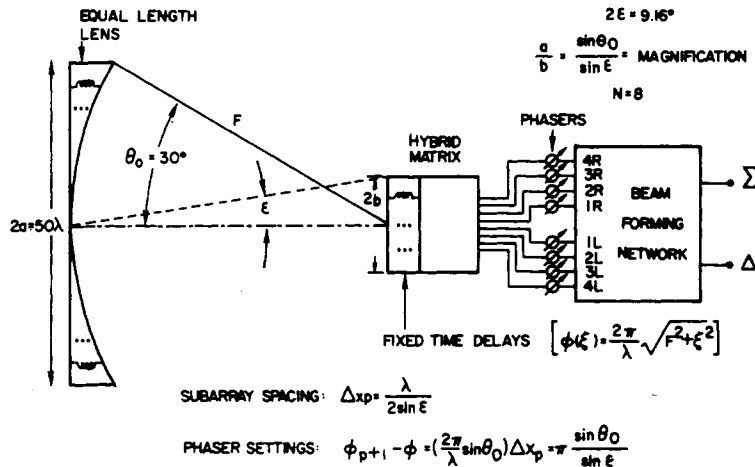


Fig. 44. Systems for limited sector scanning.



A recent investigation by Borgiotti [165] included an analytical and numerical evaluation of the dual transform antenna system of Fig. 45 for one-dimensional limited sector scan. This system is similar to the completely overlapped subarraying system described by Tang [150] but in this case there are no control elements in the final aperture. The number of control elements used is approximately equal to the theoretical minimum. The system uses a hybrid matrix and a "bootlace" lens with linear outer profile and circular inner profile to perform the two spatial transforms required for subarray formation. The geometry is also similar to that studied by McNee *et al.* [161] but with the lens objective instead of the reflector. Borgiotti presents a number of design details to facilitate parameter selection.

Fig. 46 shows a typical subarray pattern for the example studied by Borgiotti and the radiation pattern at broadside.

Notice that the near sidelobes are at the level given by the array taper and scan condition, but sidelobes and grating lobes beyond the subarray field of view are substantially suppressed. This illustrates the obvious advantages of subarraying to suppress the far sidelobes associated with phase shifter tolerances or quantization errors. The array can thus be scanned to any point within the subarray sector with good radiation characteristics.

Taken collectively, this class of limited scan system constitutes one of the major application areas of phased array activity. Most of the antenna systems described here are not yet compatible with the very low sidelobe requirements of future military systems and this remains a key area for future development. Other required developments will include broadband operation, the use of adaptive feed controls for null placement, and variable sidelobe control of hybrid systems.

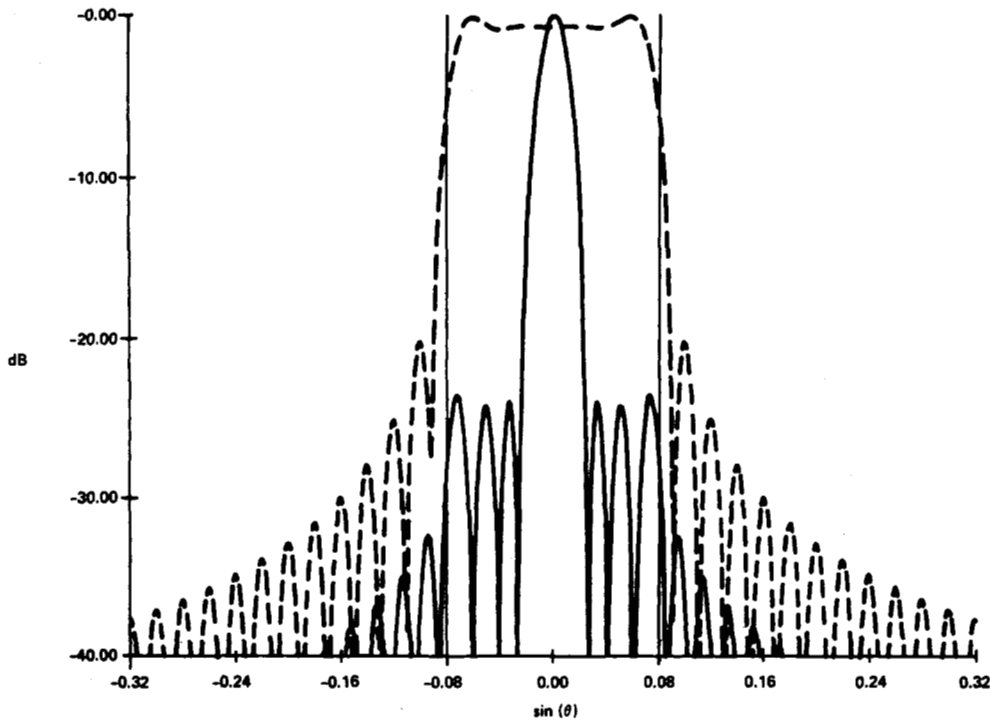


Fig. 46. Radiation pattern and subarray pattern (dashed) of overlapped subarray system (after Borgiotti [165]).

D. Wide-Band Feeds for Phase Scanned Arrays

Section I described the bandwidth limitations of phase scanned arrays as being particularly severe for large arrays. Conventional subarraying schemes with time delay at the subarray level do remove some of the bandwidth limitation, but often at the expense of increased system loss and high peak or average sidelobe levels. Two techniques for overcoming this limitation are introduced in the following section.

1) *Multiple Beam Lens Feeds:* An alternative method of designing phased array antennas which does not make use of variable time delay units has been proposed by Rotman and Franchi [166]. The concept was first derived as a two-dimensional lens configuration (azimuth scan correction only) and later extended to three dimensions (both azimuth and elevation scan correction). The basic idea is to select one of several beams in a wide-angle microwave lens antenna which would each be properly focused to point in different directions in the absence (or zero setting) of the phase shifters. Each beam can then be scanned about its zero phase shift position by means of the phase shifters at each radiating element in the lens, with a greatly enhanced bandwidth.

This concept is illustrated in Fig. 47 which shows four feed horns equally spaced along the focal arc of a two-dimensional microwave constrained lens. Energy from a transmitter can be directed to any one of the horns by means of the switching tree. Each horn, in turn, will form a beam in a different azimuth direction for the zero phase shifter setting. A typical beam for the M th horn is sketched as the solid curve (M th beam). In illumination by the phase shifters, the beam scans to either side of its no phase shift position, as illustrated by the dotted curve (phase scanned M th beam). The bandwidth limitation imposed by this phase scanning is given by (27) with θ_0 the maximum scan angle, and N the number of beam positions (4 for the example in the figure). The system bandwidth,

BEAM STEERING IN A MULTI-FEED LENS

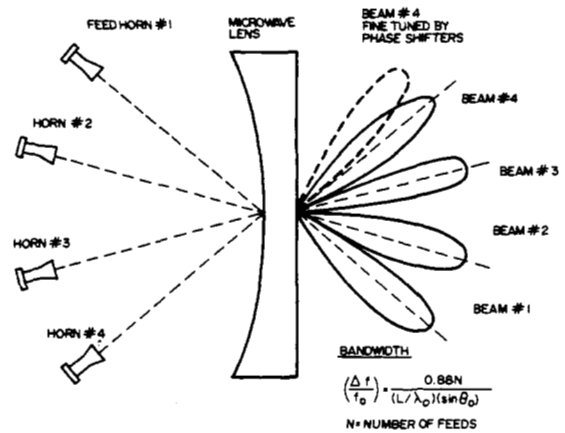


Fig. 47. Multiple beam feed for wide-band array.

given below, is wide because of the limited scan angle

$$\frac{\Delta f}{f_0} = \frac{0.88N}{(L/\lambda_0) \sin \theta_0}. \quad (93)$$

Although the illustration shows a two-dimensional configuration, Rotman and Franchi have also investigated various three-dimensional antenna concepts with limited scanning in one plane and wide angle scanning in the other. A full three-dimensional multiple beam configuration is also possible. This antenna depends upon the quality of focusing achievable with the various beams, as well as internal system reflections. In addition to potential low sidelobe behavior it is also possible to perform null steering with a system of this type by using available beams as sidelobe cancellers, much as has been done with fixed multiple beam lens systems.

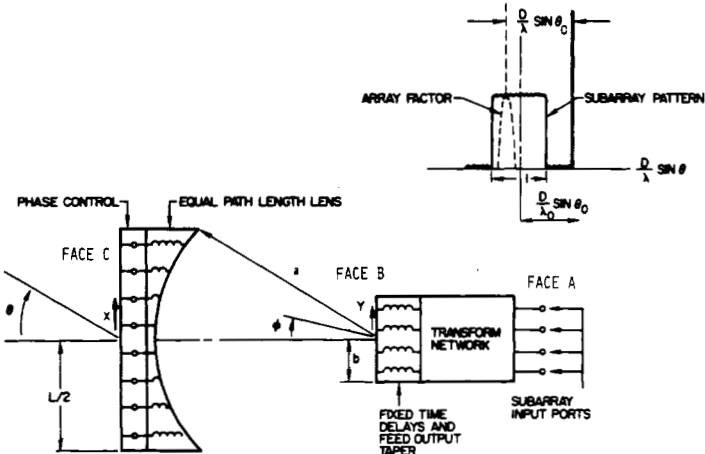


Fig. 48. Overlapped subarray feed for wide-band array.

2) Subarray Feeds for Wide Bandwidth and Pattern Control:

The various subarraying systems used for limited sector scanning can also be used with time delay devices and phase shifters to form high quality time delayed subarrays for broad-band operation. In particular the use of dual transform systems as broad-band array feeds predates [150], [167] their use as limited scan antennas and may yet be their most important application. Two-transform scanning antennas are so called because the applied excitation is subject to two spatial Fourier transforms that create the aperture illumination at the face of the phased array.

Fig. 48 shows the basic dual transform configuration. Antennas of this type have significant advantages in terms of scanning characteristics, main aperture size, element use factor (array size), and sidelobe levels. The superior sidelobe characteristics result from two factors. First, the taper imposed upon the array is translated to the main aperture and so the aperture illumination can be carefully controlled. Second, the action of the several transforms is to form a subarray at the main aperture, and the subarray radiation pattern provides further suppression of certain sidelobes. In addition, two-transform systems possess convenient properties that allow correction for surface tolerance errors in the objective, broadbanding, null steering, and adaptive pattern control at the subarray levels [168]-[170].

The basic circuit for a space fed dual transform system is illustrated in Fig. 48 using a one-dimensional circular lens of radius "a" and fixed time delays at the hybrid matrix output for subarray collimation. This specific implementation was proposed by Borgiotti [165] for the subarraying system that scanned over a limited spatial sector (Section IV-E), but here the main array has phase shifters to produce a phase tilt that scans the subarray pattern. The feed is a Fourier transformer in the form of a hybrid matrix or multiple beam lens whose purpose is to form a group of N equally spaced illumination functions (subarray illuminations) across the main array. Each function corresponds to one beam of the multiple beam feed and is therefore controlled by an individual feed input port. The main lens aperture illumination function corresponding to the p th subarray is approximately the far-field radiation pattern of the feed array evaluated at the back of the cylindrical lens, and hence, is the Fourier transform of the field array output illumination. This represents the second transform of the system.

System operation can be understood by realizing that there are two transforms within the system and that the resulting far field pattern is the Fourier transform of the main aperture illumination, so there are a total of three transforms between the input illumination and radiation pattern. As noted above, each port at face A excites one beam that illuminates face C, and so excites a subarray with maximum weighting at the beam peak, but extending across all of face C. Each subarray overlaps every other. Phase shifters in face C scan the radiated pattern of all subarrays. Because of the dual transform relationship, the subarray radiation pattern should be the same as the face B illumination apart from appropriate scaling factors and diffraction effects.

One can show that the subarray pattern is essentially zero outside of the angular region give by

$$-\frac{b}{a} \leq \sin \theta - \frac{\lambda}{\lambda_0} \sin \theta_0 \leq \frac{b}{a} \quad (94)$$

and that one can select the parameters b and a to suppress the grating lobes of the steered array by acting as a scanned angular filter. The subarray pattern of Fig. 49 provides this control which is shown as a flat topped sector pattern because no tapering is assumed at face B. Since this pattern is the same as the face B illumination it is possible to place nulls in the subarray pattern or lower the sidelobes for all subarrays by changing the illumination at face B. These topics are of intense current interest because of their possible application to wideband null steering and ultra low sidelobe pattern control.

Time delay units are used at the subarray input ports and the illumination is tapered across face A to produce a low sidelobe array factor with no beam squint. The system bandwidth is thus determined by the squint of the subarray pattern across this fixed time delayed beam, and for a very large array with $\theta_c \neq \theta_0$ the bandwidth is given approximately by $1/S_0$ where

$$S_0 = \frac{D}{\lambda_0} \sin \theta_0. \quad (95)$$

Dual transform systems offer the potential of adaptive or deterministic control at either face A or B. Control at face C is always possible but since there are many more elements at face C it is usually thought more convenient to perform this function at A or B. At face A conventional algorithms for adaptive arrays can produce nulls in the array factor. Pattern

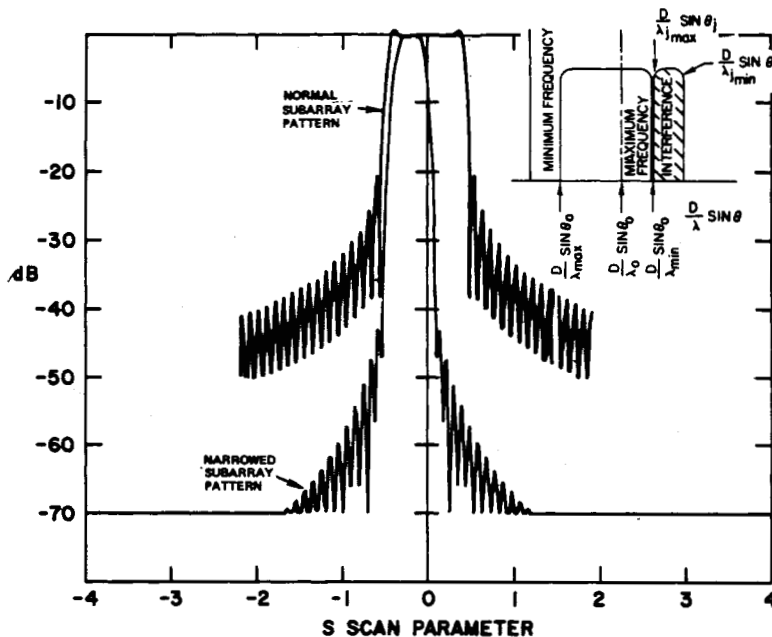


Fig. 49. Subarray pattern modification for interference suppression.

control at face *B* results in nulled subarray patterns or narrowing the pattern to exclude jammer reception at specific locations and frequencies. For example, Fig. 49 indicates that if an interfering signal radiates at some angle θ_j (with $\theta_j > \theta_0$ in this case), and if the interfering signal frequency is bounded $\lambda_{j\min} < \lambda_j < \lambda_{j\max}$ then the interfering signal is received over a distributed angular region of the subarray pattern, and indeed over proportionally the same distributed region of the feed. The interfering signal can be rejected if the subarray pattern is narrowed to satisfy the condition at the highest system frequency ($f_{\max} = c/\lambda_{\min}$)

$$\frac{\sin \theta}{\lambda_{\min}} < \frac{\sin \theta_j}{\lambda_{j\max}}. \quad (96)$$

This restriction is achieved by narrowing the radiating part of the subarray feed [170], and such pattern control could be implemented either adaptively or deterministically. The adaptive solution might differ in principle from conventional algorithms in that the weighting is applied to the subarray feed aperture, and that it could discriminate on the basis of received frequency and location of the received signal on the feed aperture. Since the received signal from any one point in space is projected to different areas on the feed surface depending upon the source frequency, then by discriminating on the basis of frequency and feed illumination the technique can accommodate null placement in the direction of any interfering source unless it occupies the same frequency spectrum limits and angular locations as the desired source.

Although overlapped subarray systems do offer a degree of control not available with other subarraying systems, the price for including these features in the subarray patterns is reduced bandwidth and increased loss [169] which must be made up using amplifiers at the subarray feed radiating face. One other factor which has not yet been thoroughly explored is that the subarray feed itself must be large enough to provide the high degree of control required by some of these applications. The

number of elements in the feed is important in determining adaptive nulling bandwidth whether the nulling is performed at the input ports (subarray input terminals) or at the output terminals. These issues and the ultimate limits of pattern control with subarray feeds are important areas of present research.

E. Lightweight Microstrip Array Technology

Section III-B describes some of the advances in printed circuit array elements. The basic microstrip elements introduced in that section have found use in a number of lightweight or conformal arrays. Of perhaps more importance is that this class of elements leads to very inexpensive array construction and is wholly compatible with developing monolithic solid-state technology that promises dramatic cost reductions within the near future. Some of the major developments in scanned microstrip arrays are summarized in this section.

Fig. 50 shows an eight-element circularly polarized receive array developed for aircraft tests with ATS-6 [171]. This L-band array, 0.36 cm thick, is scanned in one plane by three-bit switched line phase shifters. The array axial ratio was less than 2 dB over most beam positions and frequencies. The development of special compact elements, such as the shorted quarter wave patch, has reduced element size to the point where even for a two-dimensional array it is possible to keep elements, phase shifters, and feed lines all on one side of the board [172]. Fig. 51 shows such an array with 16 elements producing a measured 15.7 dB gain (compared to the maximum area gain of 17.2 dB) at 4.6 GHz. The beam was scanned to 55° in both *E* and *H* planes, VSWR was less than 2 to 1 at all beam positions, and gain fell off about 1.6 dB at ±100 MHz around the design center frequency.

One method used to gain space is to separate elements and feed with multiple layer construction, using proximity coupled printed circuit arrays [173]. Fig. 52 shows an electrically small, planar antenna composed of microstrip dipoles, electro-

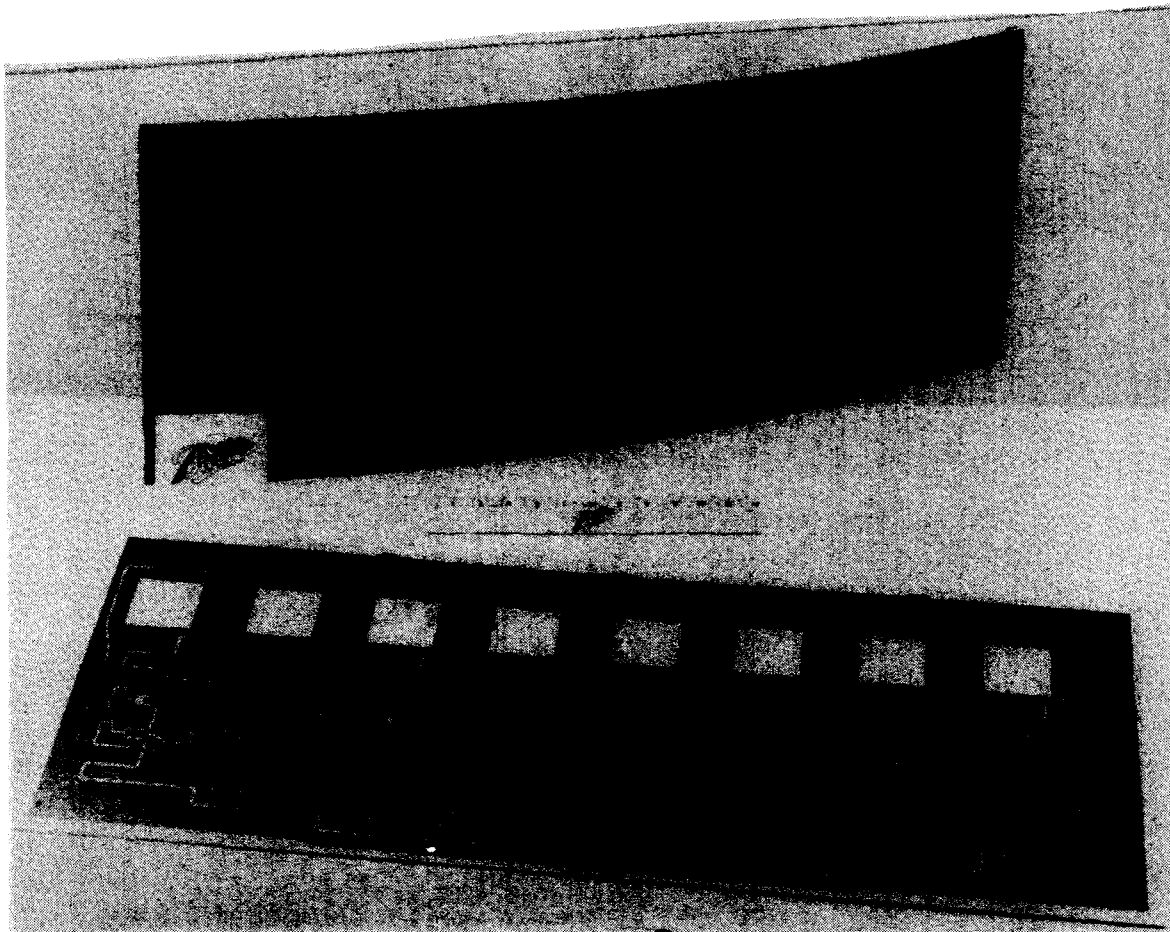


Fig. 50. Conformal array for aircraft tests with ATS-6 (after Sanford [171]).

magnetically coupled to a strip transmission line embedded in the substrate. Separating feed and elements also permits a greater freedom in element placement. The antenna shown is a 3.5λ , X-band monopulse array. The 24 elements are distributed in three rings and a separate corporate feed is used to excite each quadrant. The feed consists of an input three-way power divider, followed by three binary power dividers. Measured gain was 19.7 dB, corresponding to an aperture efficiency of 77 percent, while measured sidelobes were about -17.5 dB.

Phase scanned arrays require additional space for diode phase shifters which are often separated from the elements and placed on a separate board. An array typical [174] of this multi-board technique is shown in Fig. 53 which depicts the construction details of a 2×16 element lightweight phased array, designed to operate at 970 MHz and also to serve as a structural fuselage member of a Remotely Piloted Vehicle. The element spacing is $\lambda/2$ and a uniform excitation is provided by a 16-way stripline power divider. Azimuth scanning of $\pm 60^\circ$ is provided by four-bit diode phase shifters. The array provides a broadside gain of 16.5 dB, -13 dB sidelobes and weighs about 11.5 lbs. The cost and complexity of multi-board arrays can be minimized by using subarrays, in which the array is formed of a number of modules as shown in Fig. 54. Each module contains printed circuit radiators, phase shifters, and air stripline power dividers, all combined together as an integral unit without any interconnecting cables or connectors. For example, phase shifters and duplexing hybrids can be fabricated on an alumina ceramic substrate as a single

integrated subelement in the module. This technique lends itself to high volume production, reduces fabrication costs, and improves reliability. Subelements can be fabricated on different high- K substrates, thus reducing the space required. Proper selection of material can also aid in phase shifter head dissipation.

Large arrays present special challenges to microstrip technology, because of high feed losses. As an example of low loss, large array technology, Fig. 55 shows the Seasat, 1024 element, L-band planar array antenna which was part of a space-borne imaging radar system used for ocean surveillance. Producing a resolution of 25 m, this was one of the largest antennas flown in space. The antenna weighed 103 kg, measured 10.7×2.2 m and produced a gain of 34.9 dB with -12.8 dB sidelobes. The operating frequency was 1275 MHz, and the radiated peak power was 3000 W. The low loss substrate, a honeycomb structure with a measured ϵ_R of 1.18 provided both the required structural strength and a small substrate loss because of the large percentage of voids in the honeycomb. Coaxial cabling was used in parts of the feed network to reduce losses. Overall losses were 2.3 dB.

Microstrip arrays are ideally suited to many applications requiring narrow bandwidth (a few percent), low power, and extreme light weight or conformality. Extension of multilayer techniques will facilitate the synthesis of nulled and very low sidelobe aperture illuminations, the required development of subarray networks for wide-band and high-power operation, and integration with solid-state transmit-receive modules for increased efficiency. There is an immediate and continuing

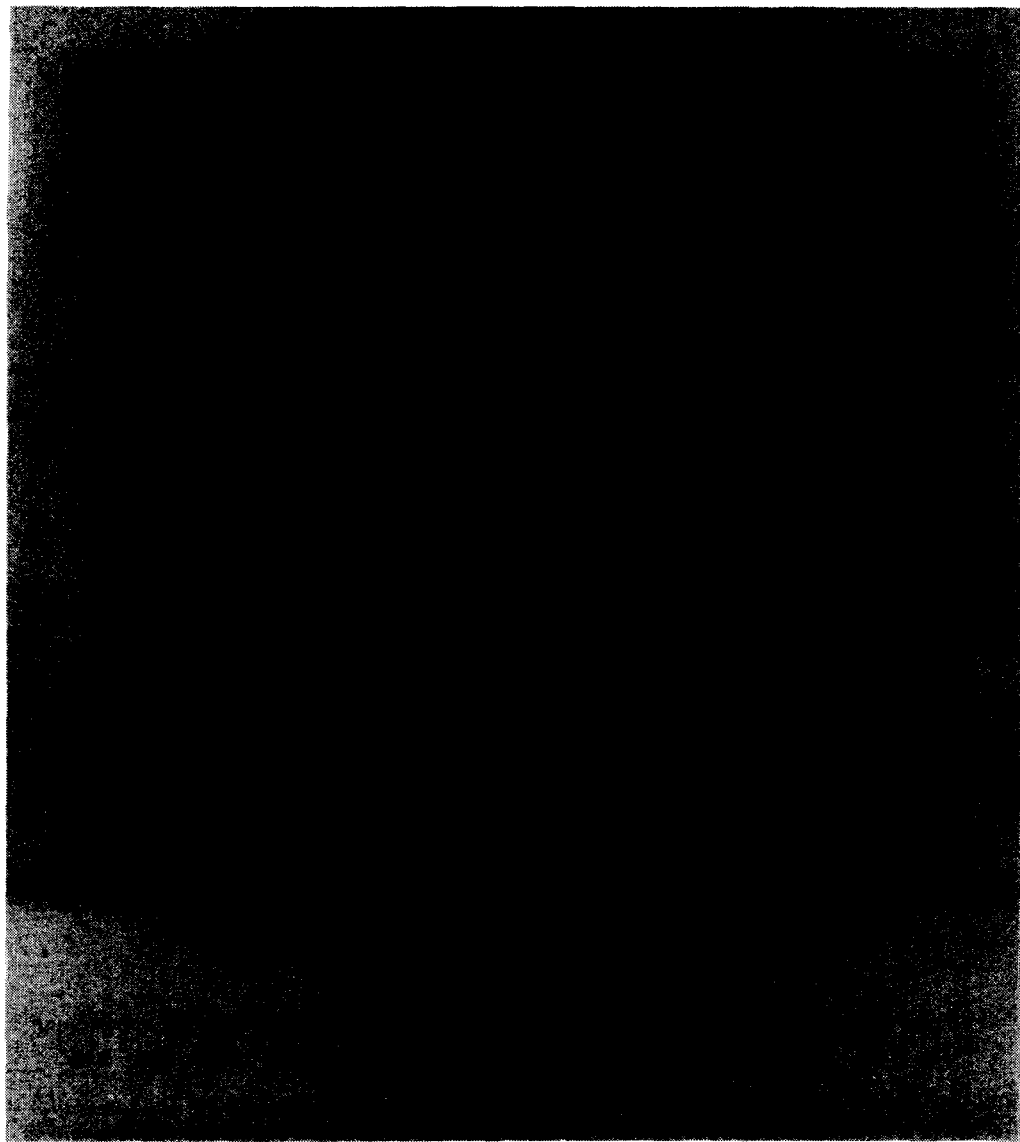


Fig. 51. Single layer microstrip phased array, with elements, phase shifters, bias, and feed lines one side of board (after Munson and Sanford [172]).

need for improved, lower cost, lightweight array antennas that will continue to stimulate development in microstrip arrays throughout the foreseeable future.

V. CONCLUSION

A review paper is a taking of stock, and it is an appropriate time to take stock of phased arrays, for the number and degree of required changes ahead will demand all of today's most advanced technology as basis for the technology of tomorrow.

Solid-state array modules, monolithic array fabrication, digital processing, optical-fiber technology, and a myriad of adaptive processes for arrays are apparently soon to change all but the basic electromagnetic aspects of array antennas. This review has sought to evaluate the electromagnetic bounds to pattern performance and to list a variety of techniques developed that will form a cornerstone of developments to come.

The theory of idealized arrays, though simple, leads to bounds on array characteristics. Many of the fundamental bounds, like bandwidth, beamwidth, and sidelobe level are well established, but other fundamental characteristics such

as null depths and cancellation bandwidth can also be derived from this basic approach.

The detailed analysis of array behavior remains a complex subject; it is described by systems of simultaneous integral or integrodifferential equations, tractable in the infinite limit or for small number of elements. The need for such detailed analysis is increasing because of the growing number of fundamentally new and different array types, the emphasis on small arrays, and arrays with sidelobes so low as to be dominated by edge effects. This paper has sought to emphasize analytical methods compatible with such arrays.

Although there have been vast advances in array development and performance, still there are limits to tolerances and dispersion in phase shifters, power dividers, and feeds that set bounds on currently achievable pattern control, even with traditional coaxial and waveguide components. The use of new transmission lines and devices will make high performance even more difficult to achieve. One example is low profile or conformal array technology where it is becoming apparent that there are fundamental inconsistencies between the components one can develop for such arrays and the requirements for very



Fig. 52. A 24-element proximity coupled microstrip dipole array (courtesy of Ball Aerospace Company).

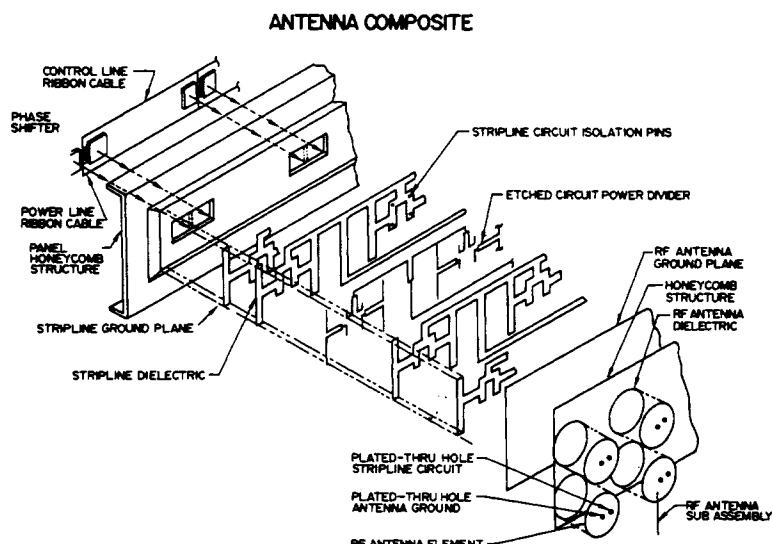


Fig. 53. Construction details of a multi-layer microstrip phased array (after Yee and Furlong [174]).



Fig. 54. A 32-element integrated subarray module at S-Band consisting of 32 disk radiators, 32 diode phase shifters, and 1 air stripline power divider (courtesy of Hughes Aircraft Company).

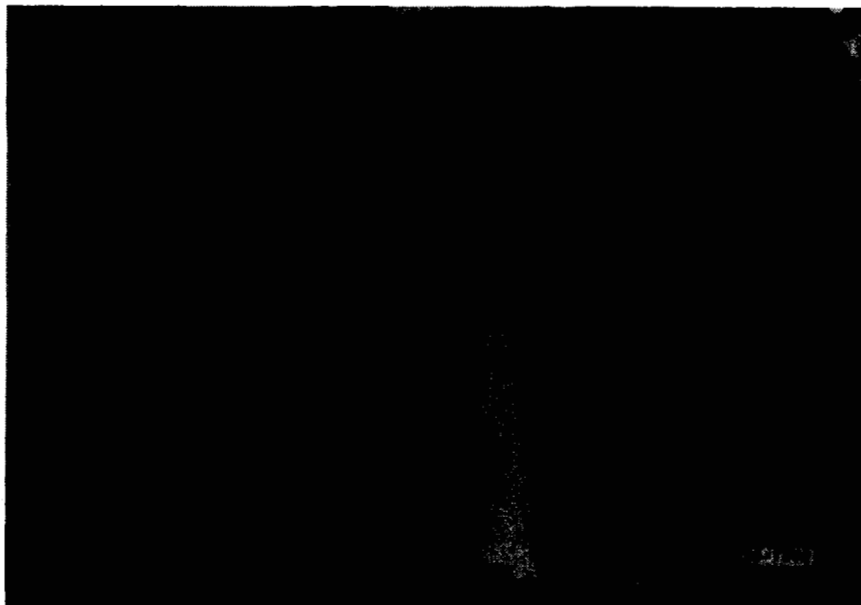


Fig. 55. The Seasat phased array antenna (10.7 X 2.2 m) (courtesy of Ball Aerospace Company).

low sidelobes, wide bandwidth, or wide-band nulls. A second example is the development of low sidelobe systems with amplifiers at each element, where it will be necessary to maintain good phase and amplitude stability, minimum dispersion and in some cases amplitude linearity, over an operating bandwidth.

Finally, although the survey of available technology for light-arrays and arrays for limited sector scanning have uncovered a wealth of technology, most of these systems have relatively high sidelobes and will require substantial advances before these low cost technologies will support the next generation of radar and communication systems.

After about twenty years of serious development one cannot

say that phased arrays are in their infancy. But if they are not, they are at least approaching a period of tremendous growth and change, and the technology of the next ten years will be very different than that of the last. Advances in solid-state devices, optical techniques, and digital logic may soon make arrays more affordable, but under the continuing pressure of military and consumer requirements they will be developed in continually larger numbers even if marginally affordable. Amid this great change in circuitry and technology the basic electromagnetic effects will still govern system performance and will always be the central issues of array evaluation. I have attempted also to make them the central issues of this review.

ACKNOWLEDGMENTS

I am grateful to numerous colleagues for discussions and facts that fill these pages, and for the excellent work that is only dimly reflected here.

In particular I thank the following for providing figures or specific data: A. Albanese of General Electric Co., E. Brookner of Raytheon Corporation, J. Gaeta of RADC, A. Kelley of Hazeltine Corporation, R. Munson and D. Huebner of Ball Aerospace Corp., R. Tang of Hughes Aircraft Co., C. Jones and B. Sickelstiel of Westinghouse Corporation, and J. Yee of Boeing Co.

In addition, I thank the two very conscientious and helpful reviewers of the PROCEEDINGS, as well as Dr. A. Schell and Dr. J. Schindler of RADC for reading the manuscript and for their comments and criticisms, and Mr. J. Dempsey of Air Force Geophysics Laboratory for editing the manuscript.

REFERENCES

- [1] L. Stark, "Microwave theory of phased array antennas—A Review," *Proc. IEEE*, vol. 62, 1661–1701, 1974.
- [2] J. F. White, "Phased array technology workshop," N. R. L., Washington, DC, *Microwave J.*, vol. 24, no. 2, pp. 16–28, 1981.
- [3] A. Forster and J. R. Garrett, "A procedure for estimating the costs of ground-based array radar systems," *Aerospace Rep. TOR-0074 (4484-02)-1*, 1974.
- [4] J. C. Sethares, J. M. Owens, and C. V. Smith, "MSW nondispersive, electronically tunable time delay elements," *Electron. Lett.*, vol. 16, no. 22, pp. 825–826, 1980.
- [5] P. Barton, "Digital beamforming for radar," *Proc. Inst. Elec. Eng.*, vol. 127, Pt. F, no. 4, pp. 266–277, 1980.
- [6] M. I. Skolnik, Ed., *Radar Handbook*. New York: McGraw-Hill, 1970.
- [7] E. Brookner, Ed., *Radar Technology*. Dedham, MA: Artech House, 1977.
- [8] R.W.P. King and C. W. Harrison, *Antennas and Waves, A Modern Approach*. Cambridge, MA: M.I.T. Press, 1969.
- [9] H. Jasic, Ed., *Antenna Engineering Handbook*. New York: McGraw-Hill, 1961.
- [10] C. H. Walter, *Traveling Wave Antennas*. New York: McGraw-Hill, 1965, pp. 121–122 and 322–325.
- [11] R. C. Hansen, Ed., *Microwave Scanning Antennas*. New York: Academic Press, 1966.
- [12] M. T. Ma, *Theory and Application of Antenna Arrays*. New York: Wiley, 1974.
- [13] R. E. Collin and F. J. Zucker, *Antenna Theory*, Parts I and II. New York: McGraw-Hill, 1969.
- [14] N. Amitay, V. Galindo, and C. P. Wu, *Theory and Analysis of Phased Array Antennas*. New York: Wiley Interscience, 1972.
- [15] J. L. Allen, "The theory of array antennas," M.I.T. Lincoln Lab. Tech. Rep. 323, 1963.
- [16] I. J. Bahl and P. Bhartia, *Microstrip Antennas*. Dedham, MA: Artech House, 1980.
- [17] R. A. Monzingo and T. W. Miller, *Introduction to Adaptive Arrays*. New York: Wiley, 1980.
- [18] A. Oliner and G. Knittel, Eds., "Phased array antennas," in *Proc. 1970 Phased Array Symp.*, 1972 (Artech House, Dedham, MA).
- [19] Special Issue on Phased Arrays, *Proc. Inst. Elec. Eng.*, vol. 127, Part F, no. 4.
- [20] Issue on Printed Circuit Antennas, AP-29 (No. 1).
- [21] Special Issue on Printed Circuit Antennas, *IEEE Trans. Antennas Propagat.*, vol. AP-29, 1981.
- [22] Special Issue on Active Adaptive Antennas, *IEEE Trans. Antennas Propagat.*, vol. AP-12, 1964.
- [23] Special Issue on Adaptive Antennas, *IEEE Trans. Antennas Propagat.*, vol. AP-24, 1976.
- [24] W. F. Gabriel, "Adaptive arrays—An introduction," *Proc. IEEE*, vol. 64, pp. 239–272, 1976.
- [25] R. S. Elliott, "The theory of antenna arrays," in *Microwave Scanning Antennas*, R. C. Hansen, Ed. New York: Academic Press, 1966, ch. 1, vol. 2.
- [26] R. J. Mailloux, L. Zahn, A. Martinez, and G. Forbes, "Multiple mode control of grating lobes in limited scan arrays," RADC-TR-76-307, AD A036323, 1976.
- [27] W. H. Von Aulock, "Properties of phased arrays," *IRE Trans. Antennas Propagat.*, pp. 1715–1727, 1960.
- [28] H. A. Wheeler, "The grating-lobe series for the impedance variation in a planar phased array antenna," *IEEE Trans. Antennas Propagat.*, vol. AP-14, pp. 707–714, 1966.
- [29] C. L. Dolph, "A current distribution for broadside arrays which optimizes the relationship between beamwidth and sidelobe level," *Proc. IRE*, vol. 34, pp. 335–345, 1946.
- [30] T. T. Taylor, "Design of line source antennas for narrow beamwidth and low sidelobes," *IEEE Trans. Antennas Propagat.*, vol. AP-3, pp. 16–28, 1955.
- [31] —, "Design of circular apertures for narrow beamwidth and low sidelobe," *IRE Trans. Antennas Propagat.*, vol. AP-8, pp. 17–22, 1960.
- [32] B. J. Strait and K. Hirasawa, "Array design for a specified pattern by matrix methods," *IEEE Trans. Antennas Propagat.*, vol. AP-17, pp. 237–239, 1969.
- [33] R. E. Elliott and R. M. Johnson, "Experimental results on a linear array designed for asymmetric sidelobes," *IEEE Trans. Antennas Propagat.*, vol. AP-26, pp. 351–352, 1978.
- [34] J. F. McIlvanna and C. J. Drane, "Maximum gain, mutual coupling and pattern control in array antennas," *Radio Electron. Eng.*, vol. 41, no. 12, pp. 569–572, 1971.
- [35] C. T. Tai, "The optimum directivity of uniformly spaced broadside arrays of dipoles," *IEEE Trans. Antennas Propagat.*, vol. AP-12, pp. 447–454, 1964.
- [36] D. K. Cheng and F. I. Tseng, "Gain optimization for arbitrary antenna arrays," *IEEE Trans. Antennas Propagat.*, vol. AP-13, pp. 973–974, 1965.
- [37] R. F. Harrington, "Antenna excitation for maximum gain," *IEEE Trans. Antennas Propagat.*, vol. AP-13, pp. 896–903, 1965.
- [38] —, *Field Computation by Moment Methods*. New York: McMillan, 1968.
- [39] S. P. Applebaum, "Adaptive arrays," SPL-TA-66-1, Syracuse University Research Corporation, Syracuse, NY (see also, *IEEE Trans. Antennas Propagat.*, vol. AP-24, pp. 585–598).
- [40] P. W. Howell, "Explorations in fixed and adaptive resolution at G. E. and SURC," *IEEE Trans. Antennas Propagat.*, vol. AP-24, pp. 575–584, 1976.
- [41] B. Widrow, P. E. Mantey, L. J. Griffiths, and B. B. Goode, "Adaptive antenna systems," *Proc. IEEE*, vol. 55, pp. 2143–2149, 1967.
- [42] P.J.D. Gething and J. B. Haseler, "Linear antenna arrays with broadened nulls," *Proc. Inst. Elec. Eng.*, vol. 121, pp. 165–168, 1979.
- [43] F. I. Tseng, "Design of array and line source antennas for Taylor patterns with a null," *IEEE Trans. Antennas Propagat.*, vol. AP-27, pp. 474–479, 1979.
- [44] H. Steyskal, *Synthesis of Antenna Patterns With Nulls*, 1961, in publication.
- [45] G. F. Farrell, Jr. and D. H. Kuhn, "Mutual coupling effects of triangular grid arrays by modal analysis," *IEEE Trans. Antennas Propagat.*, vol. AP-14, pp. 652–654, 1966.
- [46] —, "Mutual coupling in infinite planar arrays of rectangular waveguide horns," *IEEE Trans. Antennas Propagat.*, vol. AP-16, pp. 405–414, 1968.
- [47] H. Levine and J. Schwinger, "On the theory of electromagnetic wave diffraction by an aperture in an infinite plane conducting screen," *Commun. Pure Appl. Math.*, vol. 44, pp. 355–391, 1950–1951.
- [48] P. S. Carter, Jr., "Mutual impedance effects in large beam scanning arrays," *IRE Trans. Antennas Propagat.*, vol. AP-8, pp. 276–285, 1960.
- [49] R. F. Harrington, "Matrix method for field problems," *Proc. IEEE*, vol. 55, pp. 136–149, 1967.
- [50] A. J. Poggio and E. K. Miller, "A perspective on numerical methods for antennas," *Proc. 1978 Antenna Applications Symp.* (Univ. Illinois, Urbana, IL, 1978).
- [51] C. T. Tai, *Dyadic Green's Functions in Electromagnetic Theory*. Scranton, PA: Intext Educational Publishers, 1971.
- [52] A. A. Oliner and R. G. Malech, "Mutual coupling in infinite scanning arrays," in *Microwave Scanning Antennas*, R. C. Hansen, Ed. New York: Academic Press, ch. 3, vol. II, 1966.
- [53] G. N. Tsandoulas and G. H. Knittel, "The analysis and design of dual-polarization square waveguide phased arrays," *IEEE Trans. Antennas Propagat.*, vol. AP-21, pp. 796–808, 1973.
- [54] N. Amitay and V. Galindo, "The analysis of circular waveguide phased arrays," *Bell Syst. Tech. J.*, vol. 47, pp. 1903–1931, 1968.
- [55] M. H. Chen and G. N. Tsandoulas, "Bandwidth properties of quadrupole ridged circular and square waveguide radiators," *IEEE AP-S Int. Symp. Rec.*, pp. 391–394, 1973.
- [56] J. P. Montgomery, "Ridged waveguide phased array elements," *IEEE Trans. Antennas Propagat.*, vol. AP-24, 1976.
- [57] S. S. Wang and A. Hessell, "Aperture performance of a double-

- ridge rectangular waveguide in a phased array," *IEEE Trans. Antennas Propagat.*, vol. AP-26, pp. 204-214, 1978.
- [58] L. R. Lewis, A. Hessel, and G. H. Knittel, "Performance of a protruding-dielectric waveguide element in a phased array," *IEEE Trans. Antennas Propagat.*, vol. AP-20, pp. 712-722, 1972.
- [59] R. J. Mailloux and H. Steyskal, "Analysis of a dual frequency array technique," *IEEE Trans. Antennas Propagat.*, vol. AP-27, pp. 130-134, 1979.
- [60] J. K. Hsiao, "Computer aided impedance matching of an interleaved waveguide phased array," *IEEE Trans. Antennas Propagat.*, vol. AP-20, pp. 505-506, 1972.
- [61] V. Galindo and C. P. Wu, "Dielectric loaded and covered rectangular waveguide phased arrays," *Bell Syst. Tech. J.*, vol. 47, pp. 93-116, 1968.
- [62] S. W. Lee and W. R. Jones, "On the suppression of radiation nulls and broadband impedance matching of rectangular waveguide phased arrays," *IEEE Trans. Antennas Propagat.*, vol. AP-19, pp. 41-51, 1971.
- [63] R. J. Mailloux, "Surface waves and anomalous wave radiation nulls in phased arrays of TEM waveguides with fences," *IEEE Trans. Antennas Propagat.*, vol. AP-20, pp. 160-166, 1972.
- [64] E. C. Dufort, "Design of corrugated plates for phased array matching," *IEEE Trans. Antennas Propagat.*, vol. AP-16, pp. 37-46, 1968.
- [65] C. C. Chen, "Octave band waveguide radiators for wave-angle scan phased arrays, in *IEEE AP-S Int. Symp. Rec.*, pp. 376-377, 1972.
- [66] L. R. Lewis, M. Fassett, and J. Hunt, "A broadband stripline array element, in *IEEE AP-S Int. Symp. Rec.*, 1974.
- [67] V.W.H. Chang, "Infinite phased dipole array," *Proc. IEEE*, vol. 56, pp. 1892-1900, 1968.
- [68] L. Stark, "Radiation impedance of a dipole in an infinite planar phased array," *Radio Sci.*, vol. 1, pp. 361-377, 1966.
- [69] G. H. Knittel, A. Hessel, and A. A. Oliner, "Element pattern nulls in phased arrays and their relation to guided waves, *Proc. IEEE*, vol. 56, pp. 1822-1836, 1968.
- [70] J. C. Herper, F. J. Esposito, C. Rottenberg, and A. Hessel, "Surface resonances in a radome covered dipole array," in *Proc. 1977 IEEE AP Int. Symp. Digest.*, pp. 198-201, 1977.
- [71] E. Mayer and A. Hessel, "Feed region modes in dipole phased arrays," *IEEE Trans. Antennas Propagat.*, to be published.
- [72] P. Pathak and R. Kouyoumjian, "An analysis of the radiation from apertures in curved surfaces by the geometrical theory of diffraction," *Proc. IEEE*, vol. 62, pp. 1438-1447, 1974.
- [73] R. J. Mailloux, "Phased array aircraft antennas for satellite communication," *Microwave J.*, vol. 20, pp. 38-42, 1977.
- [74] C. J. Miller, "Minimizing the effects of phase quantization errors in an electronically scanned array, in *Proc. 1964 Symp. Electronically Scanned Array Techniques and Applications*, RADC-TDR-64-225, vol. 1, pp. 17-38, 1964 (RADC, Griffiss AFB, NY).
- [75] J. Brown, in Skolnik, *Radar Handbook*, vol. 11, pp. 39-40, 1970.
- [76] T. C. Cheston, "Beam steering of planar phased arrays," *Phased Array Antennas*, Oliner and Knittel, Eds. Dedham, MA: Artech House, 1972.
- [77] H. A. Wheeler, "A systematic approach to the design of a radiator element for a phased array antenna," *Proc. IEEE*, vol. 56, pp. 1940-1951, 1968.
- [78] H. A. Wheeler, "A survey of the simulator technique for designing a radiating element, in *Array Antenna*, Oliner and Knittel, Eds. (*Proceedings of the 1970 Phased Array Antenna Symposium*). Deham, MA: Artech House, 1972.
- [79] E. G. McGill and H. A. Wheeler, "Wide-angle impedance matching of a planar array antenna by a dielectric sheet," *IEEE Trans. Antennas Propagat.*, vol. AP-14, pp. 49-53, 1966.
- [80] L. R. Lewis, L. J. Kaplan, and J. D. Hanfling, "Synthesis of a waveguide phased array element," *IEEE Trans. Antennas Propagat.*, vol. AP-22, pp. 536-540, 1974.
- [81] G. Craven, "Waveguide below cutoff: A new type of microwave integrated circuit," *Microwave J.*, vol. 13, pp. 51-58, 1970.
- [82] L. Stark, "Comparison of array element types," in *Phased Array Antennas*. Dedham, MA: Artech House, 1972.
- [83] P. S. Hall and J. R. James, "Survey of design techniques for flat profile microwave antennas and arrays," *Radio Electron. Eng.*, vol. 48, pp. 549-565, 1978.
- [84] W. C. Wilkinson, "A class of printed circuit antennas," in *Proc. IEEE AP-S, Int. Symp.*, 1974.
- [85] G. R. Hanley and H. R. Perini, "Column network study for a planar array used with an unattended radar," RADC-TR-80-191, Final Rep., Mar. 1980.
- [86] R. E. Munson, "Conformal microstrip antennas and microstrip phased arrays," *IEEE Trans. Antennas Propagat.*, vol. AP-22, pp. 74-78, 1974.
- [87] Y. T. Lo, D. Solomon, and W. F. Richards, "Theory and experiment on microstrip antennas," *IEEE Trans. Antennas Propagat.*, vol. AP-27, pp. 131-145, 1979.
- [88] K. R. Carver, "A model expansion theory for the microstrip antenna," in *Proc. IEEE AP-S Int. Symp.*, 1979.
- [89] A. Derneryd, "Linearly polarized microstrip antennas," *IEEE Trans. Antennas Propagat.*, vol. AP-24, pp. 846-851, 1976.
- [90] E. H. Newman and P. Tulyathan, "Analysis of microstrip antennas using moment methods," *IEEE Trans. Antennas Propagat.*, vol. AP-29, pp. 47-54, 1981.
- [91] E. L. Coffee and K. R. Carver, "Towards the theory of microstrip antenna patterns," in *Proc. 1977 Antenna Application Symp.* (Allerton Park, IL), 1977.
- [92] G. Sanford and L. Klein, "Increasing the beamwidth of a microstrip radiating element *Int. Symp. Digest.*, pp. 126-129, 1979 (Antennas and Propagation Society, Univ. Washington).
- [93] J. Q. Howell, "Microstrip antennas," *IEEE Trans. Antennas Propagat.*, pp. 90-93, 1975.
- [94] J. Greiser, "Coplanar stripline antenna," *Microwave J.*, vol. 19, pp. 47-49, 1976.
- [95] G.A.E. Crone, N. Adatia, B. K. Watson, and N. Dang, "Corrugated waveguide polarizers for high performance feed systems," in *Proc. IEEE AP-S Int. Symp.*, 1980.
- [96] D. Davis, O. J. Digiandomenico, and J.J.A. Kempic, "A new type of circularly polarized antenna element," in *Proc. IEEE G-AP Symp. Digest*, pp. 2-23, 1976.
- [97] M. H. Chen and G. N. Tsandoulas, "A wide band square waveguide array polarizer," *IEEE Trans. Antennas Propagat.*, vol. AP-21, pp. 389-391, 1973.
- [98] G. Mathai, L. Young, and E.M.T. Jones, *Microwave Filters, Impedance Matching Networks and Coupling Structure*. New York: McGraw-Hill, 1964, ch. 9.
- [99] H. Howe, *Stripline Circuit Design*. Dedham, MA: Artech House, 1974.
- [100] L. I. Parad and R. L. Moynihan, "Split tee power divider," *IEEE Trans., Microwave Theory Tech.* vol. MTT-13, 1965.
- [101] S. G. Winchell, "A performance analysis of broadband low sidelobe array antennas," Rep. N60921-79-C-A236-100, Naval Surface Weapons Center (Pahlgren, VA), 1979.
- [102] G. E. Evans and S. G. Winchell, "A wide-band ultra-low sidelobe antenna," in *Proc. 1979 Antenna Applications Symp.*, 1979.
- [103] *Military Standardization Handbook*, U.S. Radar Equipment, MIL-HDBK-1628, Dec. 15, 1973, pp. 558-559 (see also Brookner, 1977, ch. 1).
- [104] G. C. Bandy, L. J. Hardeman, and W. F. Hayes, "MERA modules, how good in an array," *Microwaves*, pp. 39-49, 1969.
- [105] J. Butler, "Digital, matrix and intermediate-frequency scanning," in *Microwave Sensing Antennas*, R. C. Hansen, Ed. New York: Academic Press, 1969, vol. 13, ch. 3.
- [106] J. Austin and J. Forrest, "Design concepts for active phased array modules," *Proc. Inst. Elec. Eng.*, vol. 127, part F, no. 4, pp. 290-300, 1980.
- [107] J. A. Kaiser, Jr., "A retrodirective system utilizing an interferometer receive array," in *Proc. IEEE Antennas Propagation Society Symp.*, pp. 199-202, 1979.
- [108] L. Stark, C. V. Bell, R. A. Notvest, R. E. Griswold, D. A. Chelton, and R. A. Howard, "Microwave components for wideband arrays," *Proc. IEEE*, vol. 56, pp. 1908-1922, 1968.
- [109] J. F. White, "Review of semiconductor microwave phase shifters," *Proc. IEEE*, vol. 56, pp. 1924-1930, 1968.
- [110] J. F. White, *Semiconductor Control*. Dedham, MA: Artech House, 1977.
- [111] L. Stark, R. W. Burns, and W. P. Clark, "Phase shifters for arrays," in *Radar Handbook*. New York: McGraw-Hill, 1970.
- [112] W. J. Ince, "Recent advances in diode and ferrite phaser technology for phased-array radars, Part I and Part II," *Microwave J.*, vol. 15, no. 9, pp. 36-46, and no. 10, pp. 31-36, 1972.
- [113] G. N. Tsandoulas, "Unidimensionally scanned phased arrays," *IEEE Trans. Antennas Propagat.*, vol. AP-28, pp. 86-98, 1980.
- [114] W. J. Ince and D. H. Temme, "Phasers and time delay elements," *Advances in Microwaves*, vol. 4, pp. 2-183 (Academic Press New York).
- [115] L. R. Whicker and C. W. Young, "The evolution of ferrite control components," *Microwave J.*, vol. 2, no. 11, pp. 33-37, 1978.
- [116] L. R. Whicker and D. M. Bolle, "Annotated literature survey of microwave ferrite control components and materials for 1968-1974," *IEEE Trans., Microwave Theory Tech.*, vol. MTT-23, pp. 908-918, 1975.
- [117] C. R. Boyd, "Analog rotary-field ferrite phase shifters," *Microwave J.*, vol. 20, pp. 41-43, 1977.
- [118] A. G. Fox, "An adjustable waveguide phase changer," *Proc. IRE*, vol. 35, pp. 1489-1498, 1947.
- [119] D. K. Barton, "Radar technology for the 1980's," *Microwave J.*, vol. 21, no. 11, pp. 81-86, 1978.
- [120] C. G. Dahl, C. E. Fogelstrom, W. W. Gansz, and P. R. Merrill, "Low-sidelobe tactical radar antenna," in *Proc. The 1979 An-*

- tenna Applications Symp.* (Univ. Illinois, Urbana, IL), 1979.
- [121] J. T. Tillman, Jr., "The theory and design of circular array antennas," Univ. Tennessee Engineering Experiment Station Report, 1968.
- [122] J. H. Provencher, "A survey of circular symmetric arrays, in *Phased Antennas*, A. Oliner and G. Knittel, Eds. Dedham, MA: Artech House, 1972.
- [123] P. Shelton, "Application of hybrid matrices to various multimode and multibeam antenna systems," in *Proc. IEEE Washington Chapter PGAP Meet.*, 1965.
- [124] B. Sheleg, "A matrix-fed circular array for continuous scanning," *Proc. IEEE*, vol. 56, pp. 2016-2027, 1968.
- [125] G. Skahil and W. D. White, "A new technique for feeding a cylindrical array," *IEEE Trans. Antennas Propagat.*, vol. AP-13, pp. 253-256, 1975.
- [126] R. W. King, R. B. Mack, and S. S. Sandler, *Arrays of Cylindrical Dipoles*. London: Cambridge University Press, 1968, ch. 4.
- [127] G. V. Borgiotti, "Modal analysis of periodic planar phased arrays of apertures," *Proc. IEEE*, vol. 56, pp. 1881-1892, 1968.
- [128] G. V. Borgiotti and Q. Balzano, "Mutual coupling analysis of a conformal array of elements on a cylindrical surface," *IEEE Trans. Antennas Propagat.*, vol. AP-18, pp. 55-63, 1970.
- [129] —, "Analysis of element pattern design of periodic array of circular apertures on conducting cylinders," *IEEE Trans. Antennas Propagat.*, vol. AP-20, pp. 547-553, 1972.
- [130] J. C. Sureau and J. S. Hessel, "Realized gain function for a cylindrical array of open-ended waveguides," in *Phased Array Antennas*, Oliner and Knittel, Eds. Dedham, MA: Artech House, 1972.
- [131] J. C. Herper, C. Mandarino, A. Hessel, and B. Tomasic, "Performance of a dipole element in a cylindrical array-A modal approach," in *Proc. IEEE AP-S Inst. Symp.*, pp. 162-165, 1980.
- [132] K. E. Golden *et al.*, "Approximation techniques for the mutual admittance of slot antennas in metallic cones," *IEEE Trans. Antennas Propagat.*, vol. AP-22, pp. 44-48, 1974.
- [133] Q. Balzano and T. B. Dowling, "Mutual coupling analysis of arrays of aperture on cones," *IEEE Trans. Antennas Propagat.*, vol. AP-22, pp. 92-97, 1974.
- [134] A. Hessel, Y. L. Liu, and J. Shmoys, "Mutual admittance between circular apertures on a large conducting sphere," *Radio Sci.*, vol. 14, pp. 35-42, 1979.
- [135] H. Steyskal, "Analysis of circular waveguide arrays on cylinders," *IEEE Trans. Antennas Propagat.*, vol. AP-25, pp. 610-616, 1977.
- [136] H. Ahn, and A. Hessel, "Mutual coupling in arrays on concave surfaces," in *Proc. 1977 Antenna and Propagation Symp. Digest* (Stanford University, Stanford, CA), pp. 206-208, 1977.
- [137] H. Ahn, B. Tomasic and A. Hessel, "Periodic structure ray approach to analysis of arrays on concave surfaces," in *Proc. 1979 URSI Symp. Digest* (Seattle, Washington), p. 52, 1979.
- [138] Q. Balzano, "Investigation of the element pattern in cylindrical phased arrays of circular waveguides," AFCRL-72-0232, NTIS AD 742327, 1972.
- [139] R. J. Mailloux and W. G. Mavroides, "Hemispherical coverage of four-faced aircraft arrays," RADC-TR-79-176, NTIS AD A073079, 1979.
- [140] R. G. and Kouyoumjian and P. H. Pathak, "A uniform geometrical theory of diffraction for an edge in a perfectly conducting surface," *Proc. IEEE*, vol. 62, pp. 1448-1461, 1974.
- [141] L. Schwartzman and J. Stangel, "The dome antenna," *Microwave J.*, vol. 18, pp. 31-34, 1975.
- [142] H. Steyskal, A. Hessel, and J. Shmoys, "On the gain-versus-scan trade-offs and the phase gradient synthesis for a cylindrical dome antenna," *IEEE Trans. Antennas Propagat.*, vol. AP-27, pp. 825-831, 1979.
- [143] W. T. Patton, "Limited scan arrays," in *Phased Array Antennas: Proceedings of the 1970 Phased Array Antenna Symp.*, pp. 332-343, A. A. Oliner and G. H. Knittel, Eds. Dedham, MA: Artech House.
- [144] J. Stangel, "A basic theorem concerning the electronic scanning capabilities of antennas," URSI Commission VI, Spring Meet., June 11, 1974.
- [145] G. V. Borgiotti, "Degrees of freedom of an antenna scanned in a limited sector," *IEEE G-AP, Int. Symp.*, pp. 319-320, 1975.
- [146] P. W. Woodward and J. D. Lawson, "The theoretical precision with which an arbitrary radiation pattern may be obtained from a source of finite size," *J. AIEE*, vol. 95, pp. 362-370, 1948.
- [147] R. C. Hansen, "Aperture theory," in *Microwave Scanning Antennas*, R. C. Hansen, Ed. New York: Academic Press, 1966, vol. I, ch. 1.
- [148] T. E. Manwarren, A. R. Minuti, and A. Farrar, "A large-element limited scan array with random grating lobe levels," in *Proc. IEEE AP-S Int. Symp.*, pp. 321-324, 1975.
- [149] R. J. Mailloux, L. Zahn, T. Martinez, and G. Forbes, "Grating lobe control in limited scan arrays," *IEEE Trans. Antennas Propagat.*, vol. AP-27, pp. 79-85, 1979.
- [150] R. Tang, "Survey of time-delay beam steering techniques," in *Phased Array Antennas; Proceedings of the 1970 Phased Array Antenna Symp.* Dedham, MA: Artech House, pp. 254-260, 1972.
- [151] E. C. Dufort, "Constrained feeds for limited scan arrays," *IEEE Trans. Antennas Propagat.*, vol. AP-26, pp. 407-413, 1981.
- [152] R. J. Mailloux, "An overlapped subarray for limited scan application," *IEEE Trans. Antennas Propagat.*, vol. AP-22, pp. 487-489, 1974.
- [153] R. N. Assaly and L. J. Ricardi, "A theoretical study of a multi-element scanning feed system for a parabolic cylinder," *IEEE Trans. Antennas Propagat.*, vol. AP-14, pp. 601-605, 1966.
- [154] C. Winter, "Phase scanning experiments with two reflector antenna systems," *Proc. IEEE*, vol. 56, pp. 1984-1999, 1968.
- [155] C. H. Tang, "Application of limited scan design for the AGILT-RAC-16 antenna," in *Proc. 20th Annu. USAF Antenna Research and Development Symp.* (Univ. Illinois, Urbana, IL), 1970.
- [156] J. M. Howell, "Limited scan antennas," in *Proc. IEEE AP-S Int. Symp. Digest*, 1974.
- [157] A. C. Schell, "A limited sector scanning antenna," *IEEE G-AP Int. Symp.*, 1972.
- [158] R. McGahan, "A lens array limited scan antenna," in *Proc. IEEE AP-S Int. Symp.*, pp. 113-116, 1975.
- [159] W. D. Fitzgerald, "Limited electronic scanning with a near field Cassegrainian system," ESD-TR-71-271, Tech. Rep. 484, Lincoln Laboratory, AD 735661.
- [160] —, "Limited electronic scanning with a near field Gregorian system," ESD-TR-71-272, Tech. Rep. 486, Lincoln Laboratory, AD.
- [161] F. McNee, H. S. Wong, and R. Tang, "An offset lens-fed parabolic reflector for limited scan applications," in *IEEE AP-S Int. Symp. Re.*, pp. 121-123, 1975.
- [162] T. S. Bird, J. L. Boomars, and P. J. B. Clarricoats, "Multiple-beam dual-offset reflector antenna with an array feed," *Electron. Lett.*, vol. 14, pp. 439-441, 1978.
- [163] C. Dragone and M. J. Gans, "Imaging reflector arrangements to form a scanning beam using a small array," *Bell Syst. Tech. J.*, vol. 58, pp. 501-515, 1979.
- [164] C. H. Tang and C. F. Winter, "A study of the use of a phased array to achieve pencil beam over limited sector scan," AFCLR-TR-73-0482, ER 73-4292 Raytheon Co., Final Rep. Contract F19628072-C-0213, AD 768618.
- [165] G. V. Borgiotti, "An antenna for limited scan in one plane: Design criteria and numerical simulation," *IEEE Trans. Antennas Propagat.*, pp. 232-243, 1977.
- [166] W. Rotman and P. Franchi, "Cylindrical microwave lens antenna for wideband scanning application," in *Proc. Int. Symp. Digest*, IEEE AP-S, pp. 564-567.
- [167] M. H. Chen and G. N. Tsandoulas, "A dual reflector optical feed for wideband phased arrays," *IEEE Trans. Antennas Propagat.*, vol. AP-22, pp. 541-545, 1974.
- [168] R. J. Mailloux, "Subarraying feeds for low sidelobe scanned arrays," in *Proc. Int. Symp. Digest*, IEEE AP-S, pp. 30-33, 1979.
- [169] R. L. Fante, "Systems study of overlapped subarrayed scanning antennas," *IEEE Trans. Antennas Propagat.*
- [170] R. J. Mailloux, "Array and subarray pattern control features of subarraying feeds," *IEEE Trans. Antennas Propagat.*, vol. AP-29, pp. 538-544, 1981.
- [171] G. G. Sanford, "Conformal microstrip phased array for aircraft tests with ATS-6," *IEEE Trans. Antennas Propagat.*, vol. AP-26, pp. 642-646, 1981.
- [172] R. Munson and G. Sanford, "Microstrip phased array developed for 5 GHz application," in *Proc. Int. Symp. Digest Antennas and Propagation Society* (Stanford University, Stanford, CA), pp. 72-75, 1977.
- [173] D. Huebner, "An electrically small microstrip dipole planar array," in *Proc. Workshop on Printed Circuit Antenna Technology*, (New Mexico State University), paper 17, 1979.
- [174] J. Yee and W. Furlong, "An extremely lightweight fuselage integrated phased array for airborne applications," in *Proc. Workshop on Printed Circuit Antenna Technology* (New Mexico State University), paper 15, 1979.

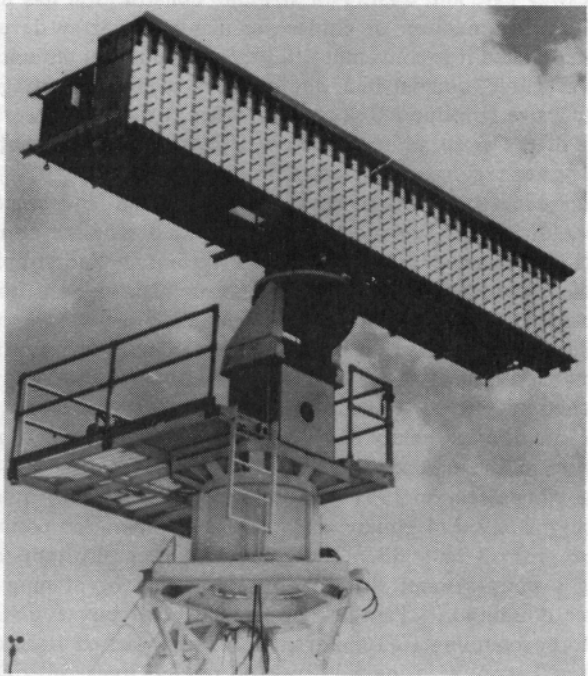


Fig. 24. *L*-Band low sidelobe array (courtesy of Westinghouse Corporation).

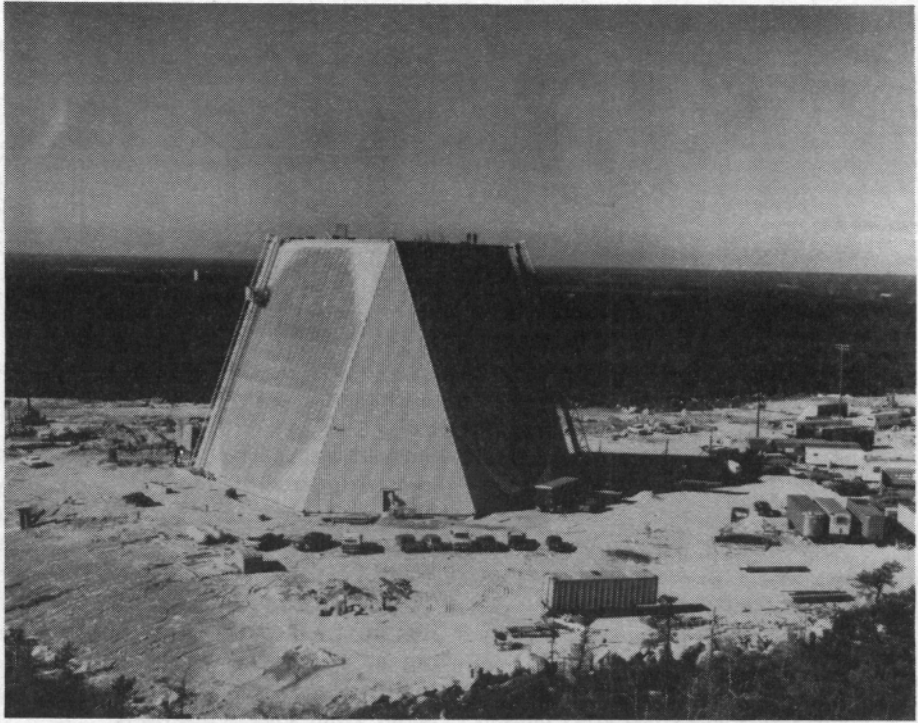


Fig. 27. Pave paws array (courtesy of Raytheon Company).



Fig. 28. Patriot array (courtesy of Raytheon Company).

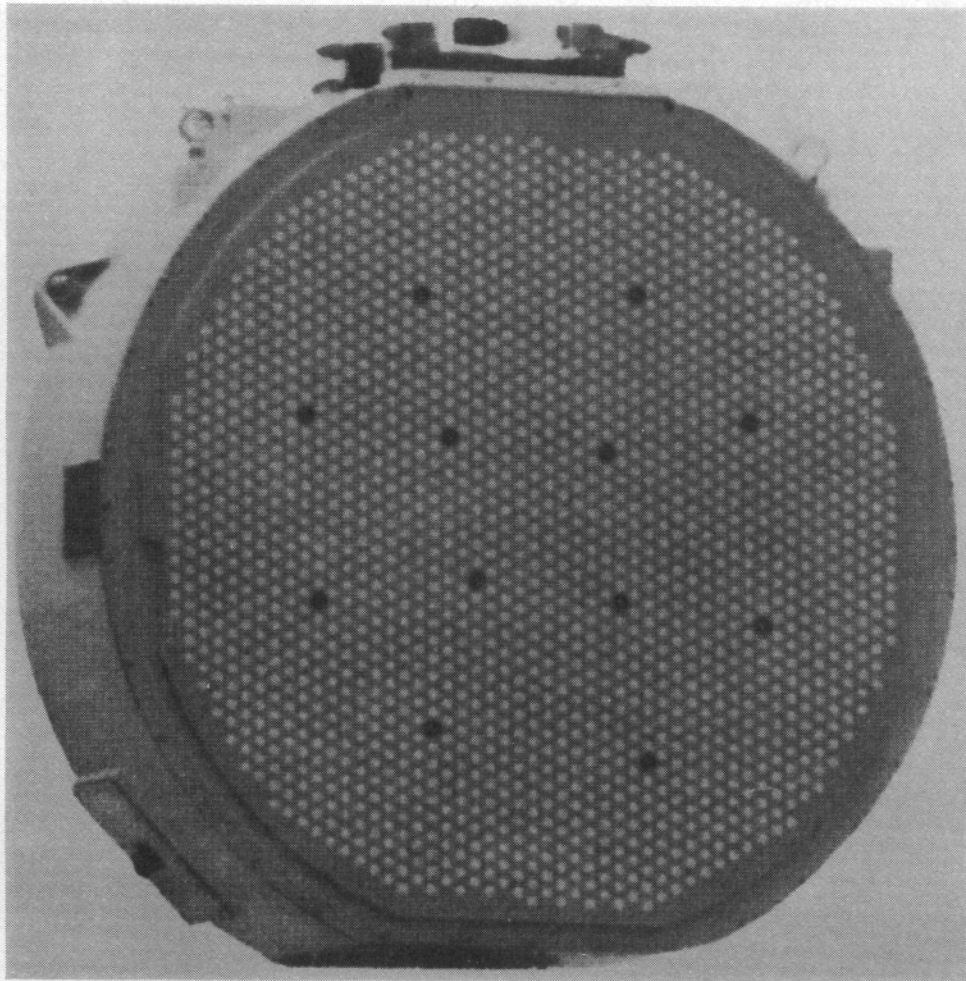


Fig. 29. Electronically agile radar array (courtesy of Westinghouse Corporation).

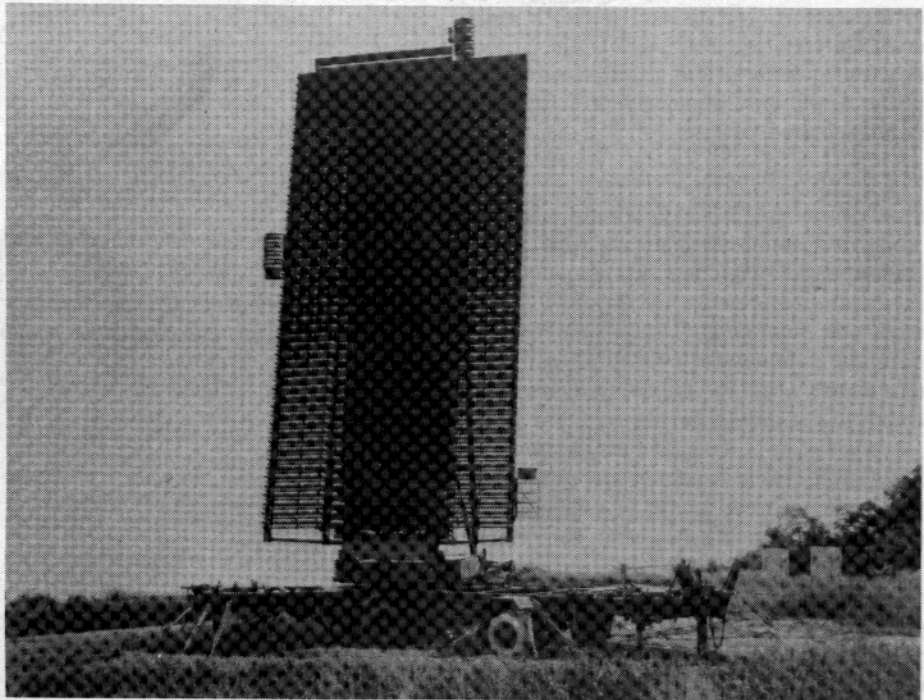


Fig. 30. TPS-59 array (courtesy of General Electric Company).

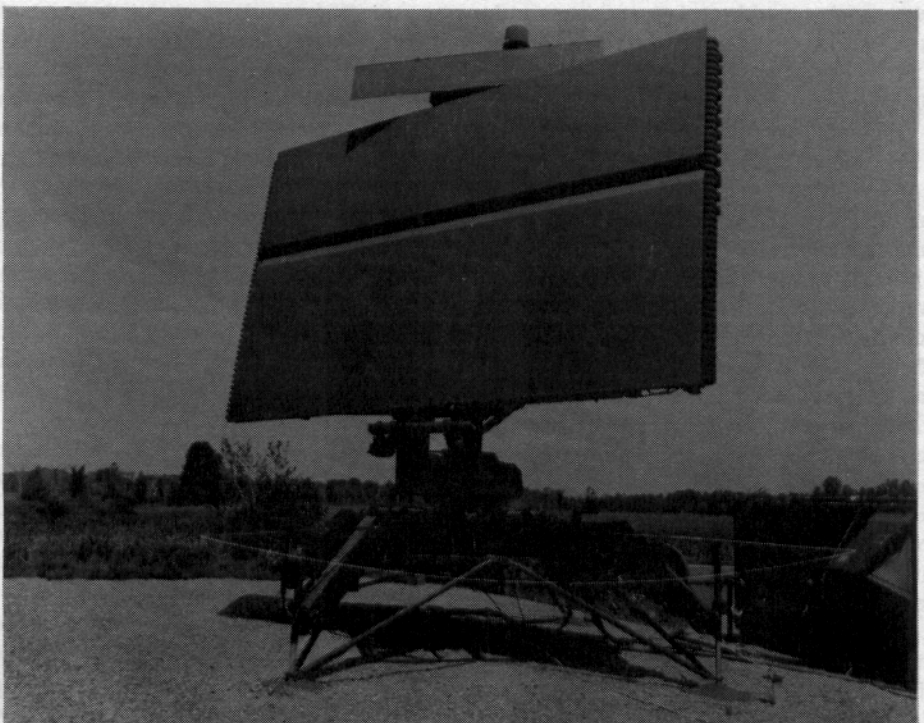


Fig. 31. Ultra-low sidelobe array.

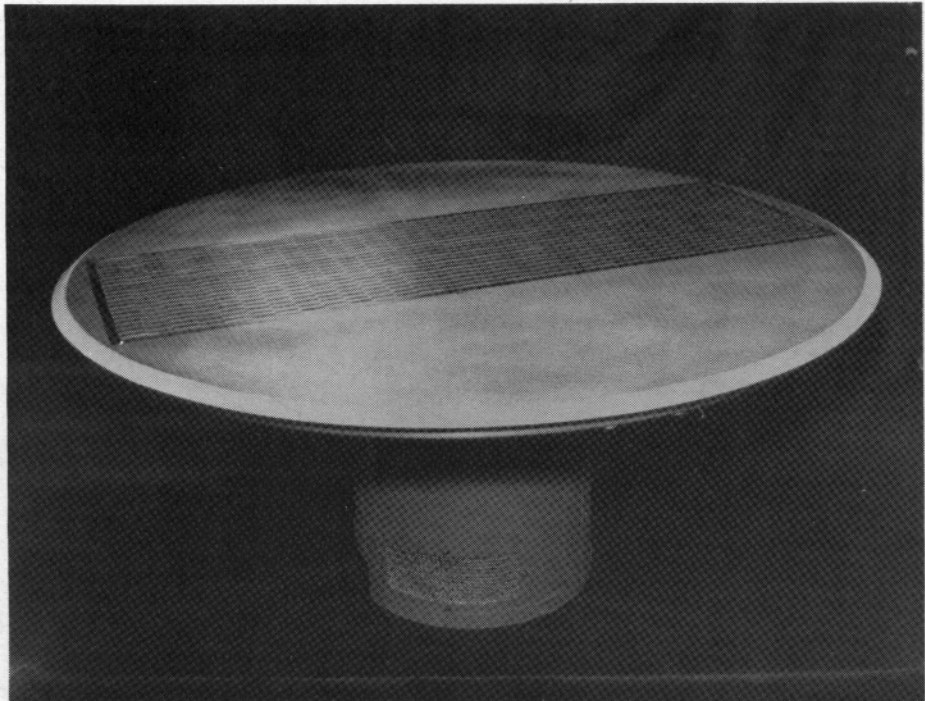


Fig. 36. Low profile array for mechanical/electronic hemispheric scan (courtesy of Hazeltine Corporation).

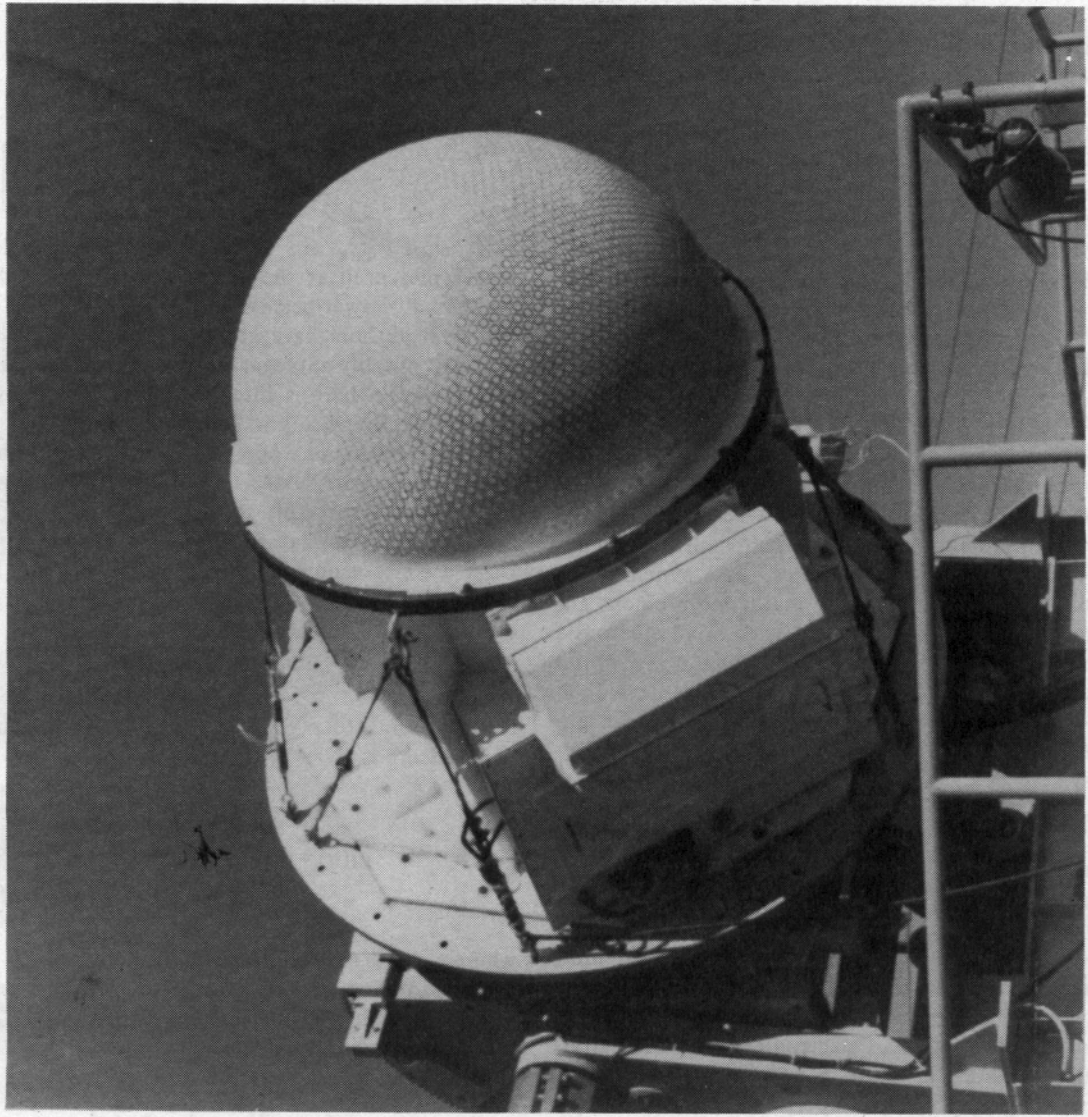


Fig. 38. The dome antenna array (courtesy of Sperry Corporation).

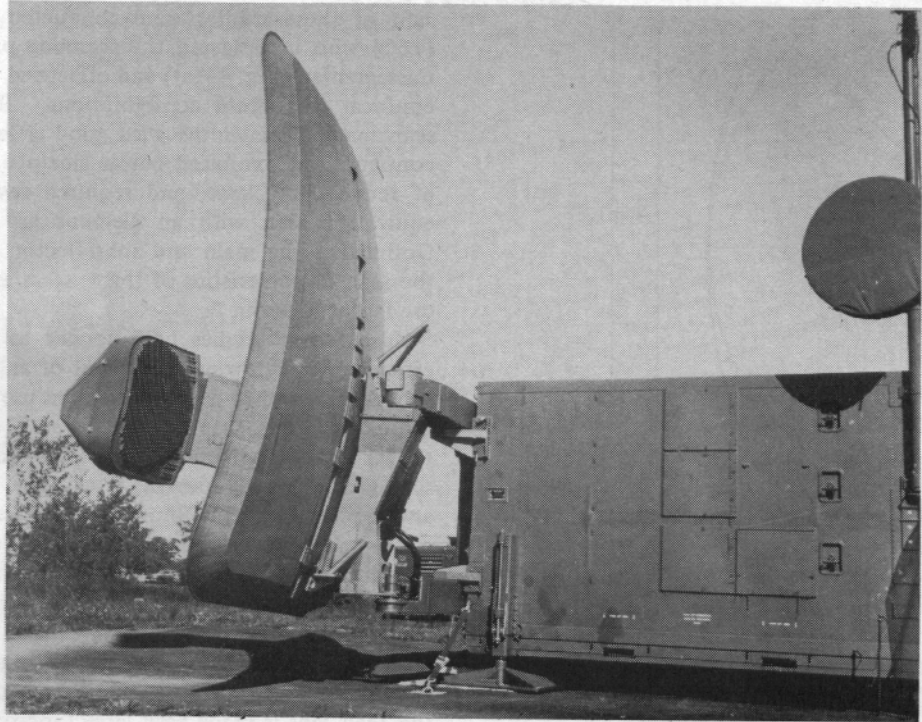


Fig. 42. Precision approach radar antenna AN/TPN-19 (courtesy of Raytheon Corporation).

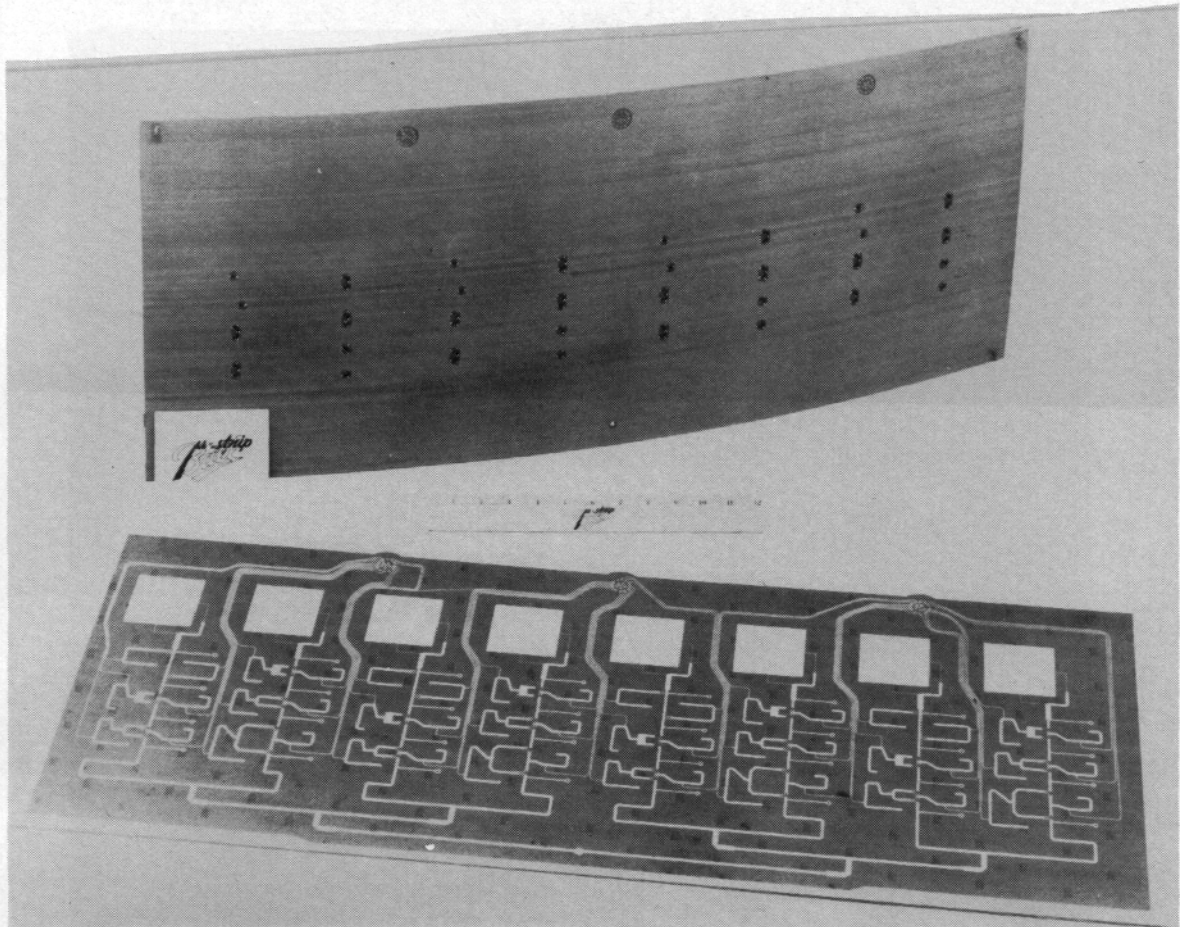


Fig. 50. Conformal array for aircraft tests with ATS-6 (after Sanford [171]).

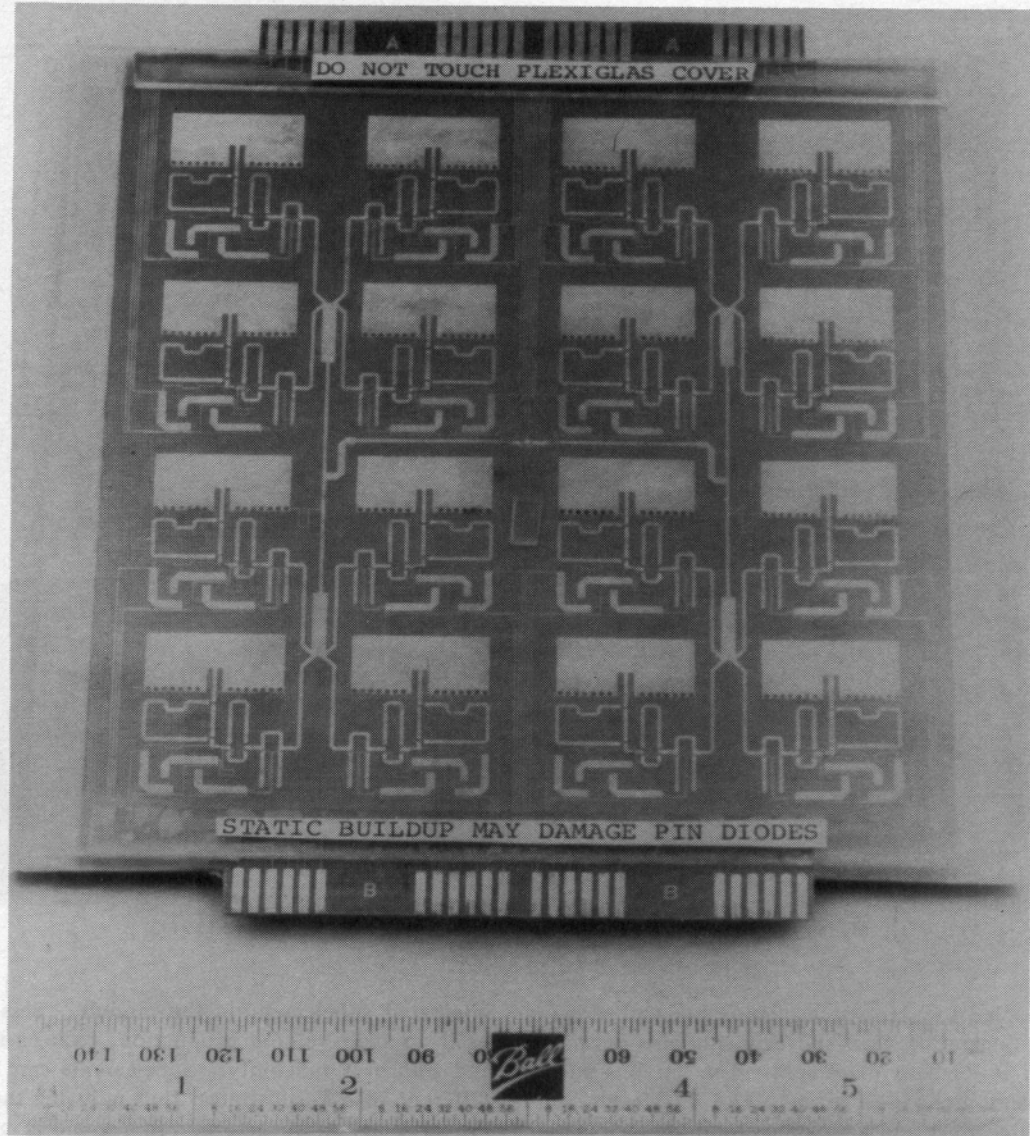


Fig. 51. Single layer microstrip phased array, with elements, phase shifters, bias, and feed lines one side of board (after Munson and Sanford [172]).

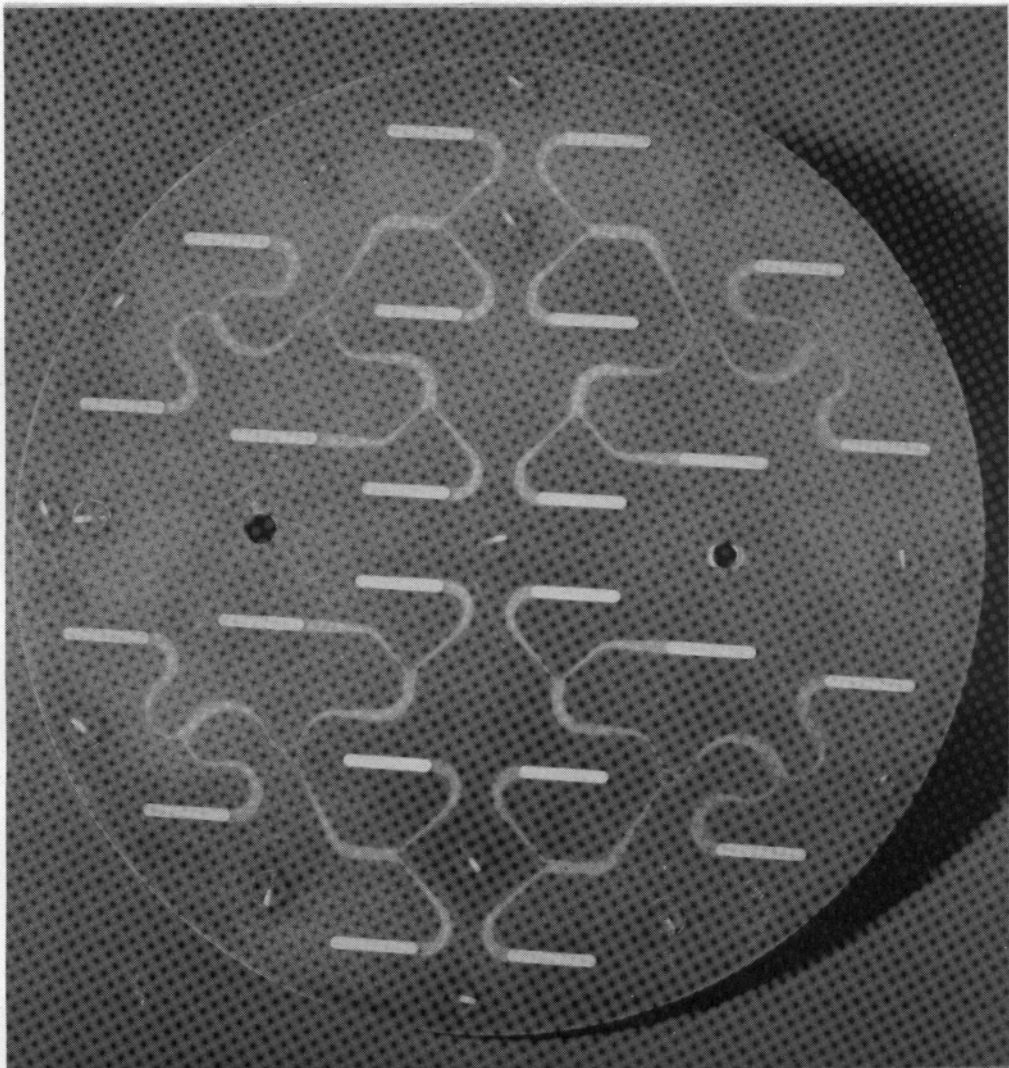


Fig. 52. A 24-element proximity coupled microstrip dipole array (courtesy of Ball Aerospace Company).